Development and Application of Electrochemical Biosensors for Multianalyte Detection in Model Organ Systems

By

Sara Lynn Melow

Dissertation

Submitted to the Faculty of the

Graduate School of Vanderbilt University

in partial fulfillment of the requirements

for the degree of

DOCTOR OF PHILOSOPHY

in

Chemistry

June 30, 2021

Nashville, Tennessee

Approved:

David E. Cliffel, Ph.D.

John A. McLean, Ph.D.

John P. Wikswo, Jr., Ph.D.

Carmelo J. Rizzo, Ph.D.

For my family.

ACKNOWLEDGMENTS

I would like to thank the financial contributions from both internal and external sources to Vanderbilt University that without, this work would not have been possible. Funding was provided by the National Institutes of Health, Environmental Protection Agency, and Vanderbilt University. The training grant I received significantly impacted my experience here, and I will forever be grateful for it. Non-financial support from the staff here like VIIBRE and the Storeroom has been so helpful, and I thank them for that!

During my graduate school time, I have worked with so many incredible people. To all of my lab members (Dilek, Ethan, Margaret, Chris, Kody, Dusty, endless naval/army students, Adam, Aaron, Evan, Dave, Pragun, Kysha, Grace, John, and Matt), thank you for providing me with help and keeping me sane. I have had the best time being in the lab with you guys. Dilek and Ethan, thanks for making our little corner so fun and letting me tell you about my crazy adventures every day. You guys made my graduate school experience the best it could be!

Without my advisors, I would most certainly never be where I am now. Thank you to my research advisor at Elmira College, Dr. Baker. You have been so supportive and I would not be here if it weren't for your help and love for analytical chemistry. Dr. Cliffel, thank you. I appreciate your hands-off approach to mentoring, allowing me to grow and become the scientist I am today. Thank you for all your help and advice when things are not working in the lab, which was more than I care to admit. I have learned from you how cultivate relationships, think critically, and solve problems creatively. Thank you!

I would like to thank the friends I have made throughout my life. First, I want to thank my friends I grew up with in Oregon, Stacie, Megan, Keziah, and Summer, for which I have felt

support near and far and through so many years of friendship. I will always treasure our relationships. Next, I would like to thank my group of seven EC girls (Danielle, Karli, Sydney, Emily, Meghan, Lauren, and Erin) I made as forever friends in college. You guys were my confidantes, my roommates, my family away from family, and for that I am forever grateful. I cannot imagine my life without you (purple and gold forever). Kelsie, you came into my life like a little sunshine beaming at me just like the bright yellow outfit with sunflowers you wore on the first day we met. It is wonderful getting to experience chemistry and grad school with you even if we are in different schools and states. Thank you for being a wonderful friend and the nicest person! Finally, I will mention my friends I made in Nashville. To Emma, it is crazy how fate works to have been friends in Oregon and then to Nashville, thank you for our Bachelor and Thai nights every week with Lucy. I loved being able to confide in you, have fun, and take my mind off any stress I had. Cara and Sophie, thank you! You guys make my life way more fun and I am so glad we got to go out downtown all the time and have Moscow Mules, you made my life way more interesting! To Kate, I am so glad to have met you (thanks, Megan)! It was so wonderful to go to the dog park with Roxy and I loved having you around to laugh and go to all the country concerts with! To all of my friends, you are my chosen family and I thank you sincerely for always being there for me!

Lastly, I want to thank my foundation that I was built upon, my family. They are the reason who I am today and why I work the hardest I can. They have supported me through everything and are who I can always count on for any help I need. Without them, I could not have completed this. To my dad (Glean), thank you for being there to help me with anything including moving in, being my handyman, and fixing my car even from hundreds of miles away. To my stepmom (Carrie), thank you for always being my go-to for hair and nail information, for which I would never look

this good without ;) To my mom (Lynn), you are always there to lend an ear for any troubles, you are my biggest cheerleader, my best adventure partner, and I hope you burst with pride, because I finally did it (I stayed in school until the end)! To my stepdad (Bruce), thank you for being there and supporting me even from many miles away. To my brother (Ross) and his family, thank you for providing me with more family and love than I could dream of. I am so proud to be your sister, aunt, and great aunt, and I can't imagine life without all of you! To Auntie Carol, I am so glad that you are my aunt and other mom, because you are the absolute most fun to be around and you have provided me with so many laughs and great memories that I will forever cherish. I have to mention my cat, Olive, with whom I have spent most of my time in graduate school with, providing many purrs to help soothe my soul after long days of lab work and stress. She provided me with companionship and made my life infinitely better. Olive you! Finally, I want to thank the newest member of my family and my best friend, Ryan Winn. I am so excited to be done with school and to marry you in a couple months (#WINNing), so that we can start our lives together. You have been my rock, my partner-in-crime, and my everything. Without you by my side, I assure you I would not have made it to where I am today and would certainly not be as happy, so thank you for everything you have done, currently do, and will do in the future.

TABLE OF CONTENTS

DEDICATION…… ii

ACKNOWLEDGMENTS……. iii

LIST OF TABLES…….. viii

LIST OF FIGURES…… ix

Chapter

I. INTRODUCTION……. 1

II. EXPERIMENTAL METHODS AND ANALYSIS…….. 8

Cleaning of Screen-Printed Electrodes…… 8
Silver/Silver Chloride Reference Electrode Preparation…… 11
Enzyme Film Deposition……...… 13
Ionophore-Based Membrane Deposition……... 13
Electrochemical Analysis…….. 13
Data Analysis……..... 15

III. A LOW-INTERFERENCE, HIGH-RESOLUTION MULTIANALYTE ELECTROCHEMICAL BIOSENSOR …….. 16

Introduction……... 16
Experimental…… 21
Results……... 33
Discussion…… 45
Conclusions……... 53
Acknowledgments…… 53

IV. MULTIANALYTE AMPEROMETRIC ELECTROCHEMICAL BIOSENSOR PLATFORM FOR ANALYSIS OF MODEL ORGAN SYSTEMS…….. 55

Introduction…….…….. 55
Experimental…… 59
Results……... 65
Discussion…… 72
Conclusions……... 80
Acknowledgments…… 80

V. DEVELOPMENT AND APPLICATION OF A DUAL AMPEROMETRIC AND POTENTIOMETRIC MULTIANALYTE BIOSENSOR…….. 82

Introduction……... 82
Experimental…… 86
Results……... 94
Discussion……... 107
Conclusions…… 112
Acknowledgments……... 113

VI. CONCLUSIONS AND OUTLOOK……. 114

Summary……. 114
Outlook…… 117

Appendix

A. DEVELOPMENT OF A CHOLESTEROL SENSOR FOR ANALYSIS OF MODEL ORGAN SYSTEMS…… 120

Introduction……. 120
Experimental……... 123
Results and Discussion…… 124
Conclusions……. 130
Acknowledgments……... 130

B. ANALYSIS OF LIVER-ON-CHIP SAMPLES USING OSMIUM-BASED ELECTROCHEMICAL BIOSENSORS…… 131

Introduction……. 131
Experimental……... 132
Results and Discussion…… 133
Conclusions……. 136
Acknowledgments……... 136

REFERENCES…… 137

CURRICULUM VITAE……. 156

LIST OF TABLES

Table **Page**

2.1 Parameters for Cleaning Electrodes …….. 10

2.2 Parameters for Evaluating the SPE Cleanliness……. 10

2.3 Parameters for Silver Plating the Reference Electrode……... 12

5.1 Treatment Protocols for Mice……..… 103

LIST OF FIGURES

Figure		Page
3.1	Redox Process for First-Generation and Os-Based Sensors	18
3.2	^{1}H-NMR of Poly(N-vinylimidazole-allylamine) and Os(bpy)$_2$Cl-PVI	24
3.3	Cyclic Voltammogram of Os(bpy)$_2$Cl-PVI	25
3.4	Continuous Measurement of Os-based GOx Sensor	29
3.5	Selectivity Assay Graph Comparing Os-Polymer and First-Generation Sensors	35
3.6	Representative calibration curves of Os-based Sensors	37
3.7	Operational Longevity of the Os-based Glucose and Lactate Oxidase Sensors	39
3.8	Glucose Consumption of AML12 Cells Treated with APAP and/or Insulin	41
3.9	Comparison Graph of Control Media with First-Generation Sensors	44
3.10	First-Generation Glucose Sensor Calibration Curve	47
3.11	Comparison Graphs for Glucose and Lactate Sensitivities for Operational Longevity	50
4.1	Drawings of SPE housing and SPE array	62
4.2	Representative Logarithmic Curves for Various Analytes	67
4.3	Representative Calibration Curves of the Linear Range of the Analytes	67
4.4	Glucose and Lactate Concentrations in Mice Macrophages After Treatment	69
5.1	Schematics of electrode housing and electrode array	89
5.2	Membrane Formulation and Sensitivity for Ammonium Sensor	95
5.3	Reference Electrode Coating Determination	97
5.4	Calibration Curves of Potentiometric Sensors	99
5.5	Operational Longevity of the Potentiometric Sensors	101

5.6 Analyte Concentrations of Mice Peritoneal Lavage Samples After Treatment …….. 104

A.1 Comparison of Cholesterol Dissolving Agents……...…..… 125

A.2 Comparison of Cholesterol Oxidase Film Modifications……. 127

A.3 Cholesterol Calibration Curve……. 129

B.1 Glucose and Lactate Metabolism in LoCs after Rosiglitazone Treatment……. 134

Chapter I

INTRODUCTION

Metabolites are products of metabolism and can have a number of functions that are involved with multiple biological processes. These are a large class of compounds that can take the form of carbohydrates, amino acids, antioxidants, neurotransmitters, organic acids, lipids, etc.[1] Glucose is important as a main nutrient for cells, but is also a part of important processes in the body including, glycolysis, glycogenolysis, and gluconeogenesis.[2] Lactate provides information on metabolic activities such as increased lactate concentrations in tissues during periods of anaerobic glycolysis.[3,4] Glutamate and dopamine are excitatory neurotransmitters that are responsible for several functions, including, learning, memory, and motor control.[5–7] A neuromodulator, acetylcholine modifies neuronal response to stimuli.[8] Superoxide is a reactive oxygen species that provides intracellular signaling, defense against foreign substances, and cell function.[9,10] Also known as vitamin C, ascorbic acid is an essential antioxidant that defends against free radicals.[11,12] Cholesterol is an essential part of the mammalian cell membranes and a part of liver homeostasis.[13,14] Ammonium is produced and consumed during cell metabolism and essential part of the urea cycle.[15] Lastly, potassium is an important mineral and helps to regulate muscle contractions and nerve signals among others.[16,17] Because metabolites serve in multiple function and are involved in multiple pathways, the ability to detect and quantify them is necessary in understanding mechanisms and processes in biological systems for monitoring health and disease.

Biosensors have been in development for decades to quantify real-time metabolite changes in concentration to monitor health and disease and examine treatments for these diseases. Glucose

monitors used by diabetics have utilized electrochemical biosensing for decades to measure glucose levels to deliver insulin more accurately.[18,19] However, it was necessary to understand more about biological systems, so sensors for other analytes, including, glutamate, acetylcholine, calcium and more have been developed.[3,6,20–22] Multiple techniques including, mass spectrometry, immunoassays, amperometry, potentiometry, and many others have been used to detect these analytes.[23–27] Mass spectrometry is used to detect many metabolites and offers high sensitivity such as determining trends of metabolites in human serum.[28] Immunoassays provide sensitive detection to specific analytes and can be used in low resource areas as seen in the on-bead detection of malarial protein biomarkers.[27] While these techniques are sensitive and have their own advantages, they suffer in temporal resolution and cannot integrate easily with biological systems for *in situ* or downstream analysis. Electrochemical biosensors utilizing enzymes and ionophores have been developed to overcome these challenges of temporal resolution and integration while maintaining sensitivity.

One of the most widely used biosensors is enzymatic-based sensors that can be used to detect metabolites, including glucose, lactate, dopamine, and reactive oxygen species.[10,24,29,30] Generally, these sensors utilize an oxidase enzyme to oxidize the analyte to generate hydrogen peroxide that can be oxidized at 0.6 V (vs. Ag/AgCl) and measured using amperometry. However, a few of the them require multiple enzymes to become a form that can finally be oxidized and measured. Dopamine readily oxidizes at 0.6 V, so tyrosinase is used for specificity and converts dopamine to a quinone that may then be reduced at a negative potential. Enzymatic instability can cause issues for these sensors as they degrade over time and require recalibration often to obtain the most accurate measurements. Combining these sensors with microfluidic systems provides automated calibration and analysis to reduce the effects of enzymatic degradation on the

measurements.[6,31] These sensors provide sensitivity, temporal resolution and can be miniaturized for integration with model organ systems for analysis of metabolites in real-time, downstream, or later on.

In addition to enzymatic-based sensors, potentiometric sensors have significantly developed to detect a wide range of analytes such as calcium, hydrogen (pH), and even gluten.[20,24,32] Potentiometric sensors measure potential across a membrane without an applied current and often utilize ionophores for selectivity.[24] The membrane composition for making these sensors is essential for the most accurate and superior sensing for specific target analytes.[24] Development in the ionophores and membrane compositions of potentiometric sensors has made these useful in biomedical, industrial, and environmental applications.[24] Drawbacks to these sensors is frequent recalibration and dependence on temperature. However, integrating these with microfluidic systems to create a platform enables automated calibration and analysis to limit these challenges. These sensors provide label-free sensing with high selectivity, and can be miniaturized for point-of-care diagnostics, wearable devices and integration with model organ systems.[33]

The development of instrumentation has enabled researchers to discover and investigate the state and interactions of biological systems. One such development is the ability to monitor multiple analytes concurrently for a better understanding of the cellular processes and pathways of toxicity in healthy and diseased states. Researchers have developed biosensors that are capable of detecting multiple analytes and even using multiple techniques simultaneously to unravel the complex pathways in biological systems.[4,18,25,29,33] By combining and using multiple analytes, a variety of physiological systems, including cellular bioenergetics, oxidative stress, antioxidant capacity, cytotoxicity, and neurotransmission can be investigated for basic scientific discoveries as well as applications to medicinal, environmental, and industrial areas.[4] Furthermore, the

addition of multiple analytes to one sensor may allow for deconvolution of pathways and mechanisms, previously unavailable with single analyte detection methods. Multianalyte detection is pivotal for better understanding the cellular processes and pathways of toxicity in model organ systems.

Currently, model organ systems are used to study disease states, toxicants, and treatments as a means to understand the risks and consequences for human health. Typically, cell culture, animal studies, and organs-on-chips (OoCs) are the primary methods for studying health and disease. Cell cultures are generally amply available, cost effective and provide the ability for high-throughput screening.[34] These studies are important for basic scientific discoveries like macrophage responses to xenobiotics.[3] Animal models are the gold standard for studies and provide a full native system to react to external sources and a full system (multiple organs) to be analyzed.[35,36] Animal studies are useful for basic science as well as understanding the overall health and disease of an animal such as the effects of TCDD on a mouse model to better understand endometriosis.[37] Finally, OoCs aim to mimic structure and biological responses of organs, including the lung, liver, and blood-brain barrier.[26,35,38,39] These provide basic scientific discoveries as well as understanding human health and disease like understanding drug metabolism in a liver-on-chip system.[26] These model organ systems can be analyzed by multianalyte biosensors to monitor their health and disease before and after perturbations.

Recognizing the usefulness of biosensors as a means to analyze the status and interactions in model organ systems requires the integration of sensors that can provide temporal and detection resolution. This will provide accurate and precise measurements for responses to perturbations in model organ systems. Previously, sensors have been developed for use and integration with OoC systems to detect metabolites like glucose, lactate, and oxygen that are involved in cellular

respiration.[31,40,41] However, many of these systems are limited in their detection resolution and the need for customizable multianalyte detection. It is necessary to develop platforms that can reduce interference and detect a larger number of analytes.

This dissertation presents the development and application of multianalyte enzymatic and potentiometric sensors to monitor health and disease in model organ systems. Chapter three discusses the development of a multianalyte osmium polymer-based sensor and its application to studying glucose and lactate metabolism. Electrochemical sensors are used by millions of patients and health care providers every year, yet these measurements are hindered by compounds that also exhibit inherent redox activity. Acetaminophen (APAP) is one such interferent that falls into this extensive class. In this work, an osmium-based redox polymer was used for electrochemical detection in a sensor that was operated at a decreased voltage, allowing for decreased interference. These sensors demonstrated better selectivity for their respective analyte over APAP, possessed higher sensitivity over a broad range of analyte concentrations, and displayed similar operational stability over seven days compared to first-generation sensors.

To test this platform under biologically-relevant conditions, glucose metabolism was monitored in a model liver cell line, Alpha Mouse Liver 12 (AML12) after treatment with APAP and/or insulin. By observing glucose metabolism as a representative indicator for the health of the cell, toxicity studies were conducted. Furthermore, to answer biological questions about insulin, specifically its interaction with liver cells, glucose metabolism in a model liver system can be investigated to gain insight into these relationships.[42] We used the AML12 cell line to study the effects of treating the cells with APAP based on its clinical relevance and hepatotoxicity, known redox activities, and insulin-dependent pathways for glucose metabolism. Glucose metabolism was dysregulated in APAP and/or insulin-treated cells. This work represents a high-resolution

electrochemical biosensor for microphysiological monitoring of glucose and lactate in the presence of an interferent.

In chapter four, we investigated a platform for detection and quantification of up to eight analytes using enzymatic-based methods to understand more about the cellular processes and pathways of toxicity. By combining sensors for multiple analytes together into one electrode array with separate channels for real-time analysis of biological systems, we may electrochemically monitor cellular respiration, oxidation processes, neurotransmission, as well as perform toxicity screenings. This is helpful of understanding the complex biological response following perturbation. Calibrations were performed to cover biologically-relevant linear ranges while maintaining sensitivity. Measuring changes in multiple analytes will allow for a better understanding of the state and interactions of a system.

This platform was used to test glucose and lactate metabolism of macrophages from mice after treatment with 2,3,7,8-tetrachlorodibenzodioxin (TCDD), lipopolysaccharide (LPS), and β-glucan. TCDD, a model immune-disrupting toxicant, is often used in studies and has shown hyperinflammatory effects in the uterine and peritoneal cavity of mice.[37,43] Mice exposed to TCDD show a phenotype similar to that of women with endometriosis.[43] This can be further amplified by a secondary trigger such as an infection like LPS.[43,44] β-glucan has been shown to train immune cells to resist infection, causing increased glucose consumption and lactate production.[45] All of these treatments disrupted glucose and lactate metabolism, indicating dysregulated cellular respiration in macrophages. Understanding the relationships between TCDD, LPS, and β-glucan and how they affect metabolism is key to determining pathways of toxicity and monitoring health and disease.

Finally, chapter five presents two potentiometric sensors that are combined with two amperometric sensors to simultaneously detect and quantify ammonium, potassium, glucose, and lactate. By combining these four sensors, there is a more in-depth analysis and the complex pathways in biological systems can begin to unravel. These potentiometric sensors were investigated to determine the membrane composition that provides the most accurate sensitivity. Furthermore, the necessity of a reference electrode coating was determined. Lastly, the sensitivity over a broad range of analyte concentrations and operational stability of the potentiometric sensors was established. To test this automated platform under biologically-relevant conditions, glucose, lactate, ammonium, and potassium metabolism was monitored in a mouse model after treatment with TCDD *in utero* and/or LPS in adulthood. These treatments significantly dysregulated metabolism for all of the analytes, and shows possible pathways of toxicity for TCDD and LPS. This work represents a customizable platform utilizing a multiplexed, multianalyte amperometric and potentiometric biosensor for microphysiological monitoring of metabolites simultaneously to provide a snapshot of the state and interactions of a biological system.

The first appendix of this dissertation describes the optimization of a cholesterol oxidase sensor for use in model organ systems. Cholesterol is difficult to dissolve, so dissolving agents were investigated with DMSO and Triton X-100 in combination as the best. Next, the sensitivity was optimized through film modifications for cholesterol oxidase, indicating poly l-lysine as providing the most sensitive film. A calibration for the cholesterol sensor was completed, showing the sensitivity to cholesterol in biologically relevant concentrations. Finally, appendix B presents a project that utilized the osmium-based sensors to detect glucose and lactate in another biological system to determine the effects of a known hepatotoxin, rosiglitazone in healthy and diseased hepatocytes.

Chapter II

EXPERIMENTAL METHODS AND ANALYSIS

This chapter provides the general electrochemical methods used throughout the studies. It will cover the cleaning of screen-printed electrodes (SPEs), Ag/AgCl reference electrode deposition, enzymatic and ionophore deposition, amperometric and potentiometric electrochemical analysis, and data analysis. More detailed methods for specific studies are described in subsequent chapters.

Cleaning of Screen-Printed Electrode

All SPEs and associated electrodes must be cleaned prior to electrode modification. These electrodes are designed in house and purchased from Pine Research (3 working electrodes; Durham, NC) and Sullins Connector Solutions (8 working electrodes; San Marcos, CA). They are first cleaned in 1 M nitric acid, then 0.5 M sulfuric acid. The SPE is attached to an edge card connector and placed in a beaker with one of the solutions with the electrodes fully submerged. The working electrodes from a potentiostat [CHI 1440 or CHI 1030 (CH Instruments, Austin, TX)] are attached to the other side of the edge card connector from the SPE. A reference cable from the potentiostat is attached to an external Ag/AgCl reference with 3 M KCl solution. Then, the counter cable from the potentiostat is attached to a flame-polished (using a Bunsen burner) platinum mesh electrode. These two electrodes are also submerged in the acid solution carefully as to not touch. In the CHI software, the technique is set to *Amperometric i-t*, and the parameters are set (**Table 2.1**). The additional electrode options in the software were selected and set to the same parameters to clean the additional electrodes on the SPE as well. After cleaning in both the nitric and sulfuric

acid solutions, the electrodes are rinsed. To evaluate the state of the electrodes, the SPE is placed back into the sulfuric acid solution. Next, the CHI software technique is set to *Cyclic Voltammetry* and the parameters are set again (**Table 2.2**). If the electrode is clean, the resulting voltammogram should not have large triangular peaks at ~0.4 V or give noisy peaks. It should be a smooth graph with three distinct reduction peaks between -0.2 and 0.1 V. If this is not the case, repeat the cleaning process with nitric and sulfuric acid.

Parameter	Setting
Initial E (V)	3 (HNO_3) 6 (H_2SO_4)
Sample Interval (s)	1
Sampling Time (s)	300
Quiet Time (s)	0
Scales during Run	1
Sensitivity (A/V)	1e-003
E1 (and others) On	Selected

Table 2.1 Parameters for Cleaning Electrodes. SPEs are cleaned in 1 M HNO_3 then 0.5 M H_2SO_4. These are set for each of the electrodes being cleaned.

Parameter	Setting
Initial E (V)	-0.2
High E (V)	0.7
Low E (V)	-0.2
Initial Scan Polarity	Positive
Scan Rate (V/s)	0.5
Sweep Segments	5
Sample Interval (s)	0.001
Quiet Time (s)	2
Sensitivity (A/V)	1e-004
E1 (and others) On	Selected

Table 2.2. Parameters for Evaluating the SPE Cleanliness. SPEs are assessed in H_2SO_4 using cyclic voltammetry. These are set for each of the electrodes to be checked.

Ag/AgCl Reference Electrode Preparation

After the SPES are cleaned thoroughly, the reference electrodes on the SPEs are coated in silver and immersed in an iron (III) chloride solution to create the Ag/AgCl interface.[18] On the three-electrode SPE, the 0.08 mm^2 electrode is plated, while the circular electrode on the eight-electrode SPE is plated. To prepare a sensor with an internal reference of Ag/AgCl, a preconditioning step and plating method were performed in a stirring silver nitrate solution (0.3 M $AgNO_3$, 1 M NH_4OH) with an external Ag/AgCl (3 M KCl) reference electrode and a flame-polished platinum mesh counter electrode. The silver electrodeposition is performed using the sweep-step function in the CHI software. The reference and counter are connected as in the cleaning procedure, but only one working electrode is connected to the reference electrode on the SPE. A preconditioning step was first applied (0.3 to 0.95 V, 0.5 V s^{-1}), which was followed by a potential hold (0.95 V, 30 s). Then, the electrode was scanned (0.95 to -0.15 V, 0.5 V s^{-1}) with a subsequent plating potential hold (-0.15 V for 450 s). Following plating, the electrode array was removed from the silver nitrate solution and immediately rinsed in deionized water and immersed and agitated in $FeCl_3$ (50 mM, 1 minute) to form a silver chloride layer, generating the internal reference electrode. In addition, the general parameters are summarized below (**Table 2.3**). The electrode is rinsed again and stored in the dark to prevent oxidation of the silver deposition.

Parameter	Setting
Initial E (V)	0.3
Sweet S. I. (V)	0.001
Step S.I. (V)	0.002
Quiet Time (s)	2
Sensitivity (A/V)	1e-004
E1 On	Selected
Scan Mode	Simultaneous

Table 2.3. Parameters for Silver Plating on Reference Electrode. SPEs are plated using these general sweep-step settings.

Enzyme Films Deposition

After cleaning the SPE and creating the reference electrode, enzyme films may be deposited on the working electrode of the SPE for selectivity and sensitivity to an analyte of interest. First, a 31 mg mL^{-1} solution of BSA in phosphate buffer solution (50 mM, pH = 7.00) was made. Then, powdered enzyme was dissolved in the BSA solution to the desired concentration described in subsequent sections. These enzymatic solutions were used immediately or stored at -18 °C until needed. In order to deposit these onto the electrode, a crosslinker is necessary for absorption to the electrode surface. Glutaraldehyde (25% wt/v in water) was added to an enzymatic solution to a concentration of 1% (v/v). For the acetylcholine sensor, this was diluted to 2% (v/v). The resulting solution was vortexed for ~5 seconds before dropcast onto a working electrode. For the 3-electrode SPE, 1 µL is deposited to cover the entire surface, while only 0.5 µL is necessary for deposition on the 8-channel working electrodes. These electrodes are air dried (in the dark) for at least an hour before use.

Ionophore Membranes Deposition

In addition to enzymatic biosensors, ionophore membrane solutions may be deposited on working electrodes for selectivity and sensitivity. Components for the formulation were mixed together and added to 1 mL of tetrahydrofuran (THF) to dissolve the components properly and for ease in deposition. This solution was vortexed for ~5 seconds. Then, the membrane solution was either immediately dropcast on the working electrodes as 0.5-µL aliquot or stored at 2 °C. If it was used, the sensors were dried overnight and stored while covered at room temperature before use.

Electrochemical Analysis

After the sensors were dried, the SPE was inserted into the electrode housing (microclinical analyzer – µCA) and connected to a pump and valve system known as the microformulator. The

three-electrode SPE with the μCA (VIIBRE; Nashville, TN) and microformulator has been detailed previously and used for multiple biological applications.[6,31,46] This sensor was inserted into the μCA, topped with water to prevent bubbles, and closed using magnets to align and screws to compress the housing. However, the eight-channel SPE was topped with a polydimethylsiloxane (PDMS) fluidic and sandwiched between two polymethylmethacrylate pieces for the housing with four screws to compress it together. Before the housing was screwed together, the channels in the PDMS fluidic were carefully aligned to the electrodes and deionized water was added on top of the SPE to prevent the formation of bubbles.

Next, this housing with either of these SPEs was connected to a microformulator, a pump and valve system. This system allows for automated calibration and sample analysis through the development of a protocol on the AMPERE (Vanderbilt Institute for Integrative Biosystems Research and Education – VIIBRE; Nashville, TN) software specific to this system. The pump (VIIBRE; Nashville, TN) can flow between 2 μL min^{-1} and 1 mL min^{-1}. The valve (VIIBRE; Nashville, TN) was used in both a 5 and 24 port variation to create flexibility in the number of calibrants and samples being analyzed. It may be necessary to tare the valve in the software for proper function. There was tubing connected between the pump, valve, debubbler, and electrodes (housing). Sensors were calibrated and then samples were analyzed. A buffer solution was used between each solution (calibrant and sample) to establish a baseline in electrochemical measurements. To ensure proper analysis and remove previous solutions, the tubing between the calibrant or sample and the valve (the first instrumentation) was primed with the correct solution.

Electrochemical analysis was performed using the *Amperometric i-t* technique in the CHI software. The CHI 1030 provided electrochemical measurements for only amperometric sensors. However, the CHI 1440 potentiostat can measure amperometrically and potentiometrically. For

amperometric detection, the protocol was set up similar to **Table 2.1** with a few adjustments. For all sensors, except dopamine, the potential was set to 0.6 V (vs. Ag/AgCl). Dopamine uses a reduction reaction, so it is set to -0.2 V (vs. Ag/AgCl). The sample times and sensitivities were determined based on what the experiment dictated. The electrode potential was set for all electrodes used and selected ON. To detect potentiometrically, the 5^{th}, 6^{th}, 7^{th}, and 8^{th} electrodes are used from the potentiostat. The electrodes were selected ON and the Gain 10 was selected ON. The amperometric sensor may or may not be selected on depending on the experimental parameters.

Data Analysis

Because the data generated from these potentiostats can be substantial and CHI does not have data analysis software built in, the use of other software is necessary. Both Microsoft Excel and MATLAB were used to reduce the data size and create a more manageable set that eases the burden for data analysis of calibration curves and sample sets. The collected data must be converted to a text file in the CHI software, so it can be used in other software. This can then be saved as Excel spreadsheet and used in Microsoft Excel or MATLAB. MATLAB provided the averages and standard deviations of a specified amount of data points that allowed the user to easily find the steady state of a calibrant or sample. Microsoft Excel may also be used to determine the steady state by manual inspection.

Chapter III

A LOW-INTERFERENCE, HIGH-RESOLUTION MULTIANALYTE ELECTROCHEMICAL BIOSENSOR[1]

Electrochemistry is a sensitive, stable, and selective analytical tool in diagnosing and monitoring health and disease.[47–49] The most widely-used electrochemical sensors are first-generation enzymatic sensors, relying on enzymes immobilized on an electrode for analyte detection. These biosensors quantify the target analyte by means of an electroactive byproduct of the enzymatic reaction, hydrogen peroxide (H_2O_2).[24,50] For instance, glucose meters, commonly used to measure blood glucose in patients with diabetes, use first-generation sensor technology and account for the large majority of first-generation electrochemical sensors used commercially.[51] However, first-generation sensors are susceptible to electroactive interferents, compounds that lead to signal contamination and therefore inaccurate results.[52,53] In this work, a polymer was developed to act as a mediator for electron transfer, allowing for decreased interference compared to first-generation sensors. Using this polymer, we quantified glucose and lactate over a background of an inherently redox-active common interferent, acetaminophen APAP, by coupling an oxidase enzyme with this osmium polymer (Os-polymer) in a sensor platform.

Although first-generation biosensors are selective for the analyte of interest against a background of electrochemically inactive species, they are still prone to interference. At the electrode surface of first-generation biosensors, H_2O_2, acting as the electron transfer mediator from the enzyme to the electrode, is oxidized with an electrode bias of 0.6 V (vs. Ag/AgCl), producing

[1] This chapter contains portions from the published research article: 1. Melow, S. L.; Miller, D. R.; Gizzie, E. A.; Cliffel, D. E.

an amperometric signal.[50] However, at this potential [0.6 V (vs. Ag/AgCl)], other electroactive species such as APAP are also oxidized, causing signal interference.[52,53] Thus, biosensors that reduce or eliminate interference are required for accurate analysis of analytes of interest.

There are a number of ways to reduce or eliminate interference including screening polymers or electron transfer mediators (co-reactants).[53–55] Although screening polymers increase selectivity by preventing larger molecules from accessing the electrode surface, they still allow smaller molecules to access the electrode and contribute to signal contamination since they use a higher potential like first-generation sensors. Furthermore, though they increase selectivity, they have decreased sensitivity due to impeded analyte diffusion.[56] However, the use of metallic co-reactants including Au, Pd, Rh, and Ru, reduce peroxide at a lower potential and therefore decrease interference.[54,57–60] Still, the instability (Rh and Pd) and expense (Au and Ru) of these materials have hamstrung their widespread implementation. Therefore, there is a need for stable and less expensive co-reactants that accurately detect analytes in all samples.

To address this need, a group of polymers that contains an osmium complex, acting as the co-reactant, were developed and incorporated into sensors. Osmium redox polymers were first developed by Heller et al. in the late 1980s to act as a mediator for electron transfer in glucose biosensors.[61] These osmium polymers are redox polymers that can be reversibly oxidized and reduced. When they are combined with an oxidase enzyme, these polymers can stably and selectively detect their respective analyte at a lower potential, thereby decreasing interference (**Figure 3.1**). Previous work has shown current densities do not vary with the Os content of the polymers, so the overall redox efficiency of these sensors similarly would not change with the Os content.[62] Since their inception, their use has extended to other analytes and biological systems[63–65] such as detecting acetylcholine release from rat frontal cortex samples.[66]

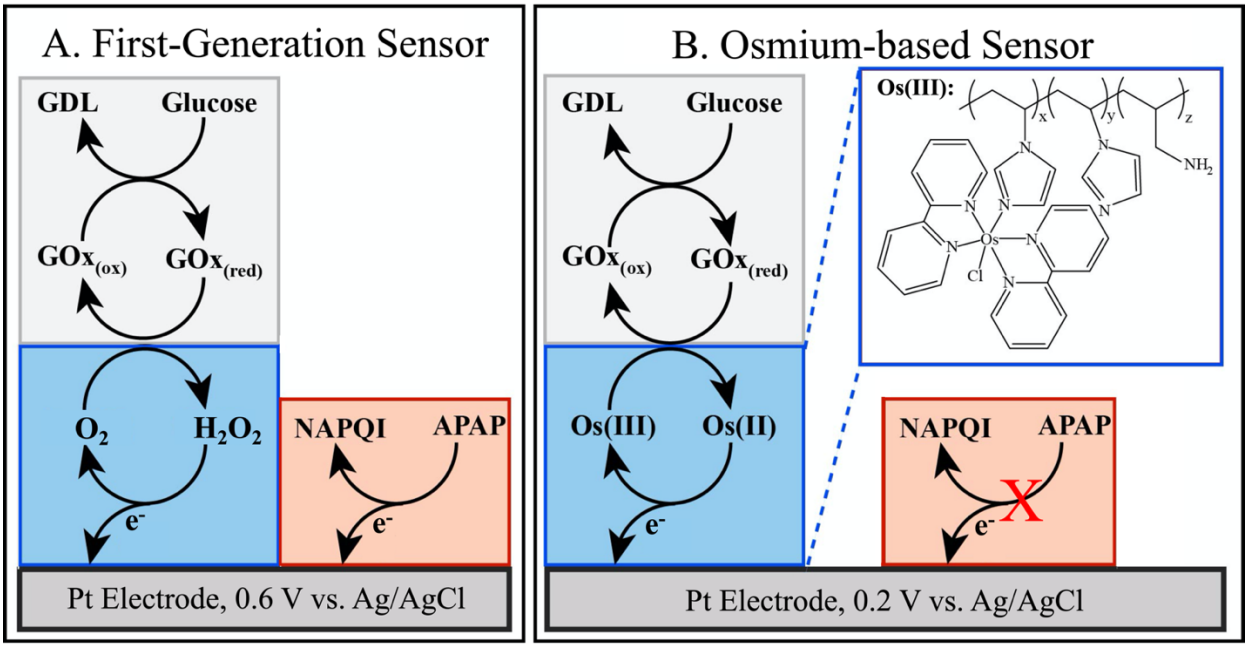

Figure 3.1. Redox Process for First-Generation and Os-Based Sensors. A) Representation of the redox process/electron flow mechanism for the first-generation GOx sensor. There is a high potential of 0.6 V (vs. Ag/AgCl) required to oxidize the H_2O_2 that also oxidizes APAP, leading to signal interference and inaccurate results. B) Representation of the redox process/electron flow mechanism for the Os-based GOx sensor. The electrode bias of 0.2 V (vs. Ag/AgCl) required for the Os-polymer and GOx system mitigates the interference from the oxidation of APAP. Inset: Representation of the Os-polymer structure.

The microclinical analyzer (μCA) provides automation, increased ease of use, real-time monitoring, and multiple analyte detection. This platform is composed of a microfluidic housing for a screen-printed electrode that is used for detection of metabolites as well as an automated pump and valve system. There is increased ease of use due to increased sample throughput and decreased user intervention from automated sensor calibration and sample input. Furthermore, the sensor and small volume-microfluidic housing allow for real-time monitoring with the ability to detect small metabolic changes.[6] Lastly, monitoring multiple analytes concurrently provides a better understanding of the cellular processes and pathways of toxicity in healthy and diseased states. This platform provides a versatile system that can be extended to many analytes and biological systems.

Because the liver has a direct role in energy and metabolism, producing, storing, and releasing glucose,[67] hepatic models are important for the comprehensive understanding of pathways and functions in the body. Alpha Mouse Liver 12 (AML12) is a cell line that models the liver and can be used to study lipid metabolism, liver injury and hepatotoxicity.[68] These cells are amply available, cost effective, and show decreased variation in quality since the cell line is both immortalized and comes from a healthy host. Furthermore, these cells most closely resemble basal and insulin-stimulated glucose metabolism in primary mouse hepatocyte cultures.[69] To answer biological questions about insulin and APAP and specifically their interactions with liver cells, glucose metabolism in a model liver system was investigated to gain insight into these relationships.

In this work, we present an Os-polymer that couples with glucose and lactate oxidases to comprise a multianalyte sensor platform for quantification that produces minimal signal interference with APAP present. Together, this system represents a new method to rapidly analyze

biological systems by electrochemically monitoring cellular viability, performing toxicity screenings, and elucidating metabolic pathways. Selectivity assays demonstrated that this platform is insensitive to APAP, an electroactive interferent, and calibrations were performed in this work to cover biologically relevant linear ranges while maintaining sensitivity. Longevity studies of the sensor performance indicated that this novel platform was ideal for interfacing with continuously operational systems such as liver-on-chips. We used the AML12 cell line to study the effects of treating the cells with APAP based on its clinical relevance and hepatotoxicity, known redox activities, and insulin-dependent pathways for glucose metabolism. The platform was applied to model liver cells to detect glucose metabolism changes and monitor the effects of insulin and APAP.

Experimental

Material Procurement

N-vinylimidazole, allylamine, azobisisobutyronitrile (AIBN), 2,2'-bipyridine, ammonium hexachoroosmate (IV), poly(ethylene glycol) diglcidyl ether (PEGDGE), potassium chloride, bovine serum albumin (BSA), GOx from *Aspergillus niger* (152.54 U mg^{-1}), LOx from *Aerococcus viridians* (11.29 U mg^{-1}), and glutaraldehyde (25% by wt. aqueous solution) were purchased from Sigma Aldrich (St. Louis, MO). Sodium phosphate monobasic and sodium phosphate dibasic (buffer) were procured from Fisher Scientific (Hampton, NH). β-D-Glucose was purchased from Calbiochem (San Diego, CA), and sodium L-lactate was purchased from Alfa Aesar (Haverhill, MA) and for use in calibrations. Dulbecco's Modified Eagle Medium supplemented with F12 (DMEM/F12), glucose-free DMEM, F12, fetal bovine serum (FBS) and a primary hepatocyte maintenance supplement kit (dexamethasone, penicillin-streptomycin (p/s), insulin, transferrin, selenium complex, BSA, linoleic acid, GlutaMAX, and HEPES) were purchased from Gibco (Gaithersburg, MD). All reagents were used as received and without additional purification.

The microclinical analyzer (μCA) housing was designed by The Vanderbilt Institute for Integrative Biosystems Research and Education (VIIBRE, Nashville, TN) and made of polymethylmethacrylate by the Vanderbilt Microfabrication Core (VMFC, Nashville, TN) that is operated by VIIBRE.[29] More detailed information for the materials of this device and the screen-printed electrodes can be found elsewhere.[6] To automate the system, rotary planar peristaltic micropumps (RPPM, US patents 9,874,285 and 9,725,687 and applications claiming priority from US patent application 13/877,925), rotary planar peristaltic five-port valves (RPPV, US patent 9,618,129), microcontrollers, and computer software were implemented in the system

(VIIBRE/VMFC). CHI 1440 and 1030 potentiostats were purchased from CH Instruments (Austin, TX) and used in the electrochemical measurements.

Synthesis and Characterization of the Os-based Metallopolymer

To produce the final Os-based redox polymer, $Os(bpy)_2Cl$-PVI, a polymer and an Os complex must be synthesized initially. First, the polymer backbone that connects the Os complex to the electrode, poly(N-vinylimidazole-allylamine) (PVI) was polymerized and purified. To randomly copolymerize with the N-vinylimidazole monomer and provide additional primary amine crosslinking sites, allylamine was mixed with the monomer in a 1:1 ratio (equimolar) in absolute ethanol (10-15 mL).[70] This mixture was then added to a septum-sealed round bottom flask and nitrogen purged (~15 minutes). Then, the initiator, AIBN (60:1 molar ratio of monomer to initiator), was dissolved in absolute ethanol (2-3 mL) and added through the septum to induce free radical polymerization in the reaction mixture.[71] After initiation, the reaction mixture was heated in an oil bath (85 °C, 2 hours) to complete polymerization, resulting in a solid. To remove the unwanted contaminants, ethanol (5-10 mL) was added to this solid, stirred overnight for full dissolution, and added dropwise to a beaker of rapidly stirring diethyl ether (40 mL), precipitating and purifying the PVI polymer. This purified PVI was collected on a coarse vacuum frit (Pyrex, Corning, NY), washed with cold diethyl ether (5-mL aliquots), and dried under vacuum until the solvent was fully removed (~30 minutes). The PVI was then further purified via dialysis against DI water using tubing with a 10 kDa mass limit. This PVI was used as the backbone for the Os complexes in all future experiments and was set aside until the Os complex was synthesized.

Next, the Os portion that forms the redox component of the final Os redox polymer was synthesized and purified. This synthesis was adapted from a previous method with slight changes made for this polymer.[72] Briefly, this Os redox compound, osmium[bis(2,2'-bipyridine)dichloride]

($Os(bpy)_2Cl_2$), was synthesized by refluxing (45 minutes) ammonium hexachloroosmate with two-molar equivalents of 2,2'-bipyridine in ethylene glycol (~50 mL) in a 100-mL round bottom flask under N_2 and cooled (2 hours). The reaction mixture was then added dropwise to the rapidly stirring aqueous solution of sodium dithionite (~0.1 g mL^{-1} in DI water, 25 mL) to reduce all Os complexes to the Os(II) state. The reaction mixture was then chilled on ice and filtered using a fine sintered glass frit (4-5.5 μm) (Pyrex, Corning, NY). Once filtered, the resulting crystals were washed with three aliquots of cold water (5 mL) and dried on the frit under vacuum (>1 hour), and then in an oven (65 °C, overnight). Oxygen exclusion may result in higher yield.

To form the final Os polymer, $Os(bpy)_2Cl$-PVI, the $Os(bpy)_2Cl_2$ and the PVI components were reacted and then ^{1}H-NMR and cyclic voltammetry (CV) were used to characterize the product. First, $Os(bpy)_2Cl_2$ and PVI were dissolved separately in absolute ethanol (10-15 mL), vortexed, and gently heated. Then, these solutions were combined together in a 100-mL round bottom flask, so the $Os(bpy)_2Cl_2$ was loaded onto the PVI backbone under reflux (1:10 molar ratio Os to imidazole) while stirring in an oil bath (48 hours at 85 °C). The reflux condenser was capped to limit ethanol evaporation during reflux. Then, the reaction mixture was cooled, and ethanol was slowly evaporated under gentle heating and N_2-stream until 6-10 mL were left. The reaction mixture was slowly added dropwise to a stirring solution of diethyl ether (~30 mL) on an ice bath. This Os polymer-ether mixture was then chilled on dry ice, and the precipitate was filtered on a fine sintered glass funnel. This precipitate was then washed with excess volumes (>30 mL) of cold ether to remove unbound $Os(bpy)_2Cl_2$ and dried under vacuum ($<10^{-4}$ Torr, overnight). The product, $Os(bpy)_2Cl$-PVI, was characterized by ^{1}H-NMR (**Figure 3.2**) and CV (**Figure 3.3)** to determine the approximate metal-loading percentage and redox potential, respectively. This product was stored in the dark and was used for all experiments (up to 3 years).

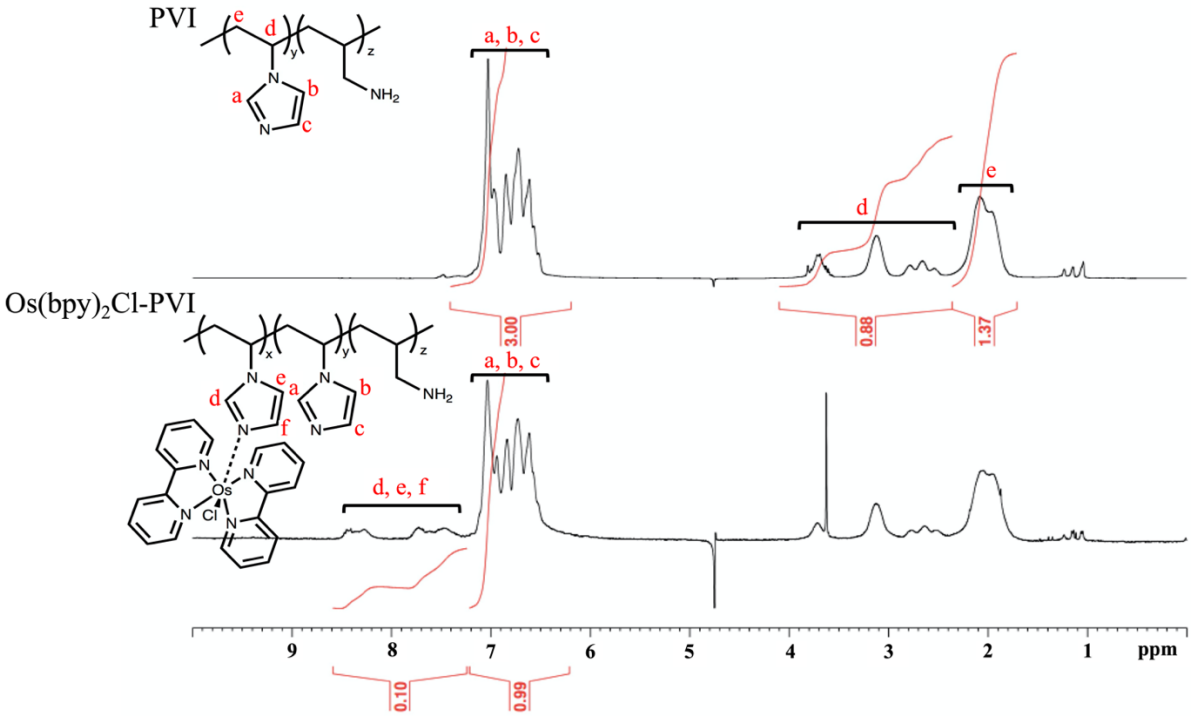

Figure 3.2 ^{1}H-NMR of Poly(N-vinylimidazole-allylamine) and Os(bpy)$_2$Cl-PVI. The ^{1}H-NMR spectra of PVI and Os-based PVI (20 mg mL^{-1} in D_2O) were collected from at least 128 scans using a 400 MHz Bruker spectrometer with water suppression. There is a multiplet at δ 6.5-7 ppm that corresponds to the protons a, b, and c on the structure for both polymers. The PVI spectrum (top) shows a single proton (d) that produced three groups of peaks. At δ 2 ppm, there are two protons (e) that produced a doublet. The Os-polymer spectrum (bottom) had imidazole protons (d, e, and f) that produced signals at δ 7.5-8.5 ppm, resulting from the Os-complex substitution on the polymer backbone.

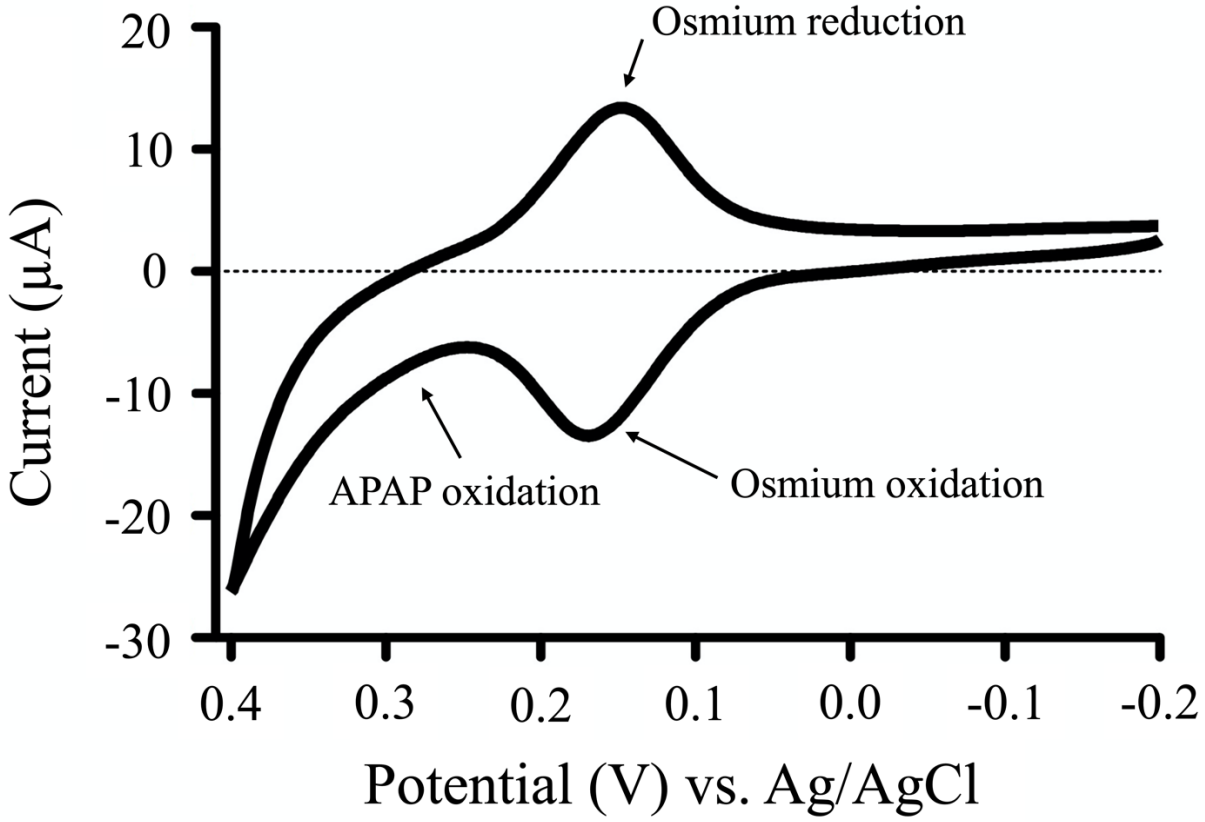

Figure 3.3 Cyclic Voltammogram of $Os(bpy)_2Cl$-PVI. The cyclic voltammogram was performed using an SPE modified with Os-polymer in a 26-μL flow chamber under a flow rate of 100 μL min^{-1}, showing the oxidation of the osmium at 0.177 V and a reduction of the osmium at 0.135 V (1 mM phosphate buffer, 120 mM KCl, 10 mM APAP, pH = 7.00). The current vs. potential is shown in the CV (-0.2 to 0.4 V, 0.5 V s^{-1}) of the Os-polymer. Oxidation of APAP began around 0.250 V (vs. Ag/AgCl). An internal reference, Ag/AgCl, and counter electrode, Pt, were used.

Electrochemical Housing Configuration

Comprised of a screen-printed electrode (SPE) in a flow chamber, the μCA was used for calibrations and sample analysis. SPEs served as the underlying substrate for this platform and were modified for sensitivity and selectivity.[29] The SPE featured three parallel 1.8 mm^2 circular working electrodes, a 19 mm^2 auxiliary electrode, and a 0.08 mm^2 reference electrode, all printed in platinum on a ceramic base. Each working electrode was modified for a specific analyte of interest. Experiments were performed using the modified SPEs in a polymethylmethacrylate flow chamber that was aligned with magnets and compressed with screws. An O-ring sandwiched tightly between the SPE face and the polymethylmethacrylate created the 26-μL flow chamber, ultimately forming the housing for the SPE, known as the μCA. This apparatus is depicted in detail elsewhere.[6,29]

Electrode Modification

To make these biosensors, reference and working electrodes were generated through electrodeposition and enzyme solution modifications. Initially to make the internal reference electrode, silver was electrodeposited on the electrode followed by immersion in an $FeCl_3$ solution, creating the Ag/AgCl interface with slight modifications from previously developed methods.[29,73] Then, working electrodes had either an Os-polymer-enzyme mixture or a first-generation enzyme solution for comparison deposited on the electrode for detection of glucose or lactate.

To prepare a sensor with an internal reference of Ag/AgCl, a preconditioning step and plating method were performed in a stirring silver nitrate solution (0.3 M $AgNO_3$, 1 M NH_4OH) with an external Ag/AgCl (3 M KCl) reference electrode and a platinum mesh counter electrode. A preconditioning step was first applied (0.3 to 0.95 V, 0.5 V s^{-1}), which was followed by a potential hold (0.95 V, 30 s). Then, the electrode was scanned (0.95 to -0.15 V, 0.5 V s^{-1}) with a

subsequent plating potential hold (-0.15 V for 450 s). Following plating, the electrode array was removed from the silver nitrate solution and immediately immersed and agitated in $FeCl_3$ (50 mM, 1 minute) to form a silver chloride layer, generating the internal reference electrode.

Next, an Os-polymer-enzyme mixture was deposited on a working electrode and dried overnight for detection of glucose or lactate. Glucose-specific electrodes were modified using a solution of GOx (0.25 mg mL^{-1} in 50 mM buffer), $Os(bpy)_2Cl$-PVI (50 mg mL^{-1} in 50 mM buffer), and PEGDGE (5% v/v). For instance, 5 µL of a more concentrated GOx solution (0.5 mg mL^{-1} in 50 mM buffer) is added to 4.5 µL of the $Os(bpy)_2Cl$-PVI solution (111 mg mL^{-1} in 50 mM buffer) and 0.5 µL of neat PEGDGE. Lactate-specific electrodes were prepared similarly with PEGDGE (5% v/v), except with LOx (2.5 mg mL^{-1} in 50 mM buffer) and $Os(bpy)_2Cl$-PVI (22.5 mg mL^{-1} in 50 mM buffer). Similarly, for a LOx Os-polymer sensor, 5 µL of a LOx solution (5 mg mL^{-1} in 50 mM buffer) is added to 4.5 µL of the $Os(bpy)_2Cl$-PVI solution (50 mg mL^{-1} in 50 mM buffer) and 0.5 µL of neat PEGDGE. These solutions were vortexed (5 seconds) in small tubes and then rested to ensure sufficient crosslinking (1 hour, room temperature). These Os-polymer-enzyme solutions were dropcast by pipetting 0.5-µL aliquots onto the working electrodes to create enzyme films. Films were dried at room temperature and then moved to the refrigerator for overnight crosslinking. After the initial use, sensors were then stored (2 °C) in buffered saline solution (2 mM buffer, 120 mM KCl, pH 7.00).

Simultaneously, first-generation enzyme-BSA crosslinked films were prepared similarly for comparative purposes. The sensors were prepared with the same enzyme concentrations used for Os-polymer sensors. However, BSA (31 mg mL^{-1}) in buffer (50 mM) replaced the Os-polymer, and glutaraldehyde (0.25% w/v) replaced the PEGDGE crosslinker in the electrode modification solutions. These solutions were also vortexed (5 seconds) but were immediately deposited, unlike

the Os-based sensors. Similar to the procedure for the Os-polymer-enzyme solutions, the enzyme-BSA-glutaraldehyde solutions were dropcast as 0.5-μL aliquots onto the working electrodes to create enzyme films. These sensors were dried at room temperature and stored in the same manner as the previously mentioned Os-polymer sensors.

Sensor Calibrations

Calibrations were completed from glucose, lactate, and APAP standards using a system comprised of automated pumps and valves, the μCA, and a potentiostat. Standards for all three of the chemicals were prepared in buffered saline solution. Each calibrant solution contained increasing quantities of glucose and lactate such that simultaneous calibrations could be performed for the analytes. Comprised of 18 calibrants, the analyte ranges used in this study were 0-23 mM for glucose (**Figure 3.4**) and 0-2.5 mM for lactate, which allowed for the linear range of each analyte to be determined. Separately, APAP was calibrated in the system with five calibrants increasing from 0 to 10 mM APAP for use in later selectivity studies. To establish a baseline for all of the calibrations, the same background buffered saline solution was flowed between every calibrant. A pump and valve system (flow rate of 100 μL min^{-1}) was used for automation, increased sample/calibrant throughput, and ease of use.[6] The μCA described above was operated in conjunction with the potentiostats to measure the calibrant signals. CHI 1440 and 1030 multichannel potentiostats were used to record the amperometric signals (glucose, lactate, and APAP, sampling frequency of 1 sec^{-1}). The potential for analyte quantification is held at 0.2 V (vs. internal Ag/AgCl) for the Os-based sensors since it is a slightly more oxidative potential relative to the redox potential of the coordination complex – $Os(bpy)_2Cl$-PVI ($Os^{3+/2+}$) or at 0.6 V (vs. internal Ag/AgCl) for the first-generation sensors.

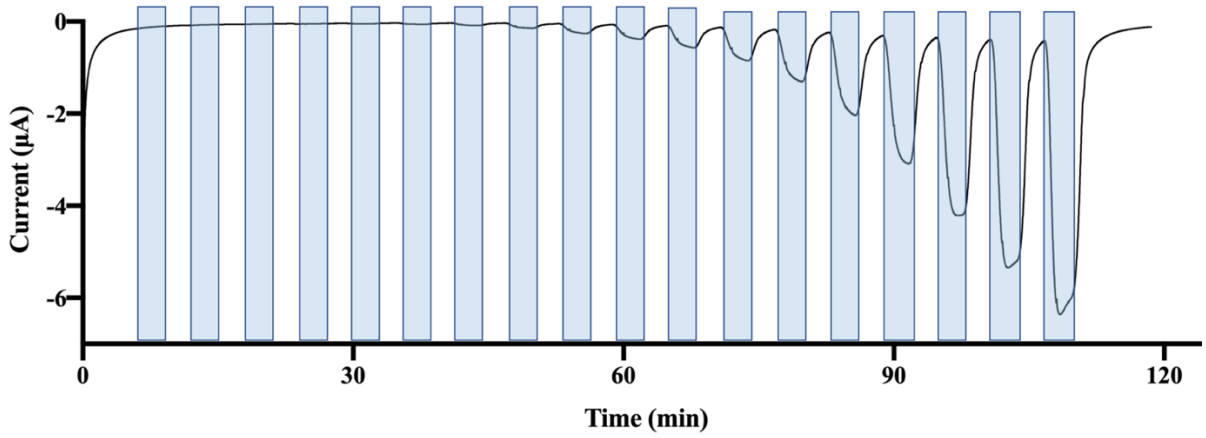

Figure 3.4. Continuous Measurement of Os-based GOx Sensor. Graphical representation of the current (µA) vs. time (min) using an Os-based GOx sensor for glucose detection. One example for a continuous measurement using this sensor for glucose with 18 calibrants ranging from 0 to 23 mM where the calibrants are highlighted in blue. There is buffered saline solution in between calibrants to obtain a steady state in current before measuring the next calibrant. Experiment was performed in buffered saline solution (ambient conditions) at 0.2 V.

Using linear and non-linear regression of the current versus concentration, limit of quantitation, the maximum limit of linearity, sensitivity of the electrode, maximum rate of reaction, and concentration at 50% saturation of the enzyme were determined. By adding the signal of the blank (buffered saline solution) to ten times the error of the blank and dividing by the sensitivity, the limit of quantitation was determined. To set the upper limit of linearity, the slope between calibration points was used to determine the approximate limit point. Subsequently, the next calibration point was added. If the slope changed by 5% or more from the previous slope without that point then the limit remained the same and the previous datapoint is the maximum limit of linearity.[6] Using the linear range of the data set (limit of quantitation to maximum limit of linearity), a regression of this data set determined the sensitivity of the electrode based on the slope of the line. A non-linear regression was performed on both of the Os-based sensors (glucose and lactate) to determine the maximum rate of reaction for the enzyme, V_{max}, and the concentration at 50% saturation of the enzyme, K_m.

Operational Longevity

Calibrations (7 calibrants within linear range) were completed daily for Os-polymer GOx and LOx sensors to ensure operational longevity for continuously operational systems. Standards for both of the analytes of interest contained increasing quantities of glucose and lactate such that simultaneous calibrations could be performed in buffered saline solution. This same buffered saline solution was also used as the baseline for all of the calibrations and flowed between every calibrant. Similar parameters were used for the sensor calibrations previously stated above. In short, the same system comprised of automated pumps (flow rate of 100 μL min^{-1}) and valves, the μCA (potential held at 0.2 V vs internal Ag/AgCl), and a potentiostats (CHI 1440/1030) were used in these experiments. However, after each calibration, the sensor was removed from the μCA and

stored (2 °C) in buffered saline solution overnight. Then on the next day, another calibration was completed until calibrations for seven days was completed.

Selectivity Assay

A selectivity assay was performed to compare the signal contribution from interference (APAP) and analyte (glucose or lactate) in first-generation and Os-polymer sensors based on selectivity coefficients. The contribution of interference in an amperometric sensor can be represented by a selectivity coefficient, $\boldsymbol{K}_{\boldsymbol{a,i}}^{\boldsymbol{amp}}$, where *a* is the analyte for a specific sensor and *i* is the interferent.[74] The amperometric selectivity coefficient is the quotient of the signal (current) produced from an interferent relative to the interferent concentration, and the current from the analyte relative to the analyte concentration. This relationship is summarized below in Equation 1.

$$\boldsymbol{K}_{\boldsymbol{a,i}}^{\boldsymbol{amp}} = \frac{\frac{\boldsymbol{i_i}}{\boldsymbol{C_i}}}{\frac{\boldsymbol{i_a}}{\boldsymbol{C_a}}} \qquad (1)$$

The signal produced at a certain concentration of the interferent, C_i, is defined as i_i. Similarly, i_a is the current detected for the specific analyte at a defined concentration, C_a. This calculation is used in a comparative study of the Os-polymer sensors and first generation sensors with respect to the analytes and model interferent. By performing a calibration with the Os-based sensors using increasing concentrations of the interferent or analyte independently, the signal contributions of interferent and analyte were separately determined. Then, $\boldsymbol{K}_{\boldsymbol{a,i}}^{\boldsymbol{amp}}$ values for the Os-polymer and first-generation sensors were calculated. The amperometric selectivity coefficients are presented as $\log(\boldsymbol{K}_{\boldsymbol{a,i}}^{\boldsymbol{amp}})$ values for ease of comparison. Sensors in which the interferent signal dominates over analyte have selectivity values that are positive (APAP-selective), whereas favorable (analyte-selective) coefficients are negative. These values are later used to demonstrate the selectivities of the sensors.

Cell Culture

AML12 cells (ATCC, Manassas, VA) were grown from cryopreserve, incubated, and plated onto a 12-well plate for treatment. The cells were first thawed from a liquid nitrogen cryopreserve and added to warmed media (DMEM/F12 with 10% FBS, 1% p/s, and a primary hepatocyte maintenance supplement kit). Then, the cell suspension was spun down (125 x g, 7 minutes). After discarding the supernatant, 1 mL of media was added to the cell pellet, and the cells were counted. Cells were subsequently added to ~10 mL of media in a T75 flask so that the flask contained ~250,000 cells (50,000 cells mL^{-1}), and it was then incubated (37°C, 5% CO_2). After the cells reached 90% confluency, they were trypsinized (0.25% w/v trypsin-EDTA), spun down (125 x g, 7 minutes), resuspended in media, and plated onto a 12-well plate (50,000 cells mL^{-1}). The cells on the well plate were grown to 90% confluency before treatment.

APAP and Insulin Treatment

To determine the effects of APAP and/or insulin on cellular metabolism, cells were subjected to one of four treatment protocols and then analyzed using the Os-based sensor. One day before the APAP treatment, the AML12 cell media was switched to a minimal media (DMEM/F12, 50% v/v, 5 mM glucose, without both serum and the primary hepatocyte maintenance supplement kit). For treatment, cell media was changed to one of four conditions: minimal media with protocol 1) no additives (media change); protocol 2) APAP only (1.4 mM); protocol 3) insulin only (10 μg mL^{-1}); or protocol 4) APAP and insulin. The treatment media was removed after 2 hours in experiments without insulin and after 24 hours in those containing insulin for analysis by a GOx Os-based sensor. Basal and treatment unconditioned media inputs were also analyzed by both types of sensors for comparison.

Results.

Synthesis and Characterization of the Os- flow rate of 100 μL min^{-1})

Prior to analysis, the Os-polymer was characterized by ^{1}H-NMR and CV. Based on the ratio of proton integration values in the ^{1}H-NMR spectra, the polymer had a metal-loading percentage of 9% (**Figure 3.2**). The redox potential of the Os-based polymer was identified as +156 mV (vs. Ag/AgCl) by CV (**Figure 3.3**). These methods confirmed the structure of the Os-polymer and that it oxidized at a lower potential than APAP as anticipated.[71]

The unloaded polymer, PVI, (**Figure 3.2 PVI**) was analyzed by ^{1}H-NMR. Peak integrations were normalized to three protons for the multiplet of peaks in the downfield region (δ 6.5-7 ppm) corresponding to the aromatic protons of the imidazole sidechain (PVI – a, b, and c). Due to the mixed tacticity of this polymer, the proton signal attributed to the single proton (PVI – d) is observed as three different groups of peaks (δ 2.4-3.6 ppm). Finally, the two protons found on the unsubstituted carbon in the polymer backbone (PVI – e) produced a doublet (δ 2 ppm).

After covalently attaching the Os-coordination compound to the polymer backbone, ^{1}H-NMR was used to calculate the amount of Os loading percentage on the PVI. Due to the sensitivity of the imidazole protons in their chemical environment, a large downfield shift was observed when the Os-complex substituted onto the imidazole side chain the (**Figure 3.2 Os(bpy)$_2$Cl-PVI**). Imidazole protons (Os(bpy)$_2$Cl-PVI – d, e, and f) produced signals further downfield than the unsubstituted polymer (δ 7.5-8.5 ppm). By comparing the integration of protons on the unmodified imidazole (PVI – a, b, and c) to the total integration of protons for both the downfield, Os-bound imidazole (Os(bpy)$_2$Cl-PVI – d, e, and f) and the unmodified (PVI – a, b, and c), an approximation for the metal-loading percentage was calculated. This relationship is summarized below in Equation 2.

$$(2)\ metal - loading\ percentage = \frac{\text{unmodified protons}}{\text{unmodified protons + bound protons}}\ X\ 100\%$$

For the Os-polymer used in these studies, there was an osmium metal-loading of approximately 9%.

Based on the cyclic voltammogram, a redox potential of 0.156 V (vs. Ag/AgCl) was determined. The electrochemical reversibility of this redox couple was evident in the ΔE_p of 21 mV. To identify the onset potential of bulk APAP relative to the $Os^{2+/3+}$ redox couple, APAP was included in this voltammogram. The onset of APAP oxidation occurred around 0.250 V (vs. Ag/AgCl). To oxidize the Os couple to the 3+ state, a potential that was slightly more positive than the peak in the oxidation portion of the voltammogram was selected. In addition, to avoid APAP interference, this potential must be less than 0.250 V (vs. Ag/AgCl), thus 0.2 V (vs. Ag/AgCl) was ideal for this sensor operation and was used in all studies and experiments.

Selectivity Assay

To compare differences between the Os-based sensors presented here and first-generation sensors, selectivities between the analyte and interferent were investigated. Direct comparison of these sensor types indicated the increased selectivity of Os-polymer sensors to the analyte of interest over a model interferent, APAP. The first-generation sensors showed approximately a 0.3-fold selectivity of glucose and 1.79-fold selectivity of lactate over APAP in the same saline buffered solution (**Figure 3.5, left**). In comparison, the Os-based sensors were approximately 40-fold more selective for glucose and 200-fold more selective for lactate over APAP in a saline buffered solution (**Figure 3.5, right**). Therefore, the Os-based sensors have about 2 orders of magnitude (100x) more selectivity for both analytes over first generation sensors.

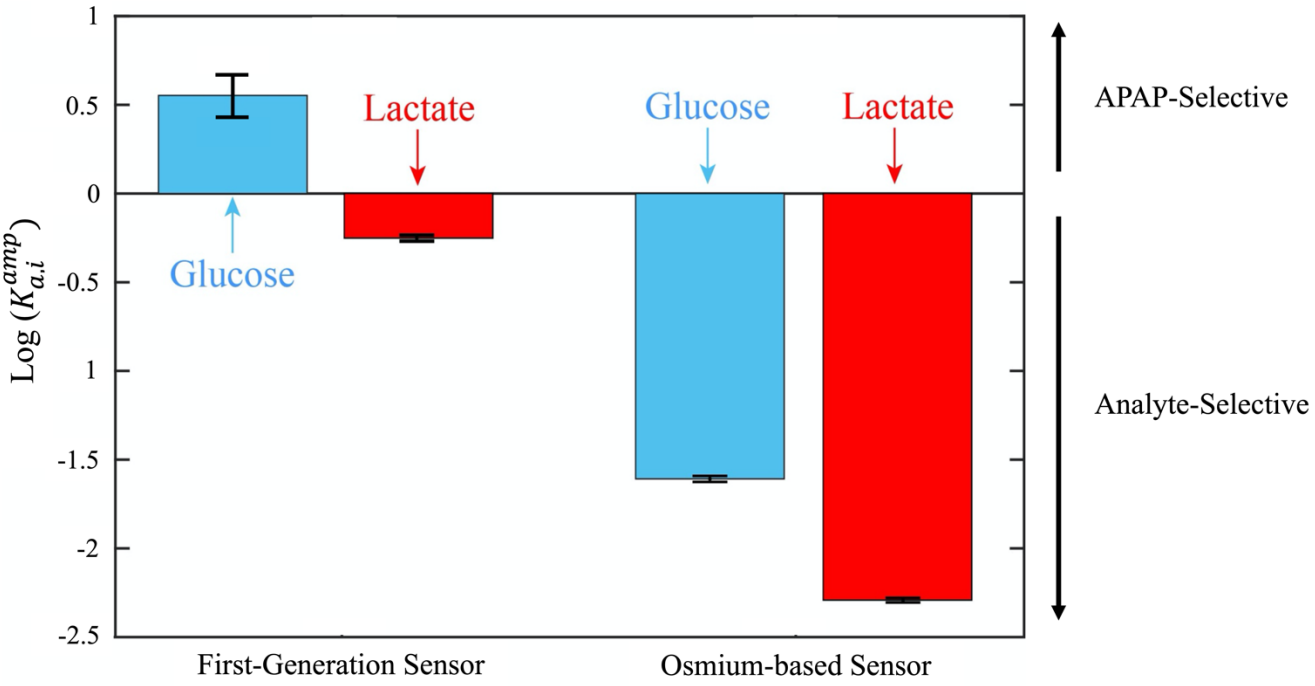

Figure 3.5. Selectivity Assay Graph Comparing Os-Polymer and First-Generation Sensors. Logarithmic representation of the selectivity coefficients for APAP with glucose (blue) and lactate (red) sensors. The first-generation sensors (left)—oxidase enzyme with BSA—had log ($K_{a,i}^{amp}$) values of 0.5 ± 0.1 for glucose and -0.25 ± 0.01 for lactate, indicating a preference of APAP over glucose and a slight preference for lactate over APAP, respectively. After coupling one of the oxidase enzymes with the Os-polymer, the Os-based sensors (right) had selectivity coefficients for glucose at -1.61 ± 0.03 and lactate at -2.29 ± 0.02, indicating a strong preference for the analyte in both cases. Potentials were held at 0.6 V (vs. Ag/AgCl) for the first-generation sensors and 0.2 V (vs. Ag/AgCl) for the Os-polymer sensors. Experiments were performed in buffered saline solution at ambient conditions. Data represented as the average with standard deviation, n = 3.

The amperometric selectivity coefficients are presented as $\log(\boldsymbol{K}_{a,i}^{amp})$ values. A positive selectivity value indicated the sensor was APAP-selective, and a negative selectivity value was analyte-selective. The first-generation sensors had a positive value for the glucose selectivity coefficient and a slightly negative coefficient for lactate. Therefore, the first-generation sensor was more selective for APAP with the glucose sensor, while the lactate sensor was only slightly more selective for the analyte. However, the Os-polymer sensors were significantly more negative for both analytes compared to the first-generation ($p < 0.01$), meaning they were more selective for the analytes. Direct comparison of these sensor types revealed the increased selectivity of Os-polymer sensors to the analyte of interest over a model interferent, APAP.

Sensor Calibrations

Calibrations were performed for glucose and lactate to compare the sensitivities of both types of sensors. The sensitivities of the first-generation and Os-based GOx sensors were 0.166 ± 0.013 μA mM^{-1} and 0.350 ± 0.006 μA mM^{-1}, respectively (**Figure 3.6, left**). A first-generation LOx sensor showed a sensitivity of 1.71 ± 0.03 μA mM^{-1}, but the Os-polymer LOx sensor had a higher sensitivity at 2.00 ± 0.05 μA mM^{-1} (**Figure 3.6, right**). Both the Os-based GOx and LOx sensors offered increased sensitivity compared to the first-generation sensors.

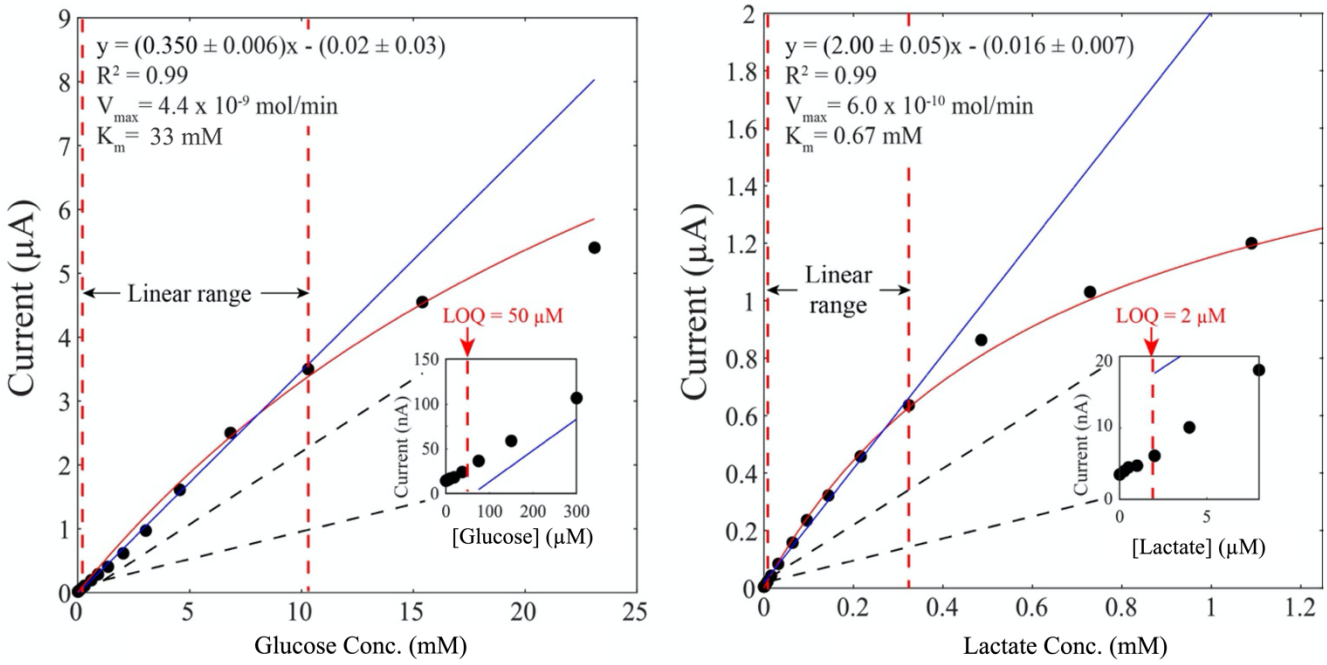

Figure 3.6. Representative Calibration Curves of Os-based Sensors. It shows anodic current vs. analyte concentration with the limits of linearity, limits of quantitation, V_{max}, and K_m for Os-based GOx (left) and LOx (right) sensors. The linear range, indicated by the two dotted red lines, were 50 µM to 10 mM and 2 to 324 µM for glucose and lactate, respectively. The slopes are represented by solid blue lines [$y = (0.350 \pm 0.006)x - (0.02 \pm 0.03)$, $R^2 = 0.99$] for the Os-polymer GOx sensor and [$y = (2.00 \pm 0.05)x - (0.016 \pm 0.007)$, $R^2 = 0.99$] for the Os-based LOx sensor. Using non-linear regression, shown in solid red, V_{max} and K_m were calculated for both analytes. For the Os-based GOx sensor, V_{max} was 4.4×10^{-9} mol min^{-1} and K_m was 33 mM. The Os-polymer LOx had a V_{max} of 6.0×10^{-10} mol min^{-1} and K_m of 0.67 mM. Inset: zoom-in of the lower concentrations of each analyte showing the lower limit of linearity (limit of quantitation). Experiments were performed in buffered saline solution (ambient conditions).

To test the linear range of the Os-based sensor, calibrations were performed for both glucose and lactate. Glucose was detected as low as 43 μM and quantified as low as 50 μM. At higher concentrations of glucose, the data began to deviate from linearity at ~10 mM, so the linear range was 50 μM to 10 mM (**Figure 3.6, left**). Non-linear regression identified the V_{max} and K_m for glucose as 4.4 x 10^{-9} mol min^{-1} and 32.9 mM, respectively. Similarly, the newly developed lactate sensor was tested to determine the linear range. The limit of detection was 1 μM while the limit of quantitation was 2 μM for lactate. The data began to deviate from linearity at 324 μM. Based on a non-linear regression model of the data, the V_{max} and K_m were 6.0 x 10^{-10} mol min^{-1} and 0.67 mM, respectively. Therefore, the linear range for the lactate sensor spanned from 2 to 324 μM (**Figure 3.6, right**). Both of the Os-based sensors offered a wide biologically-relevant linear range.

Operational Longevity

The sensitivities of the Os-based sensors were monitored over time to investigate the long-term stability of sensor performance. To do this, a calibration was carried out daily for a week for the Os-based GOx and LOx sensors. The sensitivity of the GOx sensor decreased from 420 ± 7 nA mM^{-1} to 313 ± 7 nA mM^{-1}, a 26% decrease, while the sensitivity decreased from 2460 ± 70 nA mM^{-1} to 1730 ± 70 nA mM^{-1}, a 29% decrease for the LOx sensor over the weeklong experiment (**Figure 3.7**).

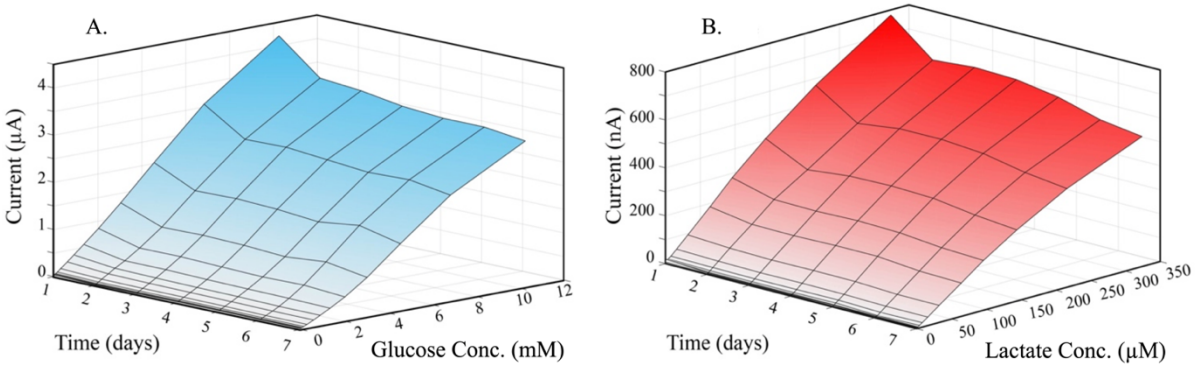

Figure 3.7. Operational Longevity of the Os-based GOx (A) and LOx (B) Sensors. These were tested by calibrating daily for seven days. Anodic (oxidative) current vs. calibration day vs. analyte concentration reported above. The sensitivity of the GOx sensor decreased from 420 ± 7 nA mM^{-1} to 313 ± 7 nA mM^{-1}, and the LOx sensor sensitivity decreased from 2460 ± 70 nA mM^{-1} to 1730 ± 70 nA mM^{-1} in the course of the week. Experiments were performed in buffered saline solution (ambient conditions) at 0.2 V. Data represented as the average, n = 3 replicates.

APAP and Insulin Treatment

To test the biological relevance of the Os-polymer sensors, AML12 glucose metabolism was observed with and without the addition of a background interferent. A glucose concentration above 5 mM (basal media concentration) denotes produced glucose while a glucose concentration below 5 mM signifies consumed glucose. Four control media samples were measured for glucose using the Os-polymer sensor. The basal media was treated with: protocol 1) no additives (4.78 ± 0.09 mM glucose, **Figure 3.8, solid blue**); protocol 2) added APAP (4.91 ± 0.05 mM glucose); protocol 3) added insulin (4.63 ± 0.14 mM glucose); and protocol 4) added both APAP and insulin (4.79 ± 0.10 mM glucose). These values are not significantly different ($p = 0.28$), so the basal media without additives is shown below as a representative for the control media. When compared to the control media, cells cultured in only basal media, protocol 1, and basal media with APAP, protocol 2, showed increased concentrations of glucose (7.15 ± 0.06 mM glucose and 6.78 ± 0.09 mM glucose, respectively) when compared to the control media (**Figure 3.8, striped**). In contrast, the glucose concentration decreased in cells challenged with protocol 3, media with insulin, (4.43 ± 0.11 mM glucose) and protocol 4, insulin-containing media from APAP-treated cells (3.83 ± 0.09 mM glucose, **Figure 3.8, checkered**) when compared to the control media.

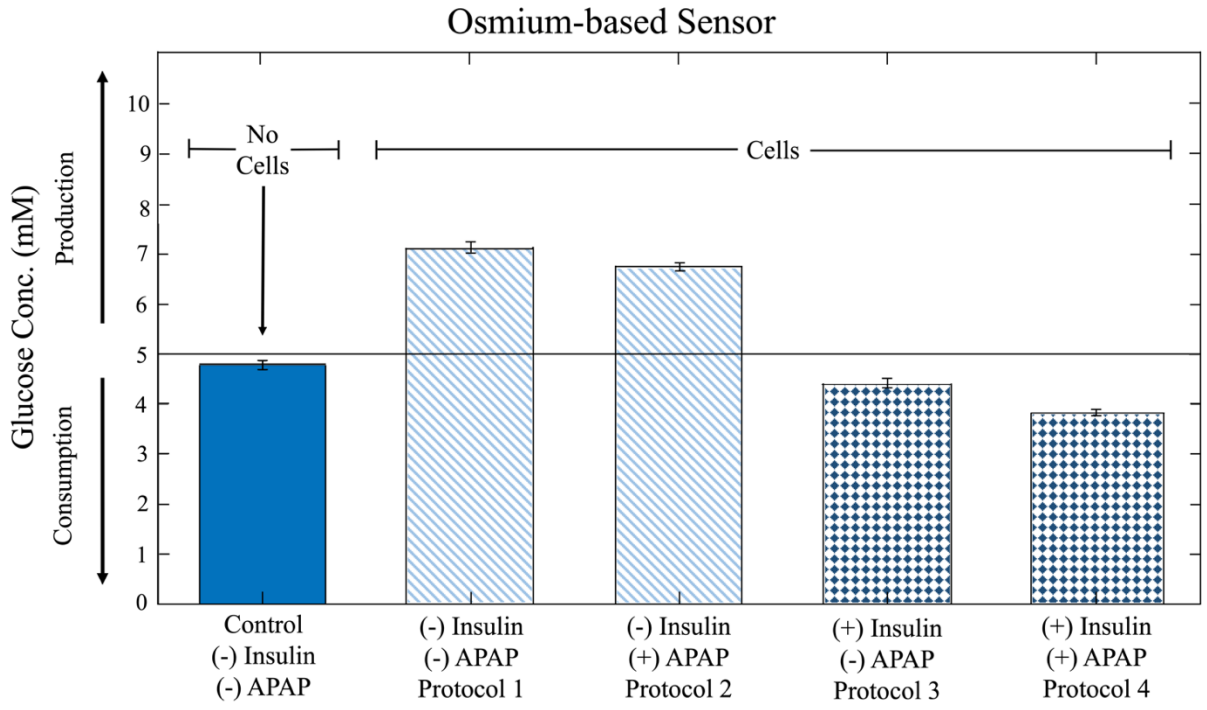

Figure 3.8. Glucose Consumption of AML12 Cells Treated with APAP and/or Insulin. Bar graph displaying the glucose concentration analyzed using an Os-based sensor vs. sample type including control and cellular samples. AML 12 cells were grown to 90% confluency in four different growth protocols and their glucose metabolism was monitored using the Os-based sensor and compared to a control without cells. Reduced glucose media is shown as the control with 4.78 ± 0.09 mM glucose. Cellular media without insulin was analyzed after two hours of exposure and is represented with stripes. Protocol 1 was the cellular media (reduced glucose DMEM/F12) without APAP and had 7.15 ± 0.06 mM glucose. Denoted as protocol 2, cells treated with APAP (1.4 mM) had 6.78 ± 0.09 mM glucose. The samples, illustrated with diamonds, were cultured in insulin-containing media and analyzed after 24 hours of exposure. The cells cultured in media with insulin (10 μg mL^{-1}) but without APAP were protocol 3 and had 4.43 ± 0.11 mM glucose, while the media from insulin- (10 μg mL^{-1}) and APAP- (1.4 mM) treated cells was protocol 4 and had 3.84 ± 0.09 mM glucose. Experiments were performed in reduced glucose DMEM/F12 media (ambient conditions). Data represented as an average and standard error with n = 3 biological replicates.

To determine the effect of insulin on glucose metabolism, AML12 cells were cultured with and without insulin and analyzed by the Os-polymer sensor. Glucose concentration changes due to the addition or removal of insulin were compared between cells treated the same (basal media or APAP-added). In comparing the cells that were left untreated and were either cultured with insulin (4.43 ± 0.11 mM glucose) or without it (7.15 ± 0.06 mM glucose), the glucose metabolism showed a significant difference ($p < 0.01$). Similarly, the APAP-treated cells were significantly different in glucose metabolism between those with (3.83 ± 0.09 mM glucose) and without insulin (6.78 ± 0.09 mM glucose) in the media ($p < 0.01$). Cells that were cultured without insulin had a larger glucose concentration than those with it.

While further examining glucose metabolism, the effect of APAP was analyzed using the Os-polymer sensor by treating cells with either basal media alone (untreated) or basal media with APAP. Samples from the media without insulin had a significantly decreased glucose concentration ($p < 0.01$) for those cells treated with APAP (6.78 ± 0.09 mM glucose) compared to the untreated cells (7.15 ± 0.06 mM glucose). The untreated cells (4.43 ± 0.11 mM glucose) had significantly increased glucose compared to the APAP-treated cells (3.83 ± 0.09 mM glucose) in media containing insulin as well ($p < 0.02$). Based on these results, the APAP-treated cells have less glucose in the media compared to the untreated cells.

To demonstrate the decreased sensitivity of the Os-based sensor to the model interferent basal media with and without APAP was analyzed using both types of sensors. When analyzed by a first-generation sensor, the basal media with insulin (3.0 ± 0.6 mM glucose) had a lower glucose concentration than the same basal media and insulin with added APAP (24 ± 2 mM glucose) (**Figure 3.9**). There was a significant difference in the basal media with and without APAP ($p < 0.01$). However, the same comparison between basal media with insulin (4.63 ± 0.14 mM glucose)

and basal media with insulin and APAP (4.79 ± 0.10 mM glucose), but analyzed by an Os-based GOx sensor was not significantly different ($p = 0.44$). Since the Os-based sensors did not show significantly different results while the first-generation sensors did, it was confirmed the Os-based sensors had decreased sensitivity to APAP.

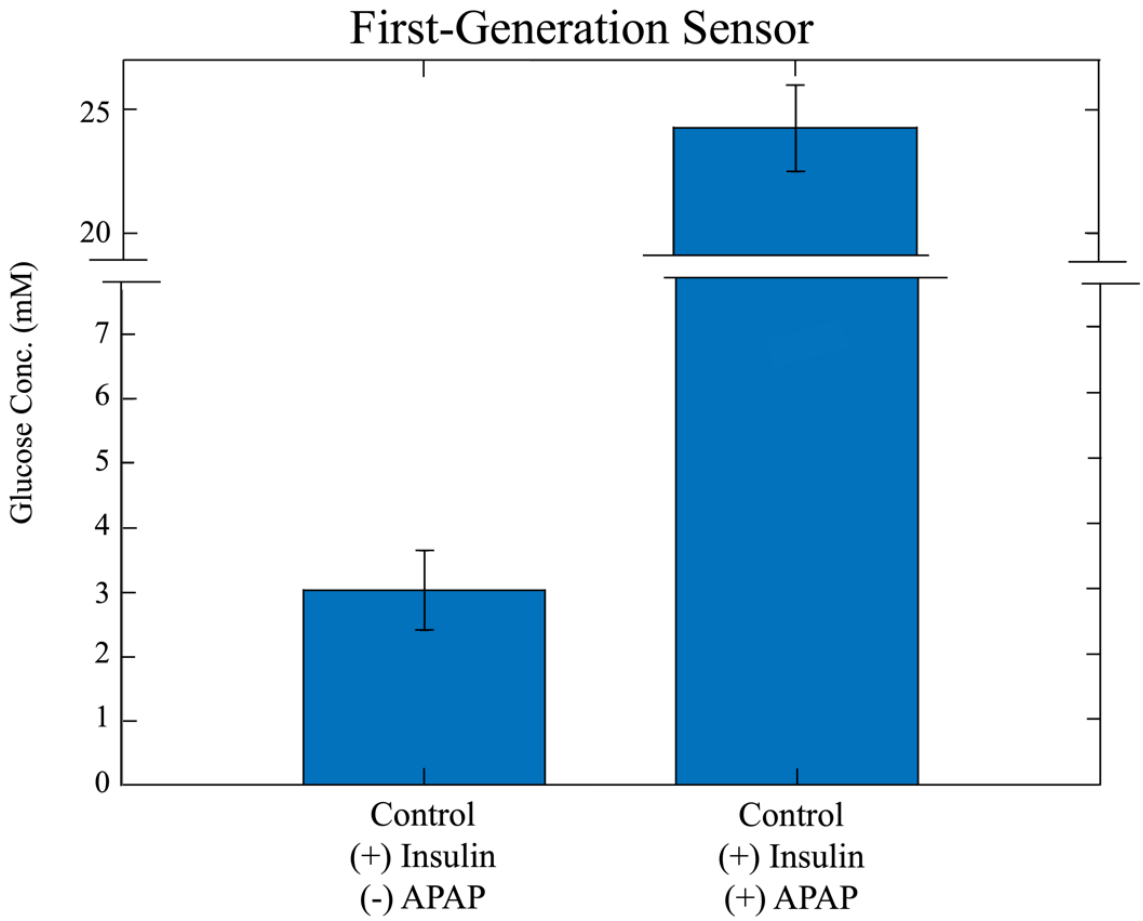

Figure 3.9. Comparison Graph of Control Media with First-Generation Sensors. Bar graph displaying the glucose concentration vs. controls (no cells) using a first-generation sensor for analysis. The glucose concentrations of the control without APAP (reduced glucose media with 10 μg mL^{-1} insulin) was 3.0 ± 0.6 mM glucose, while the same control with added APAP (1.4 mM) had 24 ± 2 mM glucose. Experiments were performed in reduced glucose DMEM/F12 media (ambient conditions). Data represented as the average and the standard error, n = 3 biological replicates.

Discussion.

Electrochemical microphysiometry is an effective method in studying cellular bioenergetics and toxicity.[4] However, electroactive signal interference may prevent accurate detection of the analytes of interest. In this work, Os-polymer sensors were used to mitigate interference by reducing the potential bias of the electrode. These sensors showed high analyte-selectivity, had a biologically-relevant linear range with increased sensitivity for the analyte compared to first-generation sensors, and established operational stability for use with model organ-on-chip systems. Together with the μCA, this system provided an easy-to-use and versatile format for sensing metabolites to improve diagnosing and monitoring health and disease.[47–49]

First, selectivities between the analyte and interferent were investigated for the developed Os-based sensors for comparison with the first-generation sensors. These Os-based sensors were approximately two orders of magnitude more selective than first-generation sensors for both analytes, demonstrating the reduced interference from APAP due to the presence of the Os-polymer that allowed for a reduced potential bias. Because the Os-based sensors were less affected by the interferent, the results from these sensors provided more accurate details about the system. This interferent insensitivity makes the high-resolution Os-polymer sensors ideal for monitoring changes in multiple biological analytes over a high background of an electroactive interferent, APAP.

Both of the new Os-based biosensors for glucose and lactate showed higher selectivity for their respective analytes compared to the redox-active interferent, APAP, since the Os-polymer allowed for a lower potential to be applied at the electrode surface. Because the Os-polymer biosensors were operated at 0.2 V (vs. Ag/AgCl), minimal APAP signal was generated. This reduced signal is expected, because 0.2 V (vs. Ag/AgCl) is well below the potential threshold for

bulk APAP oxidation. Conversely, the 0.6 V (vs. Ag/AgCl) electrode bias required to transduce a signal from the O_2-H_2O_2 couple in first-generation sensors was high enough to oxidize interferents in the solution. Additionally, the observation of an anodic (negative) current in these sensors confirmed the predicted electron flow mechanism (**Figure 3.1**), in which electron donation occurs first from the oxidase enzyme to the reduced osmium (Os^{3+}) complex and finally to the SPE.

These polymers not only decrease interference, they are also predicted to improve sensitivity of the sensor over first-generation sensors. Os-based GOx sensors have shown to have better sensitivity compared to first-generation GOx sensors (**Figure 3.10**). Because there are increase amine sites because of the imidazole there is increased crosslinking and increased electron transfer. $Os(bpy)_2Cl$-PVI had higher crosslinking efficiency with increased amine sites from the imidazole in the polymer while maintaining higher electron transfer from the osmium complex. Covalent linking of the enzyme to the hydrogel provided an enhanced pathway for electron transfer, thus increasing the sensitivity of the Os-based sensors compared to first-generation sensors.[75]

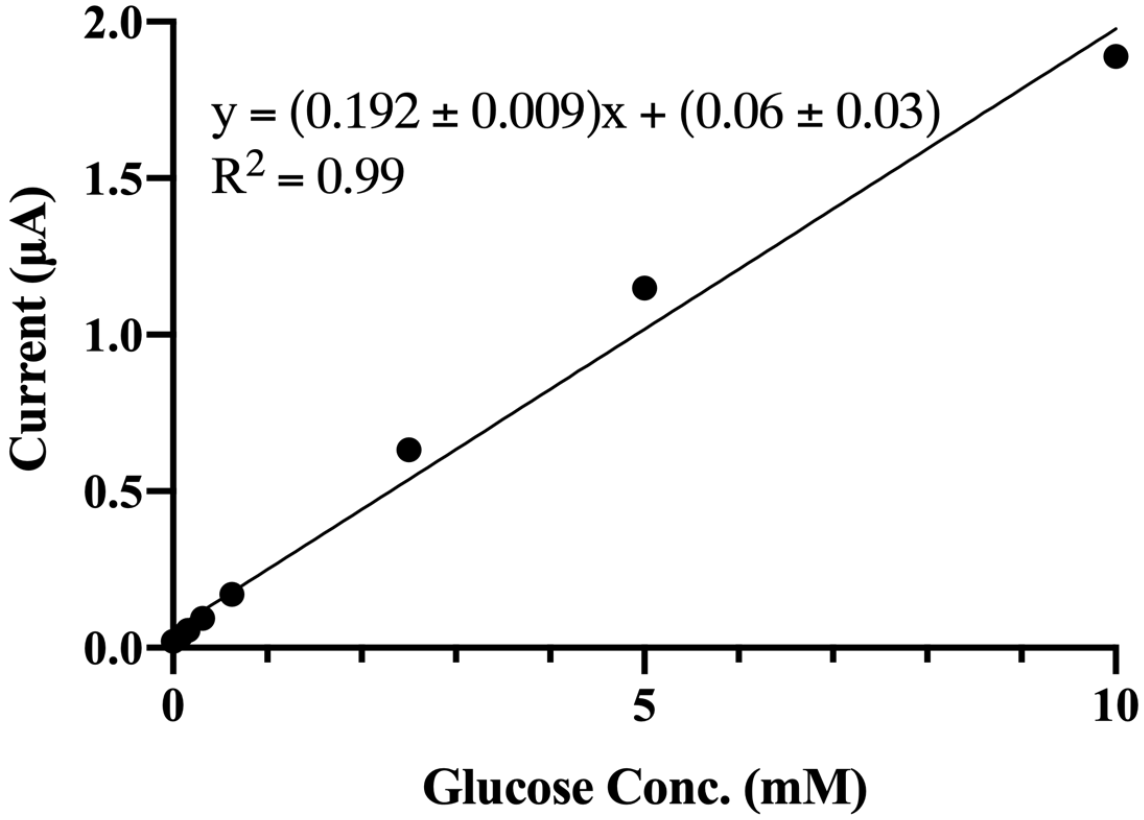

Figure 3.10. First-Generation Glucose Sensor Calibration Curve. Representative calibration curve of anodic current vs. analyte concentration showing the linear range of a first-generation GOx sensor. This shows the calibration from 0 to 10 mM. The slope is represented by a solid black line [$y = (0.192 \pm 0.009)x - (0.06 \pm 0.03)$, $R^2 = 0.99$] for the first-generation GOx sensor. Experiments were performed in buffered saline solution (ambient conditions).

Further evidence for the advantage of the Os-based sensors was the improved sensitivity while simultaneously spanning a large linear range necessary for monitoring a variety of biological processes. The first-generation sensors had a lower sensitivity for both glucose and lactate compared to the Os-polymer sensors. As predicted, the Os-polymer mediates an enhanced electron pathway, producing a higher sensitivity. More specifically, there was a 111% increase in sensitivity for the Os-polymer GOx sensors and a 17% increase in the sensitivity for Os-based LOx sensors compared to their respective first-generation sensors. This increased sensitivity allowed for a low level of detection and quantitation while still including higher concentrations which are both necessary for model organ systems and other biological applications. While there was slightly less sensitivity for Os-based glucose sensors compared to previous Os-polymer sensor, there was a slightly improved sensitivity for the Os-based LOx sensors.[76,77] Based on previous data, the V_{max} value for the glucose Os-based sensor was similar to that of a first-generation, but the lactate Os-polymer sensor was a magnitude less than a first-generation sensor.[78] The lactate sensor does not need to measure as high as the glucose so a lower V_{max} value is acceptable.[29] Furthermore, the Os-polymer GOx sensor had a slightly higher limit of quantitation but also had a much higher limit of linearity compared to a previously developed glucose Os-based sensor.[79] This is helpful for media-based detection that usually has glucose in it such as in this work with the AML12 cells. In addition, both types of these Os-polymer sensors had a higher limit of detection but a lower limit of linearity when compared to first-generation sensors.[29] These sensors offered improved sensitivity and a wide linear range for glucose (50 μM to 10 mM) and lactate (2 to 324 μM) that is suitable for monitoring cellular function and biological processes.[1,47–49,80–83]

Finally, considering the utility of this sensor platform in tandem with a continuously operational system, the longevity of sensor performance was investigated. In both sensors, after an expected initial sensitivity decrease was observed from enzymatic activity loss, the sensitivity decreased slightly and stayed stable over the weeklong study (**Figure 3.11**). These sensitivity decreases were expected in first-generation sensors as well, so the operational stability was not compromised by the addition of the Os-polymer.[29] First-generation sensors have been tested previously for longevity, showing loss of sensitivity attributed to enzyme degradation.[29] Though the first-generation sensors showed they could be used up to three weeks for glucose and two weeks for lactate, these Os-based sensors were only tested for seven days and may have longer operational longevity than tested.[29] Furthermore, the electrodes still yielded a significant analyte response, upon which a new calibration curve was prepared. Another Os-based glucose sensor showed similar stability of a week as the Os-based sensor presented here.[79] The slight decrease in sensitivity throughout the week emphasized the need for regular recalibration in continuously operational sensors. These sensors are promising for their use in monitoring multiple biological analytes over extended periods of time.

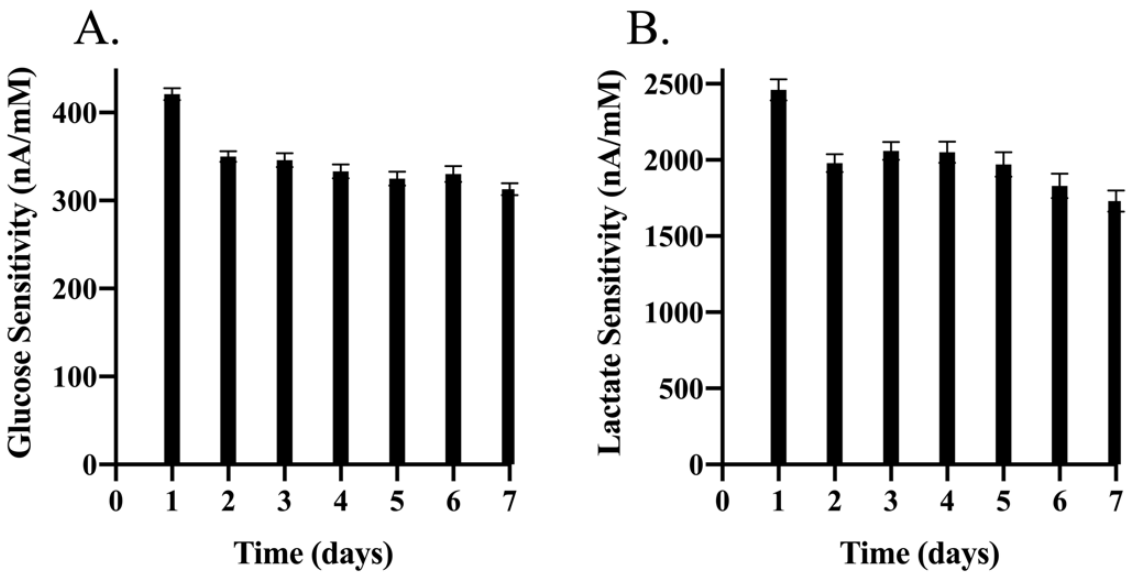

Figure 3.11. Comparison Graphs for Glucose and Lactate Sensitivities for Operational Longevity. Operational longevity of the Os-based glucose oxidase (A) and lactate oxidase (B) sensors was tested by calibrating daily for seven days. Sensitivity (nA/mM) vs. calibration day is reported above. The sensitivity of the GOx sensor decreased from 420 ± 7 nA mM^{-1} to 313 ± 7 nA mM^{-1}, and the LOx sensor sensitivity decreased from 2460 ± 70 nA mM^{-1} to 1730 ± 70 nA mM^{-1} in the course of the week. Experiments were performed in buffered saline solution (ambient conditions) at 0.2 V. Data represented as the average, n = 3 replicates.

The culturing media dysregulated glucose metabolism of AML12 cells with the addition or removal of insulin. The cells cultured in media with insulin had decreased glucose concentrations when compared to control media. Presumably, the cells were consuming glucose and exhibiting the regular insulin-stimulated glucose metabolism shown in AML12 cells.[69] Both of the samples without insulin showed increased concentrations of glucose compared to the control media. Therefore, glucose was produced, which is consistent with previous results from AML12 cells without insulin.[68,69] These results validate the Os-based sensor as an accurate detection method. Glucose metabolism of AML12 cells reversed with the addition of insulin to the culturing media.

Glucose metabolism of treated and untreated AML12 cells was investigated with a background interferent to test the Os-polymer sensors' biological relevance and application to model organ systems. Because there is a risk of liver damage with a blood level of APAP at 200 μg/mL (1.3 mM for the average person) after four hours of ingestion, a concentration of 1.4 mM APAP was chosen to induce liver changes in glucose metabolism.[84] Both sets of APAP-treated cell media had a lower glucose concentration than the accompanying untreated cells, indicating the APAP-treated cells had dysregulated glucose metabolism. The cells were likely consuming more glucose to compensate for the stress of APAP exposure and the onset of toxicity, thus changing the glucose metabolism of the cell. Therefore, we accurately measured glucose metabolism in the presence of APAP and showed the dysregulation due to the toxicant with the Os-based sensor.

Finally, a comparison of the two different sensors was investigated, highlighting the strength of the Os-polymer sensors to mitigate interference. There was a large difference between the basal media with and without APAP when analyzed by the first-generation sensor, but no

difference is seen in the same media samples analyzed by the Os-based sensors. This juxtaposition emphasized the increased resolution of the developed sensors while maintaining the integrity of the sensor for a more accurate detection method than first-generation sensors.

Conclusions.

A new multianalyte biosensor platform was constructed to directly quantify changes in glucose and lactate over high backgrounds of an electroactive interferent, APAP. Os-based redox hydrogels were utilized to mediate electron transport from the enzyme to the electrode, reducing the need for high electrode potentials, and therefore mitigating the effects of APAP on the electrochemical signal. Flow-based experiments using the μCA were performed simultaneously for glucose and lactate Os-based sensors. The automation that the μCA offers and the addition of these sensors to the ever-expanding toolbox of measurable analytes provides an efficient and versatile format. Selectivity assays indicated greatly diminished signal contributions from interferent with improved sensitivity in the Os-based sensors when compared to first-generation biosensors. The Os-polymer sensors offered a wide linear range that can be used for measuring changes in the metabolic profile of biological systems. Finally, long-term performance evaluations revealed that these sensors retain substantial analytical sensitivity after several days of use and storage, indicating that this platform can successfully be integrated in-line with a biological system for analysis. The results from cellular experiments indicated 1) the removal of insulin from basal media reversed glucose metabolism in AML12 cells; 2) APAP increased glucose consumption in the cells; and 3) the Os-based sensor had diminished signal interference compared to the first-generation sensor. This high-resolution platform can easily be translated to other applications such as glucose meters for diabetics,[52] lactate sensors for the food industry,[85] and biomimicry for pharmaceuticals (organs-on-chips).[86–90]

Acknowledgments.

The authors thank Dr. Nathan Schley and Margaret Calhoun from Vanderbilt University for assistance with the polymer and Dusty Miller and Evan Gizzie for assistance in designing and

performing experiments. The authors graciously acknowledge financial support from the Defense Threat Reduction Agency (DTRA) under award CBMXCEL-XL1-2-0001, and the Environmental Protection Agency (EPA-83573601). This work was also supported in part by the National Institute of Health training grant (ES007028), EPA (83573601), and IARPA (2017-17081500003) and using the resources of the Vanderbilt Microfabrication Core operated by the Vanderbilt Institute for Integrative Biosystems Research and Education.

Chapter IV

MULTIANALYTE AMPEROMETRIC ELECTROCHEMICAL BIOSENSOR PLATFORM FOR ANALYSIS OF MODEL ORGAN SYSTEMS

Electrochemical biosensing provides insight into the processes of biological systems.[4,18,29,31] These sensors are most commonly used to detect and quantify single analyte i.e. diabetic glucose meter.[51] Over the last several years, there has been significant development in electrochemical biosensors that provides miniaturization and increased analyte detection.[20,25,56,78,91–93] To accurately understand cellular processes and monitor health and disease, simultaneous multianalyte detection methods are critical. In this work, a multianalyte (up to eight analytes) amperometric biosensor platform is presented, allowing for the deconvolution of metabolic profiles in model organ systems. We simultaneously quantified glucose, lactate, and ascorbic acid in two mouse studies using this platform. Combining the pump and valve with this enzymatic-based electrode array allows for the quantification of a variety of analytes of interest in a multitude of biological applications.

Amperometric biosensors are used widely and allow for the detection and quantification of several analytes of interest.[4,24] Previously, detection has centered around only one analyte of interest, which does not accurately reflect the metabolic processes and overall biosignature (metabolic snapshot of the interactions in a system). Therefore, it is necessary to quantify multiple analytes simultaneously to understand the system and the interactions taking place. Recently, researchers have developed multianalyte amperometric sensors for the simultaneous detection and quantification of analytes of interest.[4,18,29] By utilizing multiple analytes, complex mechanisms and pathways can be deconvoluted and more easily understood. Many of these sensors while

helpful for detecting multiple analytes, do not allow for the customization of enzymes, restricting researchers to only those enzymes used in the respective study.[24] Furthermore, these sensors are not automated, cannot be integrated for real-time analysis, and still only detect a few analytes.[4,18,22,24,94] Since these sensors detect analytes within one chamber, there is the possibility for cross talk, and therefore inaccurate results. Thus, there is a need for a simultaneous, multianalyte, amperometric biosensor platform that is automated as well as easily customized and integrated for real-time analysis.

Addressing these needs, we investigated a multianalyte amperometric customizable electrochemical biosensor platform for simultaneous detection and quantification of up to eight analytes in model organ systems. A pump and valve are combined with this sensor for automation of calibration and sample testing.[46] With the addition of this pump and valve system and using electrochemical methods, there is the opportunity for real-time analysis in organs-on-chips (OoCs).[6] Furthermore, this biosensor has separated channels that eliminate cross-talk that has been seen in previous biosensors.[31,95,96] This system provides not only the detection of eight different analytes, it can also be used for multiple analytes with multiple replicates i.e. two analytes with four replicates or four analytes with two replicates. With the option for easy customization, researchers may utilize the enzymes used in these studies or adapt it to the enzymes/analytes that are most applicable for them.[97–101] This allows for more options of metabolite detection to determine metabolic processes and toxicity pathways.[4] This multianalyte amperometric biosensor creates a platform with the pump and valve system that allows for the addition of more metabolites to the analytical toolbox and to learn more about the cellular bioenergetics of a system.

To monitor cellular respiration, oxidative processes, and neuronal processes, it is helpful to detect metabolites to create a biosignature of a system before and after perturbation. Both

glucose and lactate play active roles in key metabolic processes and cellular respiration.[29,41,94,102,103] Superoxide is a part of the oxidative burst in macrophages and reveals the production of reactive oxygen species.[10] Ascorbic acid is a known antioxidant, reducing oxidative stress, and is also important in neuronal processes.[12,104] Lastly, glutamate, acetylcholine, and dopamine are all essential neurotransmitters, providing neuronal signaling and neuromodulation.[5–8,21] Each of these is helpful in understanding multiple metabolic processes and will allow complex problems and systems to be more easily understood.

It is currently unknown the effect 2,3,7,8-tetrachlorodibenzodioxin (TCDD), lipopolysaccharides (LPS), and β-glucan has on metabolism in mice macrophages. A model immune-disrupting toxicant, TCDD is used in studies and has shown hyperinflammatory effects in the uterine and peritoneal cavity of mice.[37,43] TCDD-exposed mice phenotypically replicate women with endometriosis, which can be exaggerated by an infection or inflammatory secondary trigger such as LPS.[43,44] β-glucan has shown to train immune cells, causing increased glucose consumption and lactate production.[45] Understanding the relationships between TCDD, LPS, and β-glucan and how they affect metabolism is key to determining pathways of toxicity and monitoring health and disease.

Applying this to a biologically-relevant system, we utilized this platform for understanding the effects of TCDD, LPS, and β-glucan on macrophages of mice. To gain insight into these interactions, glucose and lactate metabolism was investigated. Macrophages are a primary defense in the immune system against xenobiotics.[105] These are vital to understanding the pathways of toxicity and cellular processes in the body with diseases such as endometriosis.[37,45] Understanding the metabolic processes using glucose and lactate as a measure will be fundamental to understanding the whole system.[4,24,94,102,103]

Here, we present a platform for detection and quantification of up to eight analytes using enzymatic-based methods to understand more about the cellular processes and pathways of toxicity. By combining sensors for multiple analytes together into one electrode array with separate channels for real-time analysis of biological systems, we may electrochemically monitor cellular respiration, oxidation processes, neurotransmission, as well as perform toxicity screenings. Calibrations were performed to cover biologically-relevant linear ranges while maintaining sensitivity. Measuring changes in multiple analytes will allow for a better understanding of the state and interactions of a system. This platform was used to test glucose and lactate metabolism of macrophages from mice after treatment with TCDD, LPS, and β-glucan.

Experimental.

Analyte Sensor Modification

The electrode array features 11 electrodes; one platinum disk electrode, one platinum large band electrode, and nine platinum small band electrodes. The top circular electrode on the screen-printed electrode array was used as a Ag/AgCl internal reference with a large rectangular counter electrode directly below it. Below both of those sensors, there were nine small rectangular electrodes (A = 1.16 mm^2) that can be modified for analyte selectivity, but only eight of these electrodes may be used separately since two of the smaller electrodes are in series. The reference electrode was modified to make an internal Ag/AgCl reference. To make this, silver was electrodeposited on the reference electrode and then immersed in an iron (III) chloride solution.[18] Then, the working electrodes were modified with an enzymatic mixture described below.

The analytes and their respective detection enzymes include: 1) glucose (β-D-glucose, Calbiochem, La Jolla, CA) with glucose oxidase from *Aspergillus niger* (Type II, 17,300 Units g^{-1}, Sigma Aldrich, St. Louis, MO); 2) lactate (sodium L-lactate, Sigma) with lactate oxidase from *Pediococcus* sp. (20 Units mg^{-1}, Sigma); 3) glutamate (L-glutamic acid potassium salt monohydrate, Sigma) with glutamate oxidase from *Streptomyces* sp. (5 Units mg^{-1}, Sigma); 4) acetylcholine (acetylcholine chloride, Sigma) with acetylcholinesterase from *Electrophorus electricus* (137 Units mg^{-1}, Sigma), and choline oxidase from *Alcaligenes* (15 Units mg^{-1}, Sigma); 5) dopamine (3-hydroxytyramine hydrochloride, Acros Organics) with tyrosinase from mushroom (7164 Units mg^{-1}, Sigma); 6) ascorbate (L-ascorbic acid sodium salt, Acros Organics, Fair Lawn, NJ) with ascorbate oxidase from *Cucubita* sp. (1000-3000 Units mg^{-1}, Sigma); and 7) superoxide (created by combining hypoxanthine anhydrous [MP Biomedicals, Santa Ana, CA] and xanthine oxidase from bovine milk [0.5 Units mg^{-1}, Sigma]) with superoxide dismutase from bovine

erythrocytes (3,000 Units mg^{-1}, Sigma).[6,12,18,21,31,106] Every enzyme except xanthine oxidase that comes in a suspension was dissolved separately (4,000 U mL^{-1} glucose oxidase, 2,000 U mL^{-1} lactate oxidase, 50 U mL^{-1} glutamate oxidase 150 U mL^{-1} choline oxidase, 1,400 U mL^{-1} acetylcholinesterase, 72,000 U mL^{-1} tyrosinase, 1,000 U mL^{-1} ascorbate oxidase, and 5,000 U mL^{-1} superoxide dismutase) in bovine serum albumin [BSA, (800 mg/mL, Sigma)] in buffer solution [2 mM, pH 7, (Fisher Scientific, Hampton, NH)] and stored until use (-18°C) for up to one year. When required, each of these enzyme solutions (except xanthine oxidase) was mixed with glutaraldehyde (0.1% wt/v, Sigma), vortexed (~5 sec), drop-cast (0.5 µL) onto each working electrode, and air-dried (1 hour) before either use or storage [low light, 4°C, buffer solution (2 mM, pH 7), 120 mM KCl]. However, the acetylcholine sensor had acetylcholinesterase and choline oxidase combined equally (v/v) and mixed with glutaraldehyde (0.5% wt/v, Sigma), and then vortexed and drop-cast the same as the other enzyme solutions. One working electrode was left unmodified for use in conjunction with the ascorbic acid sensor.[12]

Sensor Incorporation

To incorporate these sensors into the platform, they were sealed within a specially designed housing [designed and fabricated by Vanderbilt Institute for Integrative Biosystems Research and Education (VIIBRE)] similar to previous iterations (**Figure 4.1, left**).[6] The sensor was designed in-house and fabricated by Sullins Connector Solutions (San Marcos, CA) (**Figure 4.1, right**). The bioreactor opens to insert and remove the electrode that was attached to an edge card connector linking the electrode signal to the potentiostat for analysis. Similarly, the housing interfaces with the microformulator (Vanderbilt Institute for Integrative Biosystems Research and Education)—a microfluidic pump and valve system providing automated sensor calibration and sample analysis

and accommodates a variety of flow speeds.[29] Flow must go in over the working electrodes then the flows out over the reference electrode.

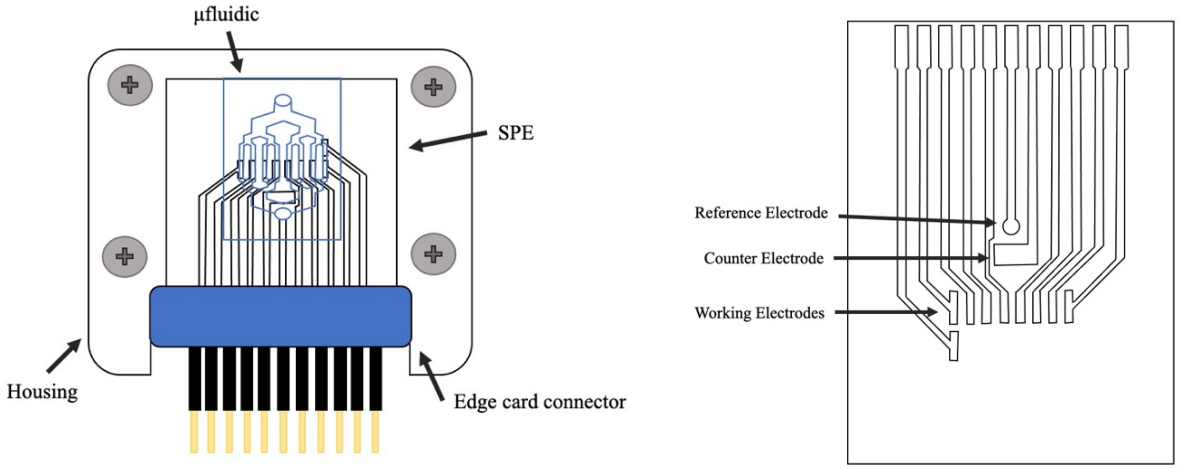

Figure 4.1. Drawings of SPE housing and SPE array. Left is the SPE, microfluidic, secured housing pieces, and edge card connector for the potentiostat. The SPE on a PMMA piece (housing) with a microfluidic on top of the SPE that create eight separate channels to reduce cross talk. The SPE is in the edge connector on the top side and is connected to the potentiostat on the bottom side (black/gold). A second PMMA piece with holes that allow for plumbing to the pump and valve system as well as the waste is placed top. Finally, this is all screwed together to make the entire SPE housing. Flow must start over the working electrodes first then the counter and finally can flow out over the reference electrode. On the right is the SPE with a circular reference electrode, a large rectangular counter electrode, and nine small rectangular working electrodes.

Characterization of analyte sensors

The limits of detection (LOD) and quantitation (LOQ), linear range, V_{max}, and K_m for each of the sensors were determined using the μCA as they were for other enzyme electrodes.[6,29] Calibrations were performed by monitoring the current generated by 24 calibrants (2.8 μM to 50 mM glucose, 0.5 μM to 8 mM lactate/glutamate/acetylcholine, 0.9 μM to 50 mM ascorbate/superoxide, and 0.3 μM to 50 mM dopamine) in buffer. Buffer for all experiments was made from a 50 mM potassium monobasic-sodium buffer (pH 7.00, Fisher) diluted in water with KCl to produce a 2 mM phosphate, 120 mM KCl, pH 7 buffered solution. Calibrants were sampled through the valve pulled by the pump at a flow rate of 100 μL/min for 2 min, and the resulting current was monitored until a steady state was reached (~3 min) using a CHI 1030 potentiostat (CH Instruments, Austin, TX) held at 0.6 V vs. Ag/AgCl except for the dopamine sensor which is held at -0.2 V vs Ag/AgCl. To establish a baseline for each of the calibrants, buffer preceded each calibrant. Calibrants were sampled using a microformulator (100 μL min^{-1} for 240 s) pump and valve system.

Biological Application

Samples were graciously provided by Dr. Kevin Osteen's Lab. Briefly, C57 BI/6 mice were treated with TCDD or PBS *in utero*. Then, two of these mice (one was TCDD-treated and one was a control with PBS) were grown to adulthood and a bone marrow isolation experiment was conducted on both mice to obtain the macrophages. These macrophages were treated with PBS, LPS, or β-glucan for either 24 hours or 3 days post injection. A reduced calibration (five calibrants) was completed then the samples were analyzed for glucose and lactate concentrations.

Calculations

Linear and nonlinear regressions were performed on the calibration data to determine the limit of detection, limits of linearity, sensitivity, V_{max}, and K_m of the sensor for each analyte. The equation for the line between six calibration points at the lower concentrations around the approximate limits was used to calculate the limits of detection and quantitation. Values from this linear regression were used for calculating the limit of detection (LOD) according to Equation 1,

$$Equation\ 1. \quad LOD = \frac{3S_E}{m}$$

where S_E is the error of the blank from the shortened calibration and m is the slope of the same calibration. Similarly, the limit of quantitation was calculated using this equation, except that the standard error was multiplied by ten instead of three. The upper limit of linearity is determined using the slope between calibration points including the limit of quantitation to the approximate saturation point based on visual inspection. If the next largest calibration point was added to the whole linear range and the subsequent slope changed by 10% or more from the previous slope without that point then the limit remained the same and the previous datapoint is the upper limit of linearity. A linear regression was then performed on the whole linear range from limit of quantitation to the upper limit of linearity, and the resulting slope provided the sensitivity of the electrode for each analyte. Because the data showed enzyme saturation and followed Michaelis-Menten kinetics, a nonlinear function could be fit to the data to determine V_{max} and K_m using Prism 9 (GraphPad software, San Diego, CA). The results yielded the values for V_{max} and K_m for each of the analytes. All *p*-values calculated in this study were found by performing two-tailed t-tests assuming unequal variance. Values of $p \geq 0.05$ are considered significant.

Results.

Calibrations were performed for all seven analytes (acetylcholine, ascorbic acid, dopamine, glucose, glutamate, lactate, and superoxide) to determine sensitivities (equations of the linear range), limit of detection, limit of quantitation, linear range, and nonlinear enzymatic kinetics (V_{max} and K_m) (**Figure 4.2**). The equations for the lines with the sensitivities of each of the analytes include, 1) acetylcholine – $y = (948 \pm 33)x + (46 \pm 4)$, $R^2 = 0.996$, (sensitivity - 948 ± 33 nA mM^{-1}); 2) ascorbic acid – $y = (1264 \pm 28)x - (30 \pm 4)$, $R^2 = 0.998$, (sensitivity - 1264 ± 28 nA mM^{-1}); 3) dopamine – $y = (13{,}794 \pm 344)x - (77 \pm 7)$, $R^2 = 0.998$, (sensitivity – 13,479 ± 344 nA mM^{-1}); 4) glucose – $y = (1329 \pm 19)x - (8 \pm 3)$, $R^2 = 0.998$, (sensitivity – 1329 ± 19 nA mM^{-1}); 5) glutamate – $y = (826 \pm 18)x - (13 \pm 4)$, $R^2 = 0.997$, (sensitivity – 826 ± 18 nA mM^{-1}); 6) lactate – $y = (738 \pm 18)x - (10 \pm 4)$, $R^2 = 0.994$, (sensitivity – 738 ± 18 nA mM^{-1}); and 7) superoxide – $y = (1120 \pm 25)x + (2 \pm 3)$, $R^2 = 0.996$, (sensitivity – 1120 ± 25 nA mM^{-1}) (**Figure 4.3**). Acetylcholine was detected at 6 μM and quantified at 22 μM. The limit of linearity was ~200 μM, making the linear range 22 to 200 μM. A Michaelis-Menten enzymatic nonlinear regression gave a V_{max} of 7.2×10^{-11} mol min^{-1} and a K_m of 0.036 mM. For ascorbic acid, the limits of detection, quantitation, and linearity were 5, 17, and 260 μM respectively. Therefore, ascorbic acid had a linear range 17 – 260 μM. A Michaelis-Menten regression determined V_{max} and K_m as 2.4×10^{-10} mol min^{-1} and 0.34 mM for ascorbic acid. Dopamine had a limit of detection of 0.8 μM and a limit of quantitation of 3 μM. Since the sensor began to saturate at 39 μM, the linear range is 3 – 39 μM. V_{max} and K_m were 3.9×10^{-10} mol min^{-1} and 0.035 mM, respectively, for dopamine. Glucose was detected as low as 5 μM and quantified as low as 18 μM. At higher concentrations of glucose, the data began to deviate from linearity at ~4 mM, so the linear range was 18 μM to 4 mM. Non-linear regression

for Michaelis-Menten enzymatic kinetics identified the V_{max} and K_m for glucose as 3.5 x 10^{-10} mol min^{-1} and 4.9 mM, respectively. The limit of detection for the glutamate sensor was 7 μM and the limit of quantitation was 24 μM. With a limit of linearity of ~440 μM, the linear range is then 24 – 440 μM. A regression for Michaelis-Menten enzymatic kinetics for glutamate showed V_{max} as 3.3 x 10^{-10} mol min^{-1} and K_m as 0.77 mM. The limit of detection for the lactate sensor was 0.6 μM while the limit of quantitation was 2 μM. The data began to deviate from linearity at ~670 μM, making the linear range for lactate 2 – 670 μM. Based on a non-linear regression model of this data, the V_{max} and K_m were 2.8 x 10^{-10} mol min^{-1} and 0.68 mM, respectively. Finally, superoxide was detected as low as 1 μM and quantified at 5 μM. The data began to deviate at ~260 μM, so the linear range for superoxide was 5 – 260 μM. The V_{max} and K_m for superoxide were 7.6 x 10^{-11} mol min^{-1} and 0.085 mM using a Michaelis-Menten model for regression, respectively.

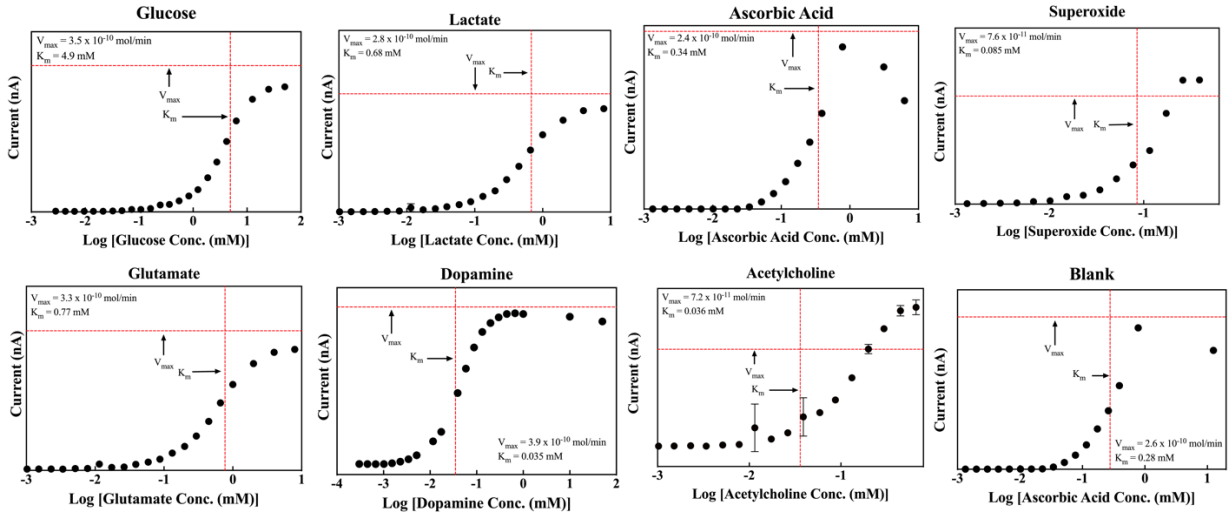

Figure 4.2. Representative Logarithmic Curves for Various Analytes. The graphs display current (nA) vs. log [analyte concentration (mM)] with V_{max}, and K_m for glucose, lactate, ascorbic acid, superoxide, glutamate, dopamine, acetylcholine, and blank sensors. Using non-linear regression of Michaelis-Menten enzymatic kinetics, V_{max} and K_m were calculated for all analytes. All current is anodic, except dopamine which results in cathodic current. The blank electrode has ascorbic acid concentrations as the analyte. V_{max} and K_m are represented as red dashed lines. Experiments were performed in buffered saline solution (ambient conditions). The calibrations had a detection time of 120 s and a flow rate of 100 µL/min.

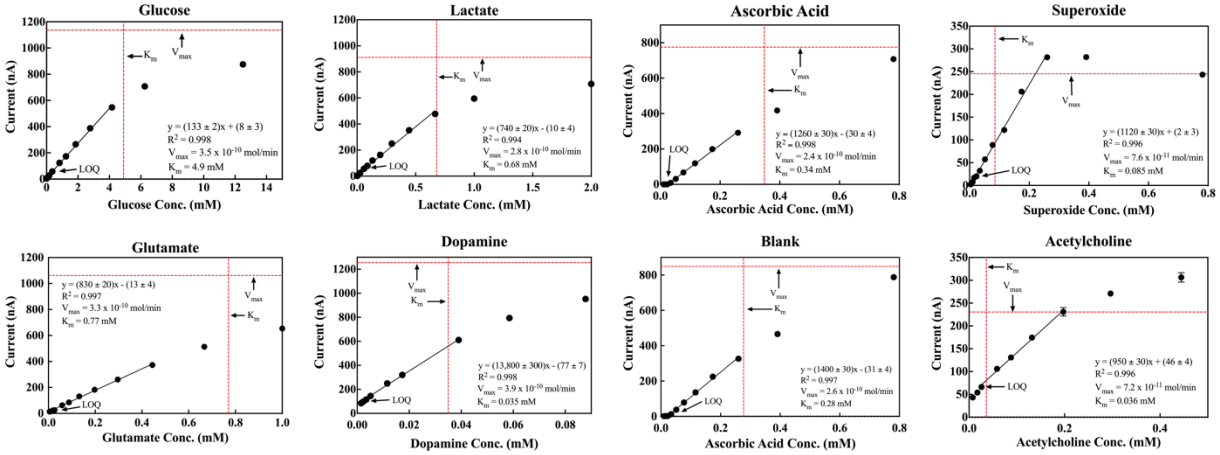

Figure 4.3. Representative Calibration Curves of the Linear Range of the Analytes. These graphs show current (nA) vs. analyte concentration (mM) with the limits of quantitation and linearity as well as the V_{max} and K_m values for all of the sensors. All of the sensors had an anodic current, except the dopamine sensor which has cathodic current. The linear ranges are represented by solid black lines with the limit of linearity as the last data point on the line. V_{max} and K_m are demarcated as red dashed lines. The limit of quantitation is also indicated on the graphs. The equations of the lines and the values for R^2, V_{max}, and K_m are shown on the graphs as well. Experiments were performed in buffered saline solution (ambient conditions). The calibrants were flowed at a rate of 100 µL/min and detected for 120 s.

Testing the biological relevance of this platform, macrophage glucose and lactate metabolism was investigated. Mice *in* utero were exposed to PBS (control, C) or TCDD (F1). The macrophages of two of these mice were treated with 1) PBS (no treatment), 2) LPS, or 3) β-glucan for either 24 hours or 3 days post injection. This gave 10 groups of mice macrophages with different treatments, designated as C-1, C-2-24, C-2-3, C-3-24, C-3-3, F1-1, F1-2-24, F1-2-3, F1-3-24, and F1-3-3. C-1 had -239 ± 2 μM glucose and -56 ± 3 μM lactate. C-2-24 showed 28.0 ± 1.0 μM glucose and 68 ± 2 μM lactate. C-2-3 had -141.3 ± 1.5 μM glucose and 28 ± 2 μM lactate. C-3-24 showed -83.3 ± 1.3 μM glucose and -40 ± 2 μM lactate. C-3-3 had -163 ± 2 μM glucose and 161.0 ± 0.6 μM lactate. F1-1 had -153.4 ± 1.3 μM glucose and 24 ± 2 μM lactate. F1-2-24 had -128 ± 2 μM glucose and 95.8 ± 0.8 μM lactate. F1-2-3 showed -153 ± 3 μM glucose and 30 ± 2 μM lactate. F1-3-24 showed -41 ± 2 μM glucose and 20 ± 3 μM lactate. F1-3-3 had -170.1 ± 0.2 μM glucose and -12 ± 2 μM lactate (**Figure 4.4**).

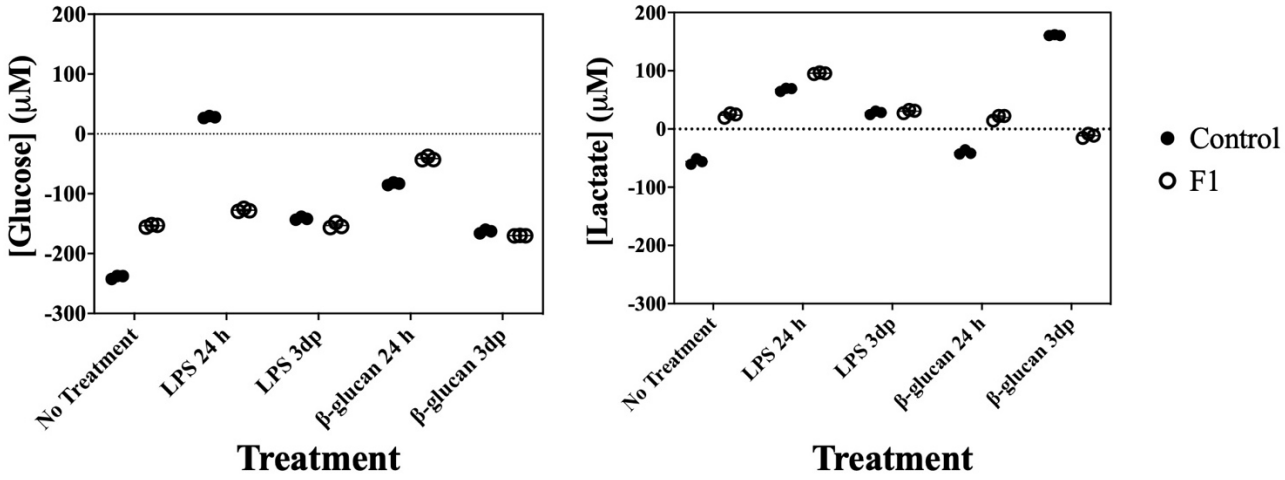

Figure 4.4. Glucose and Lactate Concentrations in Mice Macrophages After Treatment. Scatter dot plot displaying the glucose and lactate concentrations analyzed using this platform vs treatment. Five different treatments protocols were given to macrophages in mice that were either a control set or F1 (TCDD-dosed *in utero*) set. C-1 had -239 ± 2 μM glucose and -56 ± 3 μM lactate. C-2-24 showed 28.0 ± 1.0 μM glucose and 68 ± 2 μM lactate. C-2-3 had -141.3 ± 1.5 μM glucose and 28 ± 2 μM lactate. C-3-24 showed -83.3 ± 1.3 μM glucose and -40 ± 2 μM lactate. C-3-3 had -163 ± 2 μM glucose and 161.0 ± 0.6 μM lactate. F1-1 had -153.4 ± 1.3 μM glucose and 24 ± 2 μM lactate. F1-2-24 had -128 ± 2 μM glucose and 95.8 ± 0.8 μM lactate. F1-2-3 showed -153 ± 3 μM glucose and 30 ± 2 μM lactate. F1-3-24 showed -41 ± 2 μM glucose and 20 ± 3 μM lactate. F1-3-3 had -170.1 ± 0.2 μM glucose and -12 ± 2 μM lactate. Data represented as an average and standard error with technical replicates (n = 3) for both glucose and lactate.

To determine the effect that TCDD had on the mice in each treatment, glucose and lactate metabolism was compared using this platform. The analyte concentrations in macrophages from mice that were previously treated with TCDD *in utero* were compared between macrophages treated the same [PBS, LPS (24 h or 3dp), and β-glucan (24 h or 3dp)]. C-1 had significantly lower glucose and lactate concentrations compared to F1-1 ($p = 5 \times 10^{-6}$ for glucose and $p = 4 \times 10^{-5}$ for lactate). The concentrations for glucose were significantly higher and lactate was significantly lower for C-2-24 compared to F1-2-24 macrophages ($p = 8 \times 10^{-7}$ for glucose and $p = 0.0009$ for lactate). C-2-3 showed significantly higher glucose than F1-2-3 ($p = 0.03$), but the lactate concentrations were not significantly different ($p = 0.4$). C-3-24 had significantly lower glucose and lactate levels than F1-3-24 ($p = 0.0001$ and $p = 8 \times 10^{-5}$, respectively). Finally, C-3-3 was significantly higher for lactate concentrations ($p = 5 \times 10^{-5}$), but was only trending toward significantly higher glucose ($p = 0.06$). Thus, glucose and lactate were significantly different in macrophages that had previously been exposed to TCDD compared to control macrophages.

Next, the time period of treatment was investigated using glucose and lactate metabolism in both LPS and β-glucan. Glucose and lactate levels were significantly higher for C-2-24 compared to C-2-3 ($p = 5 \times 10^{-7}$ and $p = 8 \times 10^{-5}$, respectively). C-3-24 had significantly higher glucose ($p = 9 \times 10^{-6}$) and significantly lower lactate compared to C-3-3 ($p = 5 \times 10^{-5}$). The glucose and lactate levels were significantly higher when comparing F1-2-24 to F1-2-3 ($p = 0.003$ and $p = 8 \times 10^{-5}$, respectively). Lastly, F1-3-24 had significantly higher glucose and lactate concentrations compared to F1-3-3 ($p = 0.0002$ and $p = 0.001$, respectively). Glucose and lactate metabolism is significantly different between two time points.

Glucose and lactate metabolism was observed and compared for macrophages treated with either LPS or β-glucan. C-2-24 had significantly higher glucose and lactate concentrations

compared to C-3-24 ($p = 6 \times 10^{-7}$ and $p = 5 \times 10^{-6}$, respectively). Glucose was significantly higher ($p = 7 \times 10^{-6}$) while lactate was significantly lower ($p = 0.0001$) for C-2-3 when compared to C-3-3. For F1-2-24, there was significantly higher glucose and lactate levels compared to F1-3-24 ($p = 5 \times 10^{-6}$ and $p = 0.0005$, respectively). Finally, glucose and lactate concentrations were significantly higher in F1-2-3 compared to F1-3-3 ($p = 0.02$ and $p = 0.0001$, respectively). In conclusion, glucose and lactate metabolism significantly differs between the treatments of LPS and β-glucan.

To understand the effect that LPS has on the system, glucose and lactate metabolism was investigated. C-2-24 had significantly higher glucose and lactate compared to C-1 ($p = 3 \times 10^{-7}$ and $p = 2 \times 10^{-5}$, respectively). Similarly, glucose and lactate levels were significantly higher for C-2-3 than C-1 ($p = 2 \times 10^{-6}$ and $p = 7 \times 10^{-5}$, respectively). Again, F1-2-24 had significantly higher glucose and lactate concentrations compared to F1-1 ($p = 0.0002$ for glucose and $p = 0.0003$ for lactate). However, glucose was not significantly different and lactate was only trending toward significantly higher when comparing F1-2-3 to F-1 ($p = 0.9$ and $p = 0.08$, respectively). Therefore, LPS significantly dysregulates glucose and lactate metabolism.

Finally, glucose and lactate metabolism were observed to determine the effect of β-glucan on the macrophages. Glucose and lactate levels were significantly higher in C-3-24 when compared to C-1 ($p = 7 \times 10^{-6}$ and $p = 0.0001$, respectively). C-3-3 had significantly higher glucose and lactate levels compared to C-1 ($p = 3 \times 10^{-7}$ and $p = 2 \times 10^{-5}$, respectively). F1-3-24 had significantly higher glucose ($p = 3 \times 10^{-6}$) but no significant difference in lactate levels compared to F1-1. There were significantly lower concentrations of glucose and lactate in F1-3-3 when compared to F1-1 ($p = 0.005$ and $p = 0.0003$, respectively). Glucose and lactate metabolism is significantly dysregulated by the treatment of macrophages with β-glucan.

Discussion.

Measuring multiple analytes on a single sensor platform will allow for the better understanding of and insight into a biological systems' state and interactions before and after perturbations. Developing methods that allow for this, customization of analytes, and automation is pivotal. This platform showed high analyte-sensitivity and had biologically-relevant linear ranges for use with model organ systems. We then used this platform to observe glucose and lactate dysregulated metabolism due to TCDD, LPS, and β-glucan in mice macrophages. Combined with a pump and value system, this multianalyte amperometric biosensor was easy-to-use and allowed for customization to understand cellular respiration, neurotransmission, and oxidative stress for diagnosing and monitoring health and disease.

First, this multianalyte amperometric biosensor was sensitive to seven analytes and included a large linear range that is physiologically relevant for each analyte. These sensitivities are often comparable or even better than previous iterations of these analytical sensors. Glucose is two orders of magnitude higher in sensitivity compared to a similar sensor.[18] This increased sensitivity allowed for a low level of detection and quantitation that can still be used in higher concentrations that is necessary in model organ systems and biological systems. However, lactate had a slightly lower sensitivity compared to a previous sensor, but it was the same order of magnitude.[18] Thus, this will be useful in many applications as well. The glutamate sensor had the same order of magnitude in sensing, but was more than four times the sensitivity of a previously developed sensor.[6] Acetylcholine had a slightly lower sensitivity but was in the same order of magnitude, so it will still allow for the detection and quantification of acetylcholine in many applications.[21] Next, this superoxide sensor was approximately half the sensitivity of a previous sensor, but still provides an analytical signal necessary for measuring a wide range of

concentrations.[10] The ascorbic acid sensor was similar to the previously developed sensor in terms of sensitivity and only minutely more sensitive to ascorbate.[12] Lastly, dopamine had a slightly higher sensitivity but was the same order of magnitude to a similar type of sensor that was previously developed.[95] These sensitivities enabled a large linear range that can be used for a multitude of biological systems.

All of these sensors that had LODs in the single micromolar range or like for lactate and dopamine had their LOD an order of magnitude lower than that as well. However, the LOQ ranged from 2 to 24 μM (lactate and glutamate, respectively). These sensors also range from 39 μM (dopamine) to 4 mM (glucose) in the upper limit of linearity. The linear range of glucose is well suited for detection of cellular glucose consumption and other applications, but cannot detect in most media as many of them have higher concentrations than the upper limit of linearity.[18,31,78,107] The lactate sensor can detect low and higher concentrations that will be helpful in understanding lactate production from cellular respiration and other applications.[18,31,80] The glutamate sensor had a reduced linear range compared to a previous sensor but can still be used to investigate many biological processes that modify glutamate uptake and release.[6,95] The acetylcholine sensor had a larger LOQ, but a higher upper limit of linearity that allows for detection in processes that have larger increases of acetylcholine such as exposure to the environmental toxin, CPF, that increases free-floating acetylcholine.[21,95] Superoxide showed a higher limit of quantitation but encompassed a much larger upper limit of linearity that will allow for quantification of large increases in the reactive oxygen species such as in macrophage oxidative bursts.[10] Next, the ascorbic acid similarly has a higher limit of quantitation but a larger linear range with a significant increase in the upper limit of linearity that will allow for quantitation in many biological processes. This will also allow for the possibility to remove this signal from the other sensor measurements as it is an

electrochemical interferent.[12,18] Lastly, dopamine had a larger linear range that includes slightly lower concentrations for the LOQ and slightly higher concentrations for the upper limit of linearity. Dopamine is generally released at lower concentrations, so this sensor is more applicable to systems that have been treated with higher concentrations of dopamine.[95] Similar to the ascorbic acid sensor, this is also helpful as dopamine is another electrochemical interferent, so it's signal may be removed from the other sensors' signals as well for more accurate results.[95] Therefore, this new multianalyte amperometric biosensor had sensitivity to seven analytes and encompassed a wide range of concentrations that will be helpful for understanding cellular processes and pathways of toxicity to monitor health and disease of biological systems.

Finally, we investigated the values of V_{max} and K_m to further understand the usefulness of this sensor. As an analyte reaches a certain concentration, the enzyme begins to saturate. As more analyte is added, the current (signal) will not increase, and thus the enzyme has reached its maximum rate of reaction, V_{max}. The affinity of the enzyme for its substrate influences how V_{max} relates to concentration. This is quantified by the K_m value, the concentration of substrate when rate of reaction is at half of its maximum. If an enzyme has a low K_m value compared to the physiological concentrations under standard conditions, then the enzyme will turn over substrate at a constant rate regardless of concentration variations. However, a high K_m value when compared to physiological concentrations under standard conditions, will result in enzyme activity that varies with substrate concentration (depends on the availability of substrate). The glucose sensor had lower V_{max} and K_m values than previously reported (and lower K_m, than physiological concentrations) so the enzyme had a high affinity but does sacrifice in its upper limit of linearity.[18,78] Lactate had very similar values for these parameters compared to previous sensors with a higher K_m value than the physiological concentrations, so this sensor will be well suited for

many biological applications and will not sacrifice sensitivity.[18,78] Next, the glutamate sensor had slightly lower V_{max} and an order of magnitude lower K_m, meaning the limit of linearity is reduced, but this is still lower than physiological concentrations so it will be well suited for a range of biological applications.[6,95] The V_{max} and K_m values for the acetylcholine sensor were an order of magnitude lower than previously reported and lower than physiological concentrations, so this sensor loses some sensitivity and raises the limit of detection/quantification.[21,95] The superoxide sensor had a slightly lower K_m value that is around the physiological concentrations, so it will have the ability to measure the a large range of biologically-relevant concentrations.[10] For the ascorbic acid sensor, the K_m value is lower than physiological levels, so this sensor will be well suited for a variety of applications without sacrificing sensitivity.[12] Finally, the dopamine sensor had slightly increased V_{max} and K_m values were higher than previously reported and K_m is higher than most physiological concentrations, so this sensor can quantify dopamine in a wide range of biological applications. Thus, these sensors had V_{max} and K_m values that will allow for the quantification of the seven analytes.

To establish how TCDD affects a system, glucose and lactate concentrations were monitored in macrophages from mice exposed to TCDD *in utero*. TCDD is part of a large class of environmental toxicants called dioxins that affect the endocrine system and disrupt metabolism.[43] Glucose and lactate were monitored in macrophages to illustrate the capability to measure multiple replicates of a single analyte. TCDD decreased glucose consumption and increased lactate production in F1-1 compared to C-1. Perhaps, the macrophages were releasing glucose from glycogen stores or have a glucose intolerance that has led to this dysregulated metabolism.[4,108–110] These macrophages may also be depleting the glycogen stores and converting glucose straight to lactate to compensate for the stress of the toxicant and its endocrine disruption for anaerobic

respiration.[4,107,109,110] Glucose consumption was increased and lactate production was increased in F1-2-24 when compared to C-2-24. The stress of TCDD caused increased glucose consumption to promote macrophage response, dysregulating glucose metabolism in the macrophages and encouraged aerobic respiration.[45,107] Lactate is again being produced more to compensate for the toxicity and disruption, showing how TCDD dysregulated the lactate metabolism and promoted anaerobic respiration as well.[4,107] F1-2-3 consumed more glucose than C-2-3. Again, glucose metabolism is dysregulated with possibly increased glycogen storage.[4] F1-3-24 had decreased glucose consumption and increased lactate production compared to C-3-24. This set mimics several of the previous sets and likely is showing anaerobic metabolism with glucose being released from storage or a glucose intolerance.[107,111] Lastly, TCDD decreased lactate production and slightly increased glucose consumption in F-3-3 compared to C-3-3. Here, glucose metabolism is only slightly dysregulated, so maybe there was recovery from previous glucose intolerance or glycogen stores were staying filled. Furthermore, this dysregulated metabolism with decreased lactate production may be due glycogen stores not being converted back to glucose.[4,107,111] Therefore, TCDD decreased glucose consumption and dysregulated lactate production, showing TCDD affected inflammatory response, dysregulated metabolism and caused toxicity.

With increased cytokines and interleukins, LPS stimulates a strong inflammatory response within the system.[43–45,107] Glucose and lactate metabolism of macrophages provide insight into the mechanisms and toxicity of LPS in the system. C-2-24 had decreased glucose consumption and increased lactate production compared to C-1. Similarly, C-2-3 had decreased glucose consumption and increased lactate production in comparison to C-1. F1-2-24 also consumed less glucose and produced more lactate than F1-1. However, F1-2-3 had only slightly increased lactate production compared to F1-1. Based on these results, there was increased lactate production, so

the macrophages were undergoing anaerobic metabolism and were stressed from exposure to LPS.[4,45,107] In general, glucose consumption was reduced, so potentially this lactate was produced from glycogen storage.[4,109,110] Similarly, glucose was possibly released from glycogen storage or may have had a glucose intolerance, explaining the dysregulated metabolism and increased glucose seen in the results.[4,108–110] Therefore, LPS significantly dysregulated glucose metabolism and increased lactate production in mice macrophages, indicating the inflammatory response metabolic profile has been affected like in diseases such as endometriosis.

Next, we investigated the effect of β-glucan on macrophages using glucose and lactate metabolism. C-3-24 had decreased glucose consumption and increased lactate production compared to C-1. Similarly, C-3-3 showed decreased glucose consumption and increased lactate production compared to C-1. These control cells that were then exposed to β-glucan both had decreased glucose consumption and increased lactate production, so it is likely β-glucan has an effect on their metabolic profile. They may have had a glucose intolerance or glucose was released from storage.[4,108–110] Furthermore, there was increased lactate production for anaerobic respiration likely due to released glucose from storage and showed the promotion of macrophage response and immunity training.[45,107,111] However, F1-3-24 only consumed less glucose compared to F1-1. In addition, F1-3-3 had increased glucose consumption and decreased lactate production compared to F1-1. TCDD-exposed macrophage cells also treated with β-glucan seemed to reverse metabolism compared to control cells at the 3dp time point. β-glucan reversed the metabolism of the TCDD-exposed macrophages. It was training immunity and compensating for stress of TCDD by recruiting more glucose to promote macrophage response.[3,45] However, lactate was produced less or even unaffected, so glucose may have been being stored as glycogen in glycogenesis instead of completing anaerobic glycolysis.[4,107,109,110] Thus, β-glucan had a significant effect on the

macrophages, decreasing the glucose consumption in control macrophages while increasing glucose consumption in TCDD-exposed macrophages. In contrast, there was increased lactate production in control macrophages and decreased lactate production in TCDD-exposed macrophages.

Furthermore, the treatment time of LPS and β-glucan was observed using glucose and lactate metabolism. C-2-24 had reduced glucose consumption and increased lactate production compared to C-2-3. C-3-24 consumed less glucose, but produced more lactate compared to C-3-3. There was decreased glucose consumption and increased lactate production in F1-2-24 in comparison to F1-2-3. Similarly, F1-3-24 had decreased glucose consumption and increased lactate production. All of these follow anaerobic metabolism with increased lactate production.[107,111] Furthermore, it is likely glucose was released from glycogen stores or there was a glucose intolerance that is responsible for increased glucose concentrations.[2,4,110] Thus the 24 hour time point had deceased glucose consumption and increased lactate production compared to the 3 days post injection that indicated anaerobic respiration and dysregulated metabolism in inflammatory biomarkers similar to endometriosis.

Lastly, the difference in glucose and lactate metabolism was investigated for macrophages treated with either LPS or β-glucan. C-2-24 consumed less glucose and produced more lactate compared to C-3-24. There was less glucose consumption, and less lactate production in C-2-3 compared to C-3-3. When comparing F1-2-24 to F1-3-24, F1-2-24 had less glucose consumption and more lactate production. Similar to the previous set, F1-2-3 had decreased glucose consumption and increased lactate production in comparison to F1-3-3. In comparing all of these, there was decreased glucose consumption, revealing a glucose intolerance or release of glycogen stores.[2,4,110] One set had decreased lactate production, a possible consequence of decreased glucose

consumption and glucose storage instead of anaerobic respiration, indicating aerobic respiration. However, in general there was increased lactate production, showing anaerobic respiration to protect from toxicity stress. These results show how β-glucan is training the immune system and causing increased lactate production. However, there was decreased glucose consumption, so there were more complicated mechanisms of toxicity and immunity at work. Therefore, LPS caused attenuated glucose consumption and dysregulated lactate production compared to β-glucan, indicating dysregulated macrophage metabolism and possible toxicity similar to endometriosis.

Conclusions.

We present a new multianalyte amperometric biosensor platform that quantifies glucose, lactate, glutamate, acetylcholine, dopamine, ascorbic acid, and superoxide concentrations simultaneously. These are enzymatic-based and may be customized to the most applicable analytes for a biological system of interest for a versatile format. The pump and valve system provided automation for ease-of-use, while the sensor quantified multiple analytes, giving a better understanding of the state and interactions of a system. These sensors gave a high analytical sensitivity, while providing a wide linear range that may be used to understand the metabolic profiles of biological systems. We applied this system to understand the effects of TCDD, LPS, and β-glucan on the macrophages of mice in relation to health and disease. These results revealed that 1) TCDD decreased glucose consumption and dysregulated lactate production; 2) LPS dysregulated glucose consumption and increased lactate production; 3) β-glucan dysregulated glucose and lactate metabolism differently in control and TCDD-exposed macrophages; 4) LPS decreased glucose consumption more and dysregulated lactate metabolism differently than β-glucan; and 5) 24 hour treatment time period decreased glucose consumption and increased lactate production compared to the 3 day post injection time point. This platform utilizes a multianalyte amperometric biosensor and pump and valve system that can be used and translated to other biological applications to understand cellular processes and pathways of toxicity to monitor health and disease.

Acknowledgments.

This work was also supported in part by the National Institute of Health training grant (ES007028), EPA (83573601), and NIH (1R01HD102752-01) and using the resources of the Vanderbilt Microfabrication Core operated by the Vanderbilt Institute for Integrative Biosystems

Research and Education. The authors would like to thank Victoria Stephens and Kevin Osteen for providing samples and Dusty Miller for assistance in designing and performing experiments.

Chapter V

DEVELOPMENT AND APPLICATION OF A DUAL AMPEROMETRIC AND POTENTIOMETRIC MULTIANALYTE ELECTROCHEMICAL BIOSENSOR

Electrochemical detection is used as an analytical tool in a variety of applications such as monitoring environmental toxins, health, and disease.[18,22,24,25,49] The development of electrochemical biosensors has significantly expanded the analytical toolbox by allowing detection of an increasing number of analytes and by taking advantage of multiple techniques, including amperometry and potentiometry.[18,25,33] Previously, most sensors have monitored only a single analyte at a time or have focused solely on either amperometric or potentiometric detection methods.[4,18,24] However, there are a few instances of multianalyte and simultaneous amperometric and potentiometric detection.[25,33] Simultaneous and multiplexed analyte detection is critical and provides the most information for determining metabolic pathways, as well as diagnosing and monitoring health and disease. In this work, a dual enzymatic and ionophore multianalyte (up to eight analytes) electrochemical biosensor was developed, allowing for detection of more analytes using multiple techniques. We quantified glucose, lactate, ammonium, and potassium simultaneously by utilizing oxidase enzymes and ionophore-based membranes in a multianalyte multi-method sensor platform. This biosensor array provides a platform that can detect and quantify a variety of analytes of interest depending on the application.

Enzymatic sensors are the most widely-used electrochemical sensors and use amperometry as the method for detection and quantification. However, using a sensor that detects only one analyte does not account for all the necessary analytes that help to elucidate pathways and mechanisms. Previously, electrochemical sensors only detected one analyte for example, a glucose

sensor for diabetics.[4] Furthermore, sensors were only capable of one technique, for instance, amperometry or potentiometry.[24,91] However, it became necessary to quantify multiple analytes simultaneously.[29,31] In the last few years, researchers have developed multiplexed and simultaneous detection and quantification of analytes on one electrode array using amperometric and potentiometric methods.[22,25,33] This presents a larger realm of possibilities to determine the mechanisms and pathways of toxicity.[4] However, these systems have not allowed for customization to a particular biological application, thus foreclosing the possibility of detecting many different analytes.[24] In addition, these systems do not detect more than a handful of analytes simultaneously, are not automated, and cannot be fully integrated for real-time measurements.[22,24,25] Therefore, there is a need for a multiplexed platform that will provide automation and integration as well as simultaneous detection and quantification of multiple analytes.[24]

To address these needs, simultaneous and multianalyte detection and quantification in an interchangeable, automated platform was developed and investigated. A setup comprised of a pump and valve used for automation is similar to the previously developed microformulator.[46] This biosensor presents the opportunity for researchers to not only replicate this study, but it allows for the customization using different enzymes and ionophores such as glutamate oxidase or Sodium Ionophore X (used to sense the sodium ion) that were not used in this research.[6,112] By having both amperometric and potentiometric sensors together on one small chip, there are more options for metabolite detection that can then be used in model systems to determine toxicity and evaluate the potential of therapeutics.[4] Combining a pump and valve with this multiplexed, multianalyte electrochemical biosensor allows this platform to become automated and add more metabolites to the toolbox to learn more about the biosignature of a system.

Currently, the effect that 2,3,7,8-tetrachlorodibenzodioxin (TCDD) and lipopolysaccharides (LPS) has on metabolism in the peritoneal cavity of mice is unknown. TCDD is used as a model endocrine/immune disrupting toxicant for studies and has been shown to contribute to a hyperinflammatory uterine and peritoneal cavity environment.[37,43] Though mice do not menstruate, TCDD-exposed mice show remarkably similar phenotypes to women with endometriosis.[43] LPS also stimulates an inflammatory response in a biological system.[43,44,105] In addition, many reproductive failures are said to be a result of the "second hit" hypothesis: an inflammatory trigger like LPS arises after the initial problem.[43,44] Thus, it is of interest to look into these relationships and how they may affect metabolism within the mice to understand the pathways of toxicity and disease.

To answer questions about how TCDD and LPS dysregulate systems and gain insight into these relationships, glucose, lactate, ammonium, and potassium metabolism in a mouse model was investigated. Because the peritoneal cavity contains several organs and deals with many different cell types, a peritoneal lavage is important for a comprehensive understanding of pathways and functions in the body such as with endometriosis.[37,44] Glucose, lactate, ammonium, and potassium highlight a few metabolic pathways (cellular respiration and urea cycle) and are key to determining more information about the system.[4,15,17,24,94,102,103]

In this work, two potentiometric sensors were developed and used in conjunction with enzymatic-based sensors to provide more insight into the disruption of metabolic and disease pathogenesis in mice exposed to TCDD and LPS. Combining these sensors together represents a new method to rapidly analyze biological systems by electrochemically monitoring cellular viability, performing toxicity screenings, and elucidating metabolic pathways. A formulation of the potentiometric sensor membrane that exhibited the most sensitivity was determined.

Calibrations were performed to cover biologically-relevant linear ranges while maintaining sensitivity. Operational longevity studies for the sensors' performance indicated that this system could be used for interfacing with continuously operational systems such as organs-on-chips. These ionophore-based sensors were combined with enzymatic sensors for a larger biosignature that was used to test samples from a peritoneal lavage in mice. We studied the effects of TCDD and LPS on glucose, lactate, ammonium, and potassium metabolism in a mouse model.

Experimental.

Material Procurement

Dihydrogen potassium phosphate and sodium phosphate dibasic (buffer) were procured from Fisher Scientific (Hampton, NH). Dibutyl sebacate (selectophore), ammonium ionophore I, ammonium ionophore I – cocktail A (selectophore), potassium ionophore I, bovine serum albumin (BSA), GOx from *Aspergillus niger* (152.54 U mg^{-1}), LOx from *Aerococcus viridians* (11.29 U mg^{-1}), and glutaraldehyde (25% by wt. aqueous solution) were purchased from Sigma Aldrich (St. Louis, MO). β-D-Glucose was purchased from Calbiochem (San Diego, CA), and sodium L-lactate was purchased from Alfa Aesar (Haverhill, MA). Ammonium chloride was purchased from Sigma Aldrich (St. Louis, MO) and potassium chloride was purchased from Fisher Scientific (Fair Lawn, NJ) for use in calibrations. Poly(vinyl) chloride) (PVC; selectophore, high molecular weight), bis(2-ethylhexyl) sebacate (DOS; selectophore), nitrophenyl octyl ether (2-NPOE; selectophore), potassium tetrakis(4-chlorophenyl)borate (PTCPB; selectophore), and dibutyl sebacate (DBS; selectophore) were procured from Fluka Analytical (St. Louis, MO). Tetrahydrofuran (THF) was purchased from Sigma Aldrich (St. Louis, MO). All reagents were used as received and without additional purification. TCDD (99% purity) in nonane solution (50 ug/mL) was obtained from Cambridge Isotope Laboratories (Andover, MA). Lipopolysaccharide (LPS), obtained from Enzo Life Sciences (Plymouth Meeting, PA), was derived from E. coli (serotype 055:B5 S-form, TLR grade). Finally, phosphate buffer solution (PBS) 1X was purchased from Mediatech, Inc. (a Corning subsidiary; Manassas, VA).

The housing for this 8-channel sensor was designed by The Vanderbilt Institute for Integrative Biosystems Research and Education (VIIBRE, Nashville, TN) and made of polymethylmethacrylate (PMMA) by the Vanderbilt Microfabrication Core (VMFC, Nashville,

TN) that is operated by VIIBRE. Polydimethylsiloxane (PDMS) microfluidic with etched channels from VMFC. SPEs were designed in-house and fabricated by Sullins Connector Solutions (San Marcos, CA). Detailed information for the materials of a previous iteration of this device and the screen-printed electrodes can be found elsewhere.[6,18] This system is similar, but has a few different specifications that are detailed below in the *Electrochemical Housing Configuration* section. To automate the system, rotary planar peristaltic micropumps, rotary planar peristaltic twenty-five port valves, microcontrollers, and computer software (AMPERE) were implemented in the system (VIIBRE/VMFC).[46] The CHI 1440 potentiostat was purchased from CH Instruments (Austin, TX) and used in the electrochemical (amperometric and potentiometric) measurements.

For all studies, virgin female and male C57BL/6 mice were purchased from Harlan Sprague-Dawley (now Envigo; Indianapolis, IN) and housed in Vanderbilt University Medical Center's Animal Care Facility (Nashville, TN) according to National Institutes of Health and institutional guidelines for laboratory animals. All animals received food and water ad libitum. Animal rooms were maintained at a temperature of 22.8 °C–24.8 °C and a relative humidity of 40%–50% on a 12L:12D schedule. All original studies involving mice were approved by the Vanderbilt University Institutional Animal Care and Use Committee in accordance with the Animal Welfare Act.

Electrochemical Housing Configuration

The setup was comprised of a screen-printed electrode (SPE) with a PDMS microfluidic on top, held together between two pieces of PMMA housing using four screws. This setup was used for calibrations and sample analysis. SPEs served as the underlying substrate for this platform and were modified for sensitivity and selectivity.[18,29] The SPE featured nine parallel 1.16 mm^2 rectangular working electrodes (A = 1.16 mm^2), a large rectangular counter electrode, and a

circular reference electrode, all printed in platinum on a ceramic base (**Figure 5.1 – right**). Each working electrode was modified for a specific analyte of interest. The PDMS microfluidic has eight parallel channels that create separate flow chambers, ultimately forming the housing for the SPE (**Figure 5.1 – left**). Experiments were performed using the modified SPEs in the microfluidic flow chamber that was aligned to have a single channel over each of the working electrodes.

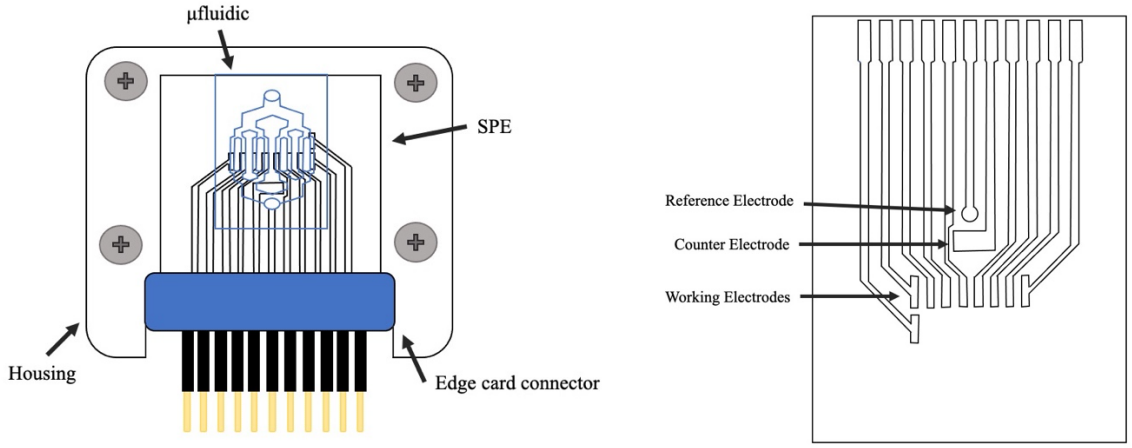

Figure 5.1. Schematics of electrode housing and electrode array. Left displays the screen-printed electrode (SPE), microfluidic (light blue), housing, and edge card connector (blue). The SPE is on a PMMA base and then a microfluidic is on top of the SPE to create eight separate channels. The SPE is inserted into the edge connector on one side, which in turn is connected to the potentiostat on the other side (black/gold). Finally, the second PMMA piece is placed top and screwed in to make the entire electrode housing. Right shows the SPE with a circular reference electrode, a large rectangular counter electrode, and nine small rectangular working electrodes.

Electrode Modification

To make these biosensors, reference and working electrodes were generated through electrodeposition and various solution modifications. To make the internal reference electrode, silver was electrodeposited on the electrode followed by immersion in an $FeCl_3$ solution, creating the Ag/AgCl interface similar to previously developed methods.[18,29,73] Then, working electrodes had either an enzymatic mixture or an ionophore membrane solution deposited on the electrode for detection of glucose, lactate, ammonium, or potassium.

Enzymatic films were prepared using an enzyme, BSA, and glutaraldehyde for selectivity and sensitivity.[18] The sensors were prepared with 0.25 mg mL^{-1} glucose oxidase and 10 mg mL^{-1} lactate oxidase. BSA (62.5 mg mL^{-1}) in buffer (50 mM) and glutaraldehyde (0.25% w/v) were used for crosslinking in the enzymatic solutions.[31] These solutions were vortexed for five seconds and then immediately deposited on the SPE. The enzyme-BSA-glutaraldehyde solutions were dropcast as 0.5-µL aliquots onto the working electrodes to create enzyme films. These sensors were dried and stored while covered at room temperature.

The ionophore membrane solutions were made from different components with varying ratios. Each of the formulations was mixed together, vortexed for five seconds, and then immediately dropcast on the electrode. Lastly, they were covered and left to dry covered overnight at room temperature. All of the following are weight by weight percentages. The microelectrode formulation was 3.50% nonactin, 0.35% PTCPB, 0.90% PVC, 32.95% DBS, and 62.30% THF.[113] The next mixture is cocktail A made from 6.9% nonactin, 92.4% 2-NPOE, and 0.7% PTCPB.[114] Formulation 1 had 1% nonactin, 66.80% DOS, and 32.20% PVC.[115] Formulation 2 was 1% nonactin or valinomycin, 33% PVC, and 66% DBS.[116] Lastly, formulation 3 was 0.20% nonactin, 69% 2-NPOE, and 30.80% PVC.[117] Each of these solutions was then added to 1 mL of THF to

dissolve all of the components and allow for the deposition of the membrane on the electrode. Similar to the enzymatic solutions, these were dropcast as 0.5-µL aliquots onto the working electrodes to create the membranes. The sensors were then dried overnight and stored while covered at room temperature. The final mixture that is used for all sensors after this set of experiments contained the pertinent ionophore for selectivity (ammonium – nonactin and potassium – valinomycin), a solvent to dissolve the materials in order to drop cast (THF), and plasticizers to harden the solution (PVC and dibutyl sebacate).

Sensor Calibrations

Calibrations were completed from ammonium chloride and potassium chloride standards using a system comprised of automated pumps and valves, the SPE and its housing, and a potentiostat. Standards for both of the chemicals were prepared in a buffer solution (2 mM buffer, pH 7.00). Comprised of 24 calibrants, the analyte ranges used in this study were 0-50 mM for both of the analytes, which allowed for the linear range of each analyte to be determined. To establish a baseline for the calibrations, the same background buffered saline solution was flowed between every calibrant. A pump and valve system (flow rate of 75 µL min^{-1}) was used for automation, increased sample/calibrant throughput, and ease of use.[6] The set up described above was operated in conjunction with the potentiostats to measure the calibrant signals. A CHI 1440 multichannel potentiostat was used to record the amperometric signals (glucose and lactate, sampling frequency of 1 sec^{-1}) as well as the potentiometric signals (ammonium and potassium, sampling frequency of 1 sec^{-1}). The potential for glucose and lactate quantification is held at 0.6 V (vs. internal Ag/AgCl).[18] No potential is applied for the other analytes as that is what is measured.

Reference Coating

To determine the usefulness of a membrane coating on the reference, a comparison study was completed with and without the reference membrane coating. A working electrode was modified with the analyte (ionophore)-sensing membrane. Then, the reference electrode was left alone as is usual with enzymatic sensors or was modified with a membrane. For the reference coating comparison, a similar procedure was followed to create the solution except the ionophore (nonactin/valinomycin) was left out of the solutions of formulation 2. The membrane solutions were dropcast as 0.5-µL aliquots onto the already coated Ag/AgCl reference electrode to create the reference coating.

Operational Longevity

Calibrations (24 calibrants within linear range) were completed for the potentiometric sensors to ensure operational longevity for continuously operational systems. The enzymatic sensors have previously shown strong operational longevity.[31] Standards for the analytes of interest contained increasing quantities of ammonium or potassium in a buffered solution. This same buffered solution was also used as the baseline for all of the calibrations and flowed between every calibrant. Similar parameters were used for the sensor calibrations previously stated above. In short, the same system comprised of automated pumps (flow rate of 75 µL min^{-1}) and valves, the SPE and housing, and the potentiostat (CHI 1440) were used in these experiments. After each calibration, the system had buffer solution flowed through constantly until the next calibration. Another calibration was analyzed until calibrations for eight days were completed.

TCDD and LPS Treatment

Virgin C57BL/6 females (N 1⁄4 25), aged 10–12 wk, were mated with intact males of similar age. Upon observation of a vaginal plug, females were separated and denoted as Day 0.5 of pregnancy (E0.5). Mice were monitored for weight gain and nipple prominence, which are

indicative of pregnancy. Pregnant mice (F0) were exposed to TCDD (10 lg kg^{-1}) in corn oil or vehicle alone by gavage on E15.5 (when organogenesis is complete). To ensure consistency across all studies, exposure of pregnant mice is routinely performed at 1100 h local time. This in utero plus lactational exposure paradigm results in direct exposure of the fetuses (F1 mice) as well as direct exposure of the fetal germ cells, which have the potential to become the F2 generation. This dose of TCDD reflects the more rapid clearance of this toxicant in mice compared with humans and is well below the LD50 for adult mice of this strain (230 lg kg^{-1}) [23]. TCDD given at this time and dose is not overtly teratogenic, and gestation length was not affected in the F0 animals; pups (F1 mice) were typically born on E20.

Calculations and Statistics

Using linear and non-linear regression of the current versus concentration, limit of quantitation, the maximum limit of linearity, and sensitivity of the electrode were determined. By dividing ten times the error of the blank (buffered saline solution) by the sensitivity, the limit of quantitation was determined.[21] Using the linear range of the data set (limit of quantitation to maximum limit of linearity), a regression of this data set produced the sensitivity of the electrode based on the slope of the line.[21]

All data were analyzed with GraphPad Prism 9 (La Jolla, CA). Data from experiments were analyzed using a two-tailed unmatched t-test. All data values are presented as mean ± SEM unless otherwise noted. A p value ≤ 0.05 was considered statistically significant.

Results.

Electrode Modification

To determine the best formulation for the potentiometric sensors, five different formulations that have commonly used membrane ingredients were measured for sensitivity. Nonactin was used as the sensing component, so the sensitivity to ammonium is used as the comparison measurement. The Microelectrode formulation has a sensitivity of 111 ± 6 mV per decade of concentration (order of magnitude of concentration), while Cocktail A had a sensitivity of 95 ± 11 mV decade^{-1}. Formulation 1 showed a sensitivity of 68 ± 5 mV decade^{-1}. Then, Formulation 2 was sensitive to ammonium at 57 ± 9 mV decade^{-1}. Lastly, Formulation 3 had a sensitivity of 138 ± 7 mV decade^{-1} (**Figure 5.2**). The comparison of these membrane formulations indicated that Formulation 2 showed the best membrane formulation because it was closest to the ideal sensitivity of 59.2 mV decade^{-1} (indicated by the red dashed line – **Figure 5.2**).

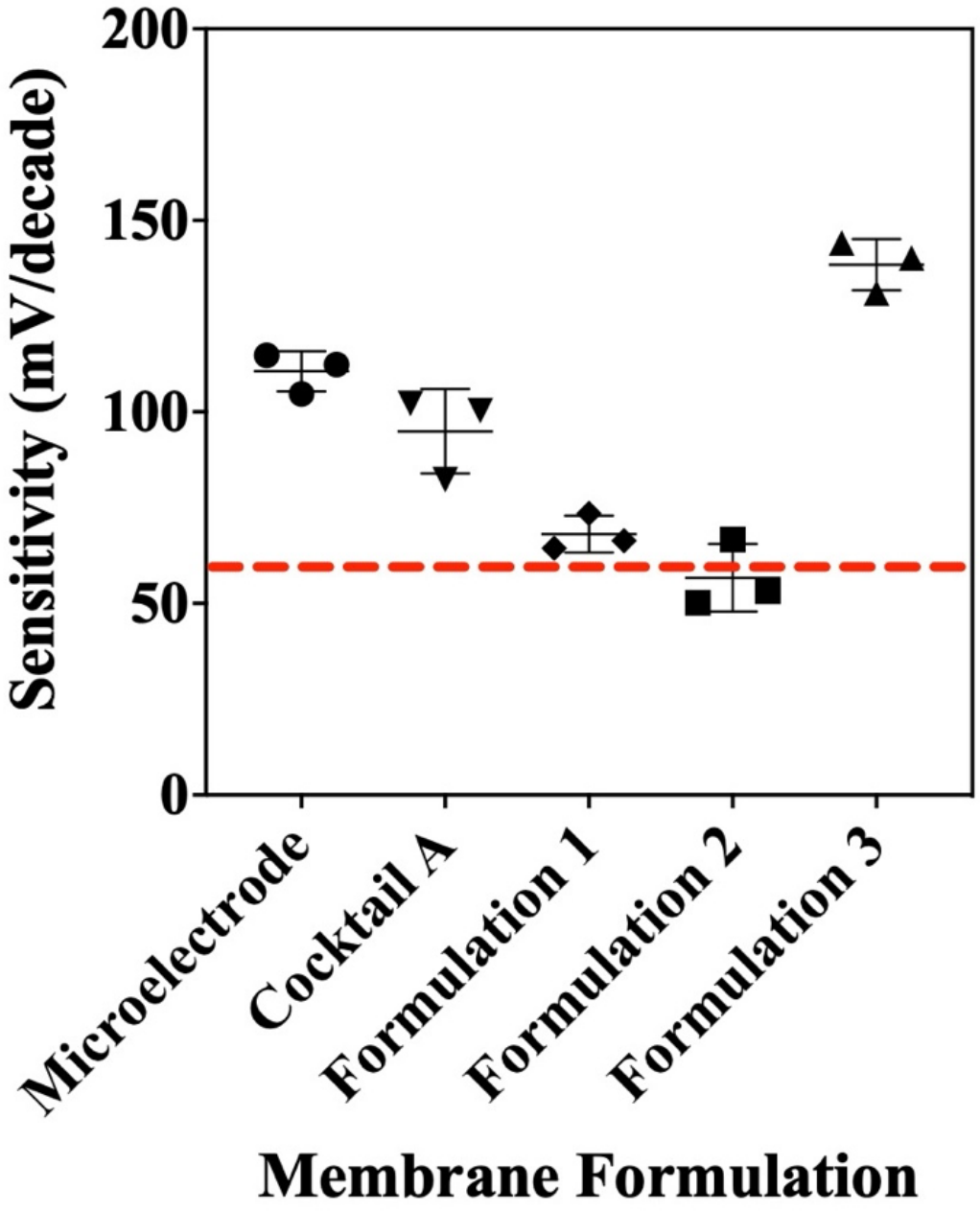

Figure 5.2. Membrane Formulation and Sensitivity for Ammonium Sensor. Scatter plot displaying the sensitivities to ammonium for different membrane formulations. The red line denotes the theoretical value for sensitivity and therefore, the membrane formulation closest will be taken as the formulation type used for all future experiments. The microelectrode formulation had a sensitivity of 111 ± 6 mV decade^{-1}. Cocktail A showed a sensitivity of 95 ± 11 mV decade^{-1}, while the Formulation 1 was 68 ± 5 mV decade^{-1}. Formulation 2 had a sensitivity of 57 ± 9 mV decade^{-1}. Lastly, Formulation 3 had a sensitivity of 138 ± 7 mV decade^{-1}. Experiments were performed in buffer (ambient conditions). Data represented as an average and standard deviation with n = 3 technical replicates.

Reference Coating

The necessity for a reference coating, which is standard generally, was investigated by comparing sensitivities to ammonium and potassium with and without the coating.[22] For the coated reference electrode with the ammonium sensor, the sensitivity was 44 ± 2 mV decade^{-1}. The uncoated reference electrode of the ammonium sensor had a sensitivity of 42 ± 9 mV decade^{-1} (**Figure 5.3, left**). Similarly, potassium sensors were tested for comparison of coated and uncoated reference electrodes. The coated reference electrode had a sensitivity of 51 ± 12 mV decade^{-1} while the coated reference electrode had a sensitivity of 38 ± 13 mV decade^{-1} (**Figure 5.3, right**). Coated and uncoated reference electrodes were not significantly different for ammonium ($p = 0.77$) and potassium ($p = 0.27$).

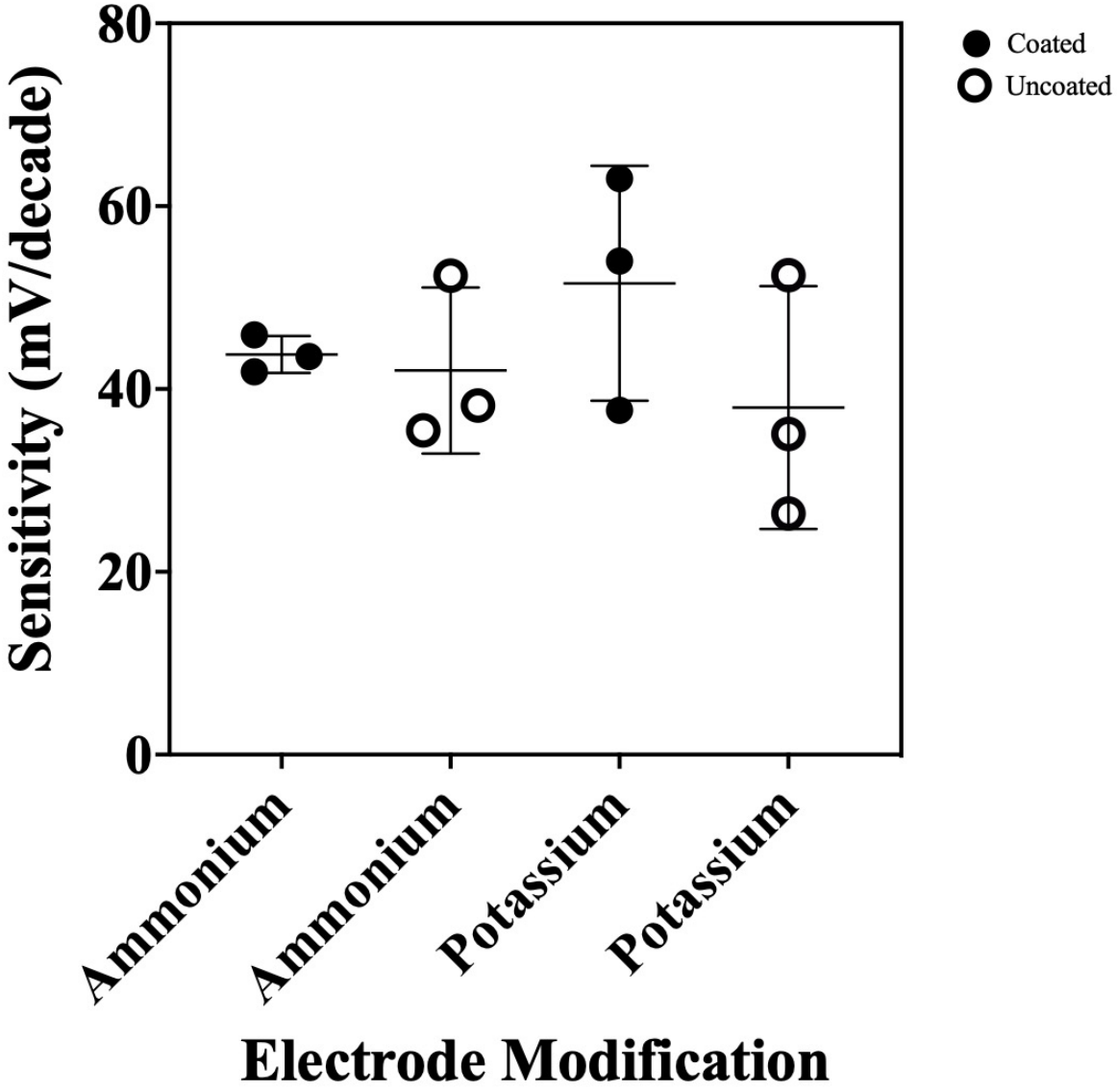

Figure 5.3. Reference Electrode Coating Determination. A scatter plot displaying the sensitivities to ammonium (left) or potassium (right) with a coated (filled circle) or uncoated (unfilled circle) reference electrode. The ammonium sensor with a coated reference had a sensitivity of 44 ± 2 mV decade^{-1}, while the uncoated reference had a sensitivity of 42 ± 9 mV decade^{-1}. This was not significantly different ($p = 0.77$). The potassium sensor with a coated reference had a sensitivity of 51 ± 12 mV decade^{-1}, and the uncoated reference electrode for potassium had a sensitivity of 38 ± 13 mV decade^{-1}. This was not significantly different ($p = 0.27$). Experiments were performed in buffer (ambient conditions). Data represented as an average and standard deviation with $n = 3$ technical replicates.

Sensor Calibrations

Calibrations were performed for both of the potentiometric sensors to determine various parameters. The sensitivity of the ammonium sensor was given by the equation, $y = (57 \pm 5)x - (77 \pm 3)$ with an R^2 of 0.99 (**Figure 5.4, left**). Similarly, the newly developed potassium sensor was tested to determine the sensitivity, which is given by the line, $y = (75 \pm 2)x + (30 \pm 9)$ with an R^2 of 0.99 (**Figure 5.4, right**). Both of these sensors showed sensitivity to their respective analytes.

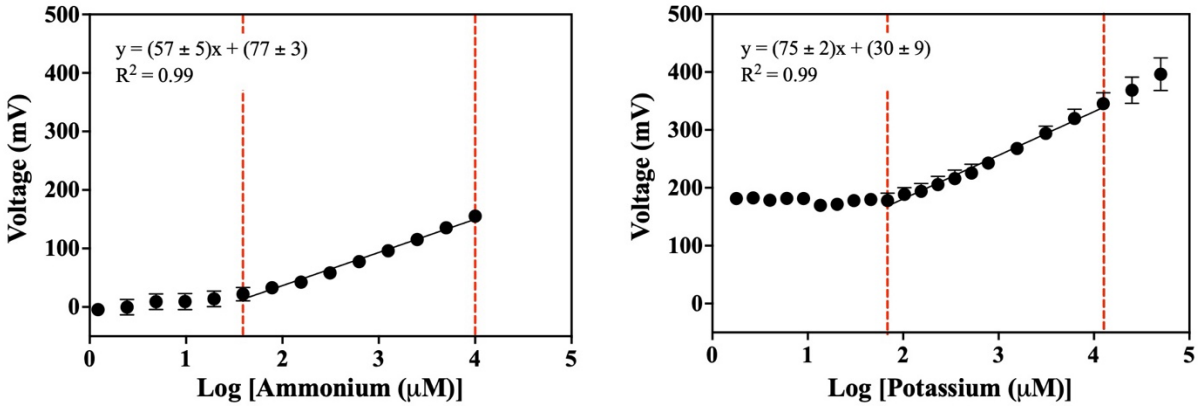

Figure 5.4. Calibration Curves of Potentiometric Sensors. These are for ammonium (left) and potassium (right) sensors with voltage vs. the logarithm of the analyte concentration, showing the linear range, sensitivity, and limits of linearity (shown as the two red dashed lines). On the left, the slope is given by the line, $y = (57 \pm 5)x - (77 \pm 3)$ with an $R^2 = 0.99$. On the right, the slope is given by the line, $y = (75 \pm 2)x + (30 \pm 9)$ with an $R^2 = 0.99$. The linear range for the ammonium sensor was 21 μM – 10 mM and for the potassium sensor it was 80 μM – 12 mM. Experiments were performed in buffer (ambient conditions). Data represented as an average and standard deviation, n = 3 technical replicates.

Calibrations were performed with 24 calibrants for ammonium and potassium to test the linear range. Ammonium was detected as low as 3 μM and quantified as low as 21 μM. At higher concentrations of ammonium, the data began to deviate from linearity at 10 mM, thus the linear range for ammonium was 21 μM – 10 mM (**Figure 5.4, left).** Similarly, the potassium sensor was tested to determine the linear range. The limit of detection was 3 μM while the limit of quantitation was 80 μM. The data began to deviate from linearity at 12 mM, making the linear range 80 μM – 12 mM (**Figure 5.4, right**). Both of these sensors offered a wide biologically-relevant linear range.

Operational Longevity

The sensitivities of the potentiometric sensors were monitored over time to investigate the long-term stability of sensor performance. To accomplish this, a calibration was carried out frequently over a total of eight days for the ammonium and potassium sensors. The sensitivity of the ammonium sensor decreased from 57 ± 5 mv decade^{-1} to 32 ± 2 mV decade^{-1}, a 44% decrease. The sensitivity of the potassium sensor decreased from 75 ± 2 mV decade^{-1} to 42.2 ± 0.5 mV decade^{-1}, a 44% decrease (**Figure 5.5**).

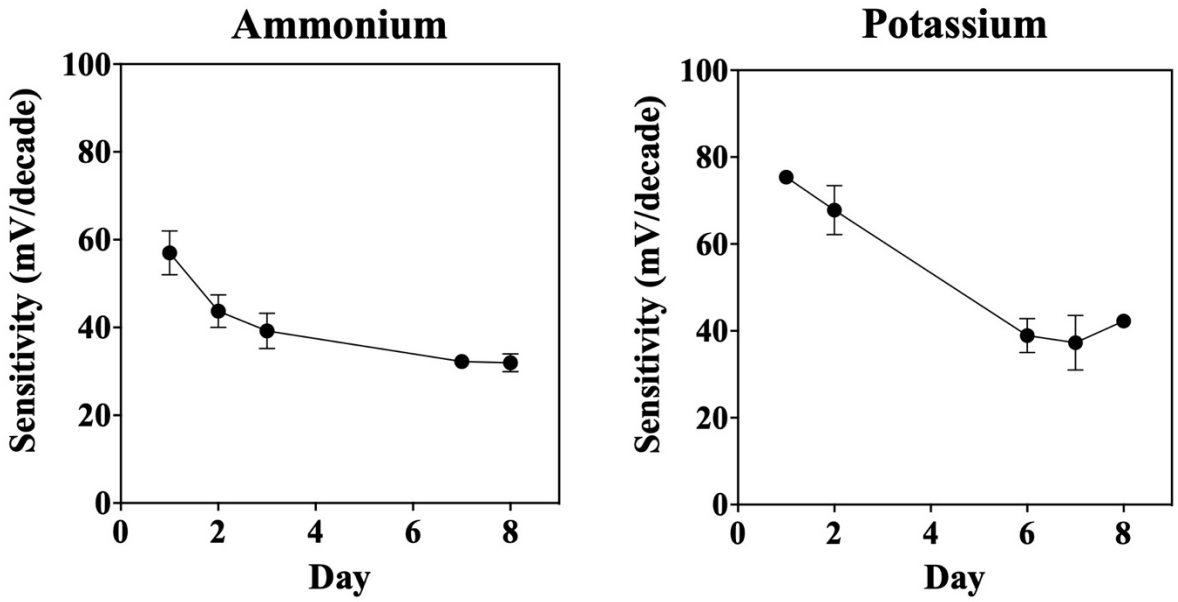

Figure 5.5. Operational Longevity of the Potentiometric Sensors. These graphs display the data from ammonium (left) and potassium (right) sensors that were tested by calibrating frequently over an eight-day period. The sensitivity (mV decade^{-1}) vs. calibration day is reported above. The sensitivity of the ammonium sensor decreased from 57 ± 5 mv decade^{-1} to 32 ± 2 mV decade^{-1}, and the potassium sensor sensitivity decreased from 75 ± 2 mV decade^{-1} to 42.2 ± 0.5 mV decade^{-1} in the course of the study. Experiments were performed in buffer solution (ambient conditions). Data is represented as the average with SEM, n = 3 technical replicates.

Biological Samples

To test the biological relevance of the potentiometric sensors, ammonium and potassium as well as glucose and lactate were quantified in samples from peritoneal lavages of mice. These sensors were also used in conjunction with amperometric sensors to quantify glucose and lactate. The mice consisted of two groups of treatment: group A) control mice and group B) mice exposed to TCDD in utero (F1). Then, each group was given two protocols for treatment: protocol 1) treated with LPS protocol 2) treated with PBS (no LPS) (**Table 5.1**). This gave four groups of mice with different treatments, denoted as A1, A2, B1, and B2. A1 showed 126 ± 17 μM glucose, 198 ± 35 μM lactate, 1.3 ± 0.3 mM ammonium, and 1.8 ± 0.5 mM potassium. B2 had 123 ± 69 μM glucose, 231 ± 43 μM lactate, 0.4 ± 0.4 mM ammonium, and 0.8 ± 0.7 mM potassium. A2 had 174 ± 27 μM glucose, 182 ± 21 μM lactate, 1.1 ± 0.3 mM ammonium, and 1.4 ± 0.1 mM potassium. Lastly, B1 showed 230 ± 41 μM glucose, 236 ± 24 μM lactate, 0.3 ± 0.1 mM ammonium, and 0.8 ± 0.4 mM potassium (**Figure 5.6**).

Group and Protocol Letter and Number	Mice Name	Exposed to TCDD in utero	Exposed to LPS
A1	Control with LPS	No	Yes
A2	Control with PBS	No	No
B1	F1 with LPS	Yes	Yes
B2	F1 with PBS	Yes	No

Table 5.1. Treatment Protocols for Mice. This contains the group and protocol letters and numbers for the treatments. There are also the names of the groups as well as their respective treatments.

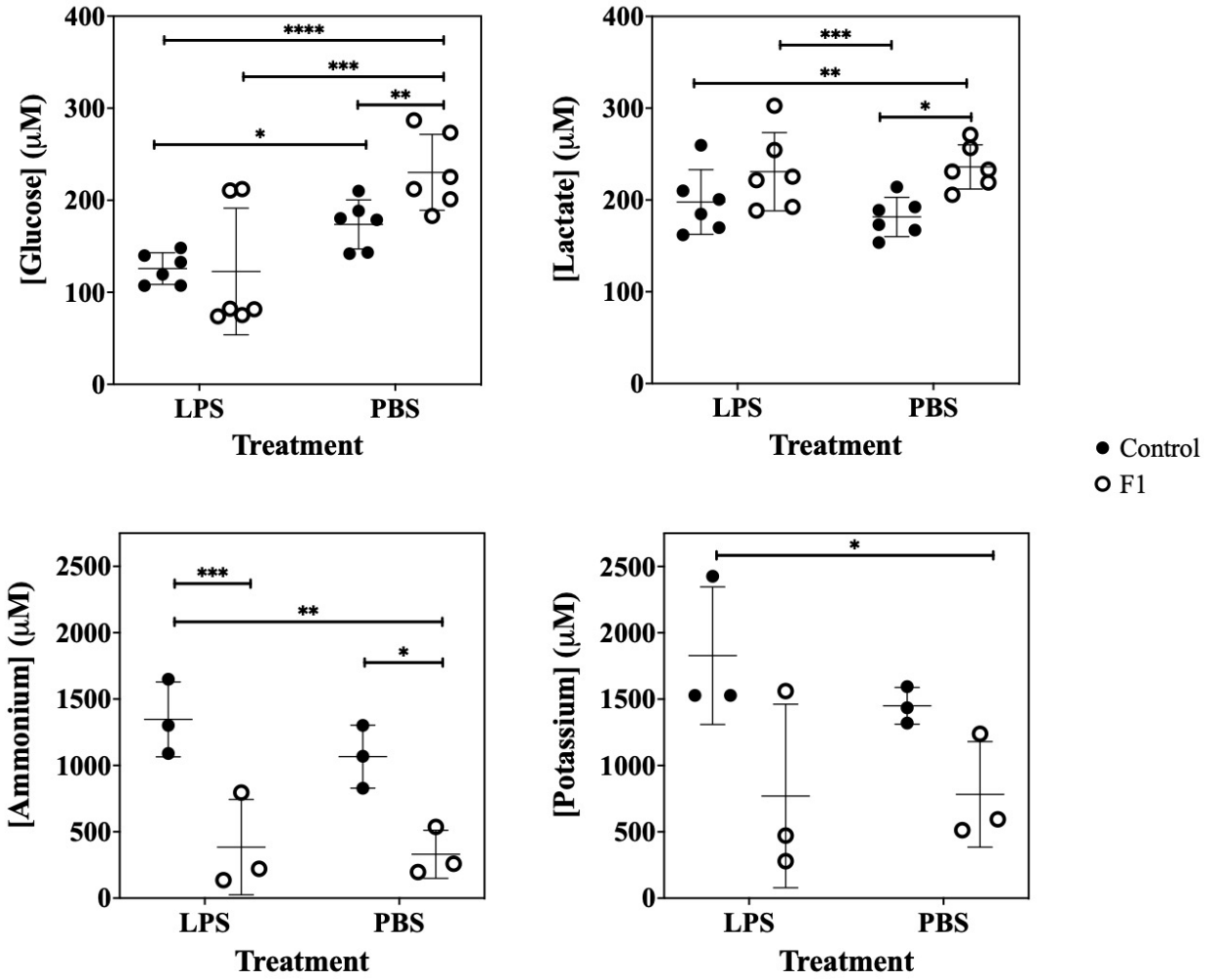

Figure 5.6. Analyte Concentrations of Mice Peritoneal Lavage Samples After Treatment. Scatter dot plot displaying the glucose, lactate, ammonium, and potassium concentrations analyzed using the multianalyte dual amperometric and potentiometric sensor vs. treatment type. Two different types of mice were given two treatment protocols (**Table 1**) A1 showed 126 ± 17 μM glucose, 198 ± 35 μM lactate, 1.3 ± 0.3 mM ammonium, and 1.8 ± 0.5 mM potassium. B2, F1 mice treated with LPS had 123 ± 69 μM glucose, 231 ± 43 μM lactate, 0.4 ± 0.4 mM ammonium, and 0.8 ± 0.7 mM potassium. A2 had 174 ± 27 μM glucose, 182 ± 21 μM lactate, 1.1 ± 0.3 mM ammonium, and 1.4 ± 0.1 mM potassium. Lastly, B1 had 230 ± 41 μM glucose, 236 ± 24 μM lactate, 0.3 ± 0.1 mM ammonium, and 0.8 ± 0.4 mM potassium. Starred experiments denote significantly different results. Data is represented as an average and standard deviation with biological replicates for ammonium and potassium (n = 3) and the addition of two technical replicates (n = 6) for glucose and lactate.

Glucose, lactate, ammonium, and potassium metabolism was observed for mice treated with and without LPS. Glucose levels were significantly lower for A1 compared to A2 ($p = 0.005$). Similarly, the glucose concentrations were significantly lower for those treated with B1 compared to B2 ($p = 0.01$). Lactate, ammonium, and potassium levels were not significantly different for the same type of mice treated with LPS compared to PBS. Glucose metabolism was dysregulated in mice treated with LPS compared to those treated with PBS.

To determine the effect of TCDD, control and F1 mice were compared for glucose, lactate, ammonium, and potassium metabolism using this newly developed sensor. The concentrations of the analytes produced from mice that were previously treated with TCDD *in utero* were compared between mice treated the same (PBS or LPS). The concentration of glucose for A2 was significantly lower than with the B2 ($p = 0.02$). However, A1 was not significantly different from B1. Lactate levels were significantly lower in A2 compared to B2 ($p = 0.002$). Similar to glucose, the concentration of lactate in A1 was not significantly different from the B1. The concentration of ammonium was significantly lower for B1 compared to A1 and B2 compared to A2 ($p = 0.01$ and $p = 0.02$, respectively). Potassium levels were trending toward the B2 having a lower concentration than the A2 ($p = 0.09$). Lastly, the A1 were not significantly different in potassium levels from the B1. Therefore, glucose, lactate, and ammonium had significantly differing concentrations for F1 mice compared to control mice.

While investigating all of these parameters, there were some analytes that were significantly different in concentrations between all of the treatment protocols. The concentration of glucose was significantly higher in B2 compared to the A1 ($p = 0.0008$). The levels of lactate for the same set of mice when compared was trending toward B2 having a higher concentration than A1 ($p = 0.06$). Interestingly, ammonium and potassium had significantly lower concentrations

for the B2 compared to A1 ($p = 0.01$ and $p = 0.05$, respectively). Then, B1 had significantly higher lactate compared to A2 ($p = 0.04$). Finally, the ammonium levels were trending toward the B1 having significantly lower ammonium than the A2 ($p = 0.06$). Thus, many of the analyte concentrations differed significantly between all of the variables.

Discussion.

Electrochemistry can be used for studying cellular and *in vivo* bioenergetics and toxicity pathways. The need to measure and quantify more analytes was the impetus for developing a platform that is easily customizable and applicable to a variety of different applications. In this work, we present two potentiometric sensors for ammonium and potassium, in tandem with enzymatic sensors to comprise this platform for use with model systems. These potentiometric sensors 1) used the most accurate membrane formulation, 2) showed that coating the reference electrode with a membrane was nonessential, 3) showed a biologically-relevant linear range with sensitivity to their respective analyte, and 4) established operational longevity for use in model organ systems. We used this platform to analyze samples from a mouse model to show metabolism dysregulation due to TCDD and LPS. Together with a pump and valve system, this biosensor provided an easy-to-use and versatile format to build a larger biosignature, diagnose and monitor health and disease, and further develop new therapeutics.

First, the sensitivities to ammonium were investigated to determine the formulation that produces a sensitivity closest to the ideal sensitivity. The formulation for the potentiometric sensor was determined to be the best based on the sensitivity of the electrode to ammonium. Potentiometric sensors obey the Nernst Equation ($E = E° - \frac{0.0592}{n}\log Q$).[33] This reveals the theoretical slope of potentiometric sensors based on the associated ion charge of n.[33] Thus, both of the sensors developed here will have a theoretical slope of 0.0592 V decade^{-1} (59.2 mV decade^{-1}), since "n" (the number of electrons) is equal to one.[118] The sensitivity that is closest to 59.2 mV decade^{-1} represented the best formulation and was used for future experiments.[118] Formulation 2 had the closest sensitivity to the theoretical value and allowed for a more accurate determination of the analyte concentrations in biological systems.

Next, the need for a reference electrode coating was determined. Reference electrodes are often coated to get a more accurate signal for the sensor by reduce potential drift.[22,119] However, this data suggested that the reference electrode coating is not necessary and does not significantly change the sensitivity to the analyte for either of the sensors. Thus, a reference coating was not used in future experiments. Because a reference coating was not necessary for the potentiometric sensors, the same reference electrode can be used for amperometric and potentiometric detection on a single SPE.

The ammonium and potassium sensors were sensitive to their respective analytes and spanned a large linear range necessary for monitoring a variety of biological processes. The sensitivities allowed for a low level of detection and quantitation while also including higher concentrations. It is possible that the linear range extends beyond the upper limit of linearity, but calibrants with higher concentrations of analytes were not tested, since higher concentrations are not physiologically relevant. The sensitivity of the ammonium sensor exhibited near-Nernstian behavior (a theoretical sensitivity of 59.2 mV decade^{-1} according to the Nernstian equation).[120] Thus, it is performing as it should and will provide accurate results. The potassium sensor had a slightly super-Nernstian response, providing accurate results, but emphasizing the need for calibrations before sample testing. Using this as a platform would allow for use not only these analytes but also other ions for instance, sodium. It is possible to use the same membrane with a different ionophore, making this an interchangeable system that allows for customization to a variety of applications.

Finally, since this can be used in tandem with continuously operational systems, the longevity of the potentiometric sensors was established. The operational longevity of the amperometric sensors has previously been established with a few weeks of stability after an initial

loss of sensitivity due to enzyme degradation.[29] In both sensors, there was a decrease in sensitivity initially in the first few days that then stabilizes after approximately seven days. These were tested for up to eight days, but it is possible they can be used for longer. Furthermore, these potentiometric sensors still yielded a substantial response to analytes after eight days, allowing another calibration to be completed, even though they seem to have a decreased sensitivity compared to other electrodes.[25,121] These sensitivity decreases emphasized the need for regular recalibration in continuously operational sensors. Therefore, the developed potentiometric sensors are promising for their use in monitoring multiple ion-based biological analytes over extended periods of time and in combination with enzymatic-based sensors to be used as a platform.

LPS elicits a strong inflammatory response with resulting increased cytokines and interleukins in the system.[43,44,105] Here, the glucose was decreased in A1 and B1 compared to A2 and B2, respectively, indicating dysregulated glucose metabolism. This is showing that the mice are under significant stress from LPS and compensating by recruiting more glucose to promote macrophage response, thus changing the glucose metabolism in the peritoneal cavity of the mice.[105] However, the other analytes were not significantly different, showing a slight metabolic profile change, but not enough to change the whole system. Even though glucose was consumed more, it is possible that lactate was unaffected if glucose produced lactate and was stored as glycogen.[2,4] Glucose metabolism in the peritoneal cavity of mice is dysregulated due to LPS, but the other metabolites are unaffected, showing that the inflammatory response does have an effect on metabolism similar to endometriosis.

Dioxins are a family of environmental contaminants with TCDD considered to be the most toxic and can disrupt several different cellular processes.[43] B2 mice showed dysregulated glucose, lactate, and ammonium compared to A2. The mice treated with only TCDD had increased glucose

concentrations when compared to control mice, indicating a dysregulation in glucose metabolism. Perhaps the perturbed mice were releasing glucose (glycogen stores) or revealing a new glucose intolerance, which explains the improper metabolism and the increased glucose seen in the results.[2,4,108,122] Both of these may be done to compensate for the stress of TCDD and the onset of its toxicity and endocrine disruption, thus changing the glucose metabolism of the mice's peritoneal cavity.[108] This sheds more light on the possible effects endometriosis as a disease has on a body's metabolic profile. However, B1 and A1 did not show differences which may shed light on how LPS affects the system. Similar to glucose, lactate also had increased concentrations for B2 mice compared to A2 mice. The mice were generating more lactate by perhaps depleting their glycogen stores or converting glucose straight to lactate to protect from toxicity stress and endocrine disruption.[2,4] Again, the B1 and A1 mice did not show a difference in lactate concentrations which may be a result of LPS again changing the system after TCDD has changed the system. Lastly, ammonium had reversed results compared to glucose and lactate and showed decreased concentrations in the B1 mice and B2 mice compared to the A1 mice and A2 mice, respectively. This may be a result of ammonium levels increasing in the liver/blood stream, which indicates possible liver or kidney failure.[15,122,123] Potassium levels were trending toward decreased concentrations in the B2 mice compared to A2 mice. This may also account for the dysregulated glucose metabolism.[124] Dysregulated potassium metabolism is most likely the result of distressed kidneys as they are responsible for potassium homeostasis.[17] Because the ion concentrations in the peritoneal cavity were lowered, there were signs of distress and toxicity. In general, glucose, lactate, and ammonium metabolisms were dysregulated in mice treated with TCDD, similar to the endocrine disruption with endometriosis.

Interestingly, in comparing some of the peritoneal cavity samples with treatment of TCDD and/or LPS, there was significant metabolite dysregulation. B2 mice compared to A1 mice had increased glucose, trending toward increased lactate, and decreased ammonium and potassium. This is possibly a result of LPS forcing cells to consume more glucose while TCDD promotes glucose intolerance or storage. Lactate may reveal that the mice were producing even more lactate when treated with TCDD as it has dysregulated their metabolism even more than a dysregulated metabolism with LPS. Lowered ammonium and potassium concentrations may be the result of dysregulated metabolic pathways and showing signs of the onset of toxicity by increasing the concentrations of these ions in the liver/kidneys. Then, B1 mice compared to A2 mice showed significantly increased lactate concentrations and trending toward decreased ammonium levels. Thus, lactate is produced heavily when the peritoneal cavity is hit with both inflammatory agents, and ammonium is reduced in the system with ammonium concentrated in the liver and kidneys, perhaps.[43] Both of these reveal the significant metabolite dysregulation when dosed with both toxicants. Thus, the metabolic profile of the peritoneal cavity changes with TCDD and/or LPS.

Conclusions.

A new multianalyte dual amperometric and potentiometric biosensor platform was investigated to quantify changes in glucose, lactate, ammonium, and potassium simultaneously. Enzyme and ionophore-based membranes were used for multiplexed analysis and combined on the biosensor array with a pump and valve for automation and customization. The developed potentiometric sensors were combined with amperometric sensors to provide a platform for a broader and more thorough profile of cellular function and toxicity pathways that is customizable to a variety of applications. We developed potentiometric sensors to have a membrane formulation that will allow for the most accurate results. The sensors offered a wide linear range that can be used for measuring metabolic biosignatures in systems. Lastly, these sensors retain strong analytical sensitivity after at least eight days of use, showing that the platform may be integrated with organ-on-chip systems for real-time analysis of a number of analytes. Applying this platform to a model organ system like the peritoneal lavage mice samples provides biological context and demonstrates the translation to a multitude of applications. These results showed that 1) LPS increased glucose consumption; 2) TCDD by itself decreased glucose consumption, increased lactate production, decreased ammonium levels, and slightly decreased potassium concentrations; 3) TCDD decreased glucose consumption, slightly increased lactate production, and lowered ammonium and potassium concentrations compared to the LPS dysregulated metabolisms; and 4) TCDD and LPS together increased lactate production and decreased ammonium concentrations. With the addition of these sensors and use of this platform, we can examine a biosignature before and after a model organ system has been perturbed to understand metabolite dysregulation and pathways of toxicity.

Acknowledgements.

This work was also supported in part by the National Institute of Health training grant (ES007028), EPA (83573601), and NIH (1R01HD102752-01) and using the resources of the Vanderbilt Microfabrication Core operated by the Vanderbilt Institute for Integrative Biosystems Research and Education. The authors would like to acknowledge Pragun Tuladhar for the assistance of designing and performing experiments and Victoria Stephens and Kevin Osteen for providing samples.

Chapter VI

CONCLUSIONS AND OUTLOOK

Summary

This dissertation describes the development and application of multianalyte electrochemical biosensors for understanding the cellular processes and mechanisms of toxicity in model organ systems. Previously, there have been studies detailing the development of multianalyte biosensors for several different analytes. However, these sensors are restricted by their low resolution, inability to integrate with model organ systems, inability for customization, and detection of only a few analytes. The studies shown here seek to not only validate the ability of electrochemical biosensors to analyze complex biological processes, but establish platforms for future work to further investigate model organ systems.

For chapter 3, a glucose and lactate osmium polymer-based sensor was developed and used to measure metabolism in AML12 cells after treatment with APAP and/or insulin. The osmium-based redox polymer was used for electrochemical detection in this sensor and operated at a decreased voltage, allowing for decreased interference. These sensors demonstrated higher selectivity (40-fold for glucose and 200-fold for lactate) over APAP, possessed higher sensitivity (0.350 ± 0.006 μA mM^{-1} for glucose and 2.00 ± 0.05 μA mM^{-1} for lactate) over a biologically-relevant range of analyte concentrations (50 μM – 10 mM for glucose and 2-324 μM for lactate), and displayed comparable operational stability (26% decrease for glucose and 29% decrease for lactate) compared to first-generation sensors. To test this platform under biologically-relevant conditions, glucose metabolism was monitored in AML12 cells after treatment with APAP and/or

insulin. This sensor revealed that the removal of insulin from basal media reversed glucose metabolism in AML12 cells. In addition, it indicated that APAP reduced production of glucose in the cells. Lastly, the Os-based sensor mitigated APAP interference compared to the first-generation sensor. These studies illustrated the effectiveness of this high-resolution platform that can be translated to other biological systems to understand cellular processes without concern for interference.

To further understand cellular processes, a platform capable of the detection and quantification of up to eight analytes using enzymatic-based sensors was developed. In chapter four, the sensor was characterized using calibrations to obtain the high analytical sensitivities and the wide biologically-relevant linear ranges for seven different analytes. These sensors can be customized and are combined with a pump and valve system that provided an easy-to-use and versatile format. This system was applied to analyze glucose and lactate metabolism of samples from mice macrophages treated with TCDD, LPS, and β-glucan. The sensors revealed 1) TCDD decreased glucose consumption and dysregulated lactate production; 2) LPS dysregulated glucose consumption and increased lactate production; 3) β-glucan dysregulated glucose and lactate metabolism differently in control and TCDD-exposed macrophages; 4) LPS decreased glucose consumption more and dysregulated lactate metabolism differently than β-glucan; and 5) 24 hour treatment time period decreased glucose consumption and increased lactate production compared to the 3 day post injection time point. Measuring changes in multiple analytes will allow for a better understanding of the state and interactions of a system.

Finally, a similar platform was developed to detect and quantify changes in analytes using amperometry and potentiometry. Chapter five details the development of two potentiometric sensors combined with two amperometric sensors to simultaneously detect and

quantify ammonium, potassium, glucose, and lactate. The membrane formulation that provides the most accurate sensitivity was found to be 1% ionophore, 33% poly(vinyl chloride), and 66% dibutyl sebacate. It was also determined that a reference electrode coating was not necessary. The potentiometric sensors had sensitivities of 57 ± 2 mV per decade of concentration for ammonium and 75 ± 3 mV decade^{-1} for potassium. This included a broad range of analyte concentrations (21 μM – 10 mM for ammonium 80 μM – 12 mM for potassium). Finally, these were characterized for operational stability (44% decrease for both ammonium and potassium) over eight days. These sensors were used to detect the dysregulated metabolism of each of the analytes from peritoneal lavage mice samples. Based on this data, LPS increased glucose consumption, while TCDD decreased glucose consumption, increased lactate production, decreased ammonium levels, and slightly decreased potassium concentrations. Comparing the two treatments showed that TCDD decreased glucose consumption, slightly increased lactate production, and lowered ammonium and potassium concentrations compared to the LPS treated mice. Lastly, TCDD and LPS together increased lactate production and raised ammonium concentrations. Overall, this work represents a customizable platform utilizing a multiplexed, multianalyte amperometric and potentiometric biosensor for microphysiological monitoring of metabolites simultaneously to provide a snapshot of the state and interactions of a biological system.

Outlook

Important to several biological processes, including biosynthesis, neurotransmission, cellular respiration, metabolites are important aspects in understanding these complex processes. Electrochemical biosensors that can detect a multitude of analytes will allow for the evaluation of new and old systems to gain new insights on pathways of toxicity and cellular processes and can show dysregulated metabolism in diseases like Parkinson's or after perturbations like LPS.[4,24,107] Thus, it is vital to detect and quantify metabolites to identify pathways of toxicity, monitor disease progression, and develop novel therapeutics.

There have been many methods developed and used to detect and quantify metabolites, electrochemical biosensors provide the opportunity for low cost, rapid, selective, stable, and sensitive means to detect multiple analytes. These analytes comprise a biosignature, a snapshot of the state and interactions of a system, that is used in analyzing biological applications. This makes them highly translational, for instance to the clinic for personalized medicine or in wearable monitors (smart bands).[4] Enzymatic- and ionophore-based sensors, like those described in this work, provide all of these benefits unlike some of the other methods described previously.

Although enzymatic sensors show great promise, they do have some drawbacks that prevent them from being fully effective in model organ systems. First, these sensors show lowered enzymatic activity due to degradation, resulting in lowered sensitivity and a reduced operational stability of the sensor. Glutaraldehyde is used as a common crosslinker (as it is in these studies) for absorption of the enzyme onto the electrode surface. However, this crosslinking does not promote enzymatic stability. Newer means of adsorption have been developed such as sol-gels that maintain higher enzymatic activity.[76,125,126] These and the development of new methods will be helpful in improving the effectiveness of enzymatic sensor.

Next, these enzymatic sensors are susceptible to electroactive interference that can lead to signal contamination and inaccurate results. Because enzymatic sensors often use oxidase enzymes that rely on hydrogen peroxide oxidation, APAP and other interferents can also be oxidized at the same potential. Significant research and development has been completed including this work to reduce and mitigate this interference using conductive polymers and nanomaterials to lower the potential for oxidation or change the sensor function entirely.[18,50,62] Applying these to more analytes enables a better understanding of complex pathways and mechanisms. Screening polymers such as m-phenylenediamine may also be used to reduce interference by preventing larger molecules from accessing the electrode surface. All of these methods have improved sensitivity and selectivity of enzymatic sensors by mitigating interference. Developing sensors with better sensitivity and selectivity provides more opportunities for analysis of processes and systems not previously understood due to interference.

Similarly, ionophore-based sensors are quite specific and low cost, but also have limitations that must be considered. These sensors suffer from limitations that prevent them from being fully effective in biological applications. One such drawback is the stability of the sensors. The incorporation of polymers such as poly(3,4-ethylenedioxythiophene) doped with poly(styrene sulfonate) and optimization and development of membrane compositions have proven helpful for improving stability in sensors.[20,24] Furthermore, these sensors often suffer from selectivity issues between ions. The addition of components to the membrane such as polymers and carbon paste has demonstrated enhanced sensing capabilities of ions.[24] Lastly, ionophore-based sensors often have shortened linear ranges. Again, these may be improved through the integration of polymers like PVC and ion exchangers like dibutyl phthalate.[24,118] Once these issues have been addressed,

the sensors can be translated to multiple other ions and used to unravel the complex biological processes in model organ systems.

Since electrochemical biosensors can be used for real-time analysis, it is helpful to understand how they can integrate within or downstream of OoC systems. Using the sensors with OoCs provides the opportunity for observing human cellular processes and pathways of toxicity to monitor health and disease. While these sensors have the capability to be integrated, they suffer from interference from the cellular media as well as diffusion, causing inaccurate results and lowered resolution. Work has been done to reduce these effects through alternative cell media, the addition of polymers, and lower flow rates, these methods are not perfect. Thus, electrochemical biosensors need further optimization for use in real-time analysis of model organ systems like OoCs.

Metabolites are an important aspect of every biological process and are required for proper function. The development of electrochemical biosensors to monitor multiple analytes provides new insight about the pathways of toxicity and cellular processes. These sensors provide a low-cost, sensitive, selective, and stable method for detection and quantification of multiple analytes. While there are improvements that can be made to electrochemical sensors, the future is bright for using these for integration with model organ systems to monitor health and disease.

Appendix A

DEVELOPMENT OF A CHOLESTEROL AMPEROMETRIC BIOSENSOR FOR ANALYSIS OF MODEL ORGAN SYSTEMS

Drug-induced liver injury is responsible for 5% of all hospital visits.[127] Organ-on-chip (OoC) devices are being developed to faithfully reproduce human organs and organ systems unlike traditional tissue culture techniques and animal models. Model organ systems such as OoCs are the key to gaining insight in monitoring cellular function and toxicity and developing new therapeutics. These devices provide 3D models that recapitulate the native environment and allow for perfusion of cells. To monitor the health of the OoCs over time and in response to various stimuli, several analytical tools have been developed. However, time dependent analysis is needed to observe metabolic processes, pathways for disease, and mechanisms of toxicity in the organ for use in identifying toxicant doses and time regimes, tracking changes in metabolic and signaling activity, and observing metabolic pathway shifts. This may then be used to influence the use of other methods that provide high-information content in terms of molecular-level responses like mass spectrometry. Therefore, metabolic processes and mechanisms of toxicity may be established as well as development of new therapeutics may progress.

Cholesterol is an important biomarker for overall health as it is used in every cell in the body. It is vital to many organs as a structural component of cellular membranes and can be helpful or harmful for them with varying concentrations.[128] Since the liver is responsible for the regulation and synthesis of cholesterol, deviations can indicate the status of liver function.[129] Higher concentrations of cholesterol suggest that it is synthesizing too much cholesterol or regulating

improperly. Lower concentrations of cholesterol indicate that it is not synthesizing enough or regulating it improperly.

The liver-on-chip (LoC), a model liver system, is key to gaining insight in monitoring toxicity as it is the metabolic center. Time-dependent analysis is needed to observe metabolic processes, pathways for disease, and mechanisms of toxicity. This is important for identifying toxicant doses and time regimes that are the most effective/toxic, tracking changes in metabolic and signaling activity in the organ-on-chip (OoC), and observing metabolic pathway shifts such as from anaerobic to aerobic. This may then be used to influence further in-depth analysis with other methods, like mass spectrometry, that provide high-information content. These are necessary for further development of therapeutics and monitoring toxicity in OoCs toward predictive toxicology and biomimicry.

To answer this need, we developed a cholesterol sensor to be combined with LoC to gain a better understanding of health and disease in the liver as well as its responses to chemical and physical perturbations.[24] The microclinical analyzer (μCA) accomplishes this by measuring the concentration of cholesterol (and it is possible to measure other analytes simultaneously) in the effluent from LoCs via electrochemistry in real time. Electrochemical analysis represents a powerful tool for bioenergetic profiling.[130] The biosignature measures the secretome of the cell of a LoC that can be analyzed using specific biomarkers for liver stress as well as glucose, lactate, dissolved oxygen, and pH biosensors previously developed.[29] Thus, by creating new sensors, more information will be gathered about the system which will help build a larger and more descriptive biosignature for the system. Together, they will ultimately allow for monitoring cellular function, elucidating metabolic pathways, performing toxicity screens, and developing new therapeutics. These will give greater insight into the cellular function and provide more information on the

identifying the toxicant doses and time regimes, tracking changes in metabolic and signaling activity, and observing metabolic pathway shifts. This new sensor will be a valuable resource for the wider scientific community to pursue more studies in chemical and physical perturbations in real time for toxicity and development of new therapeutics studies that have not been possible before due to the limitations of current analytical tools.

Experimental.

By using a cholesterol oxidase (12.5 mg mL^{-1} in BSA/buffer solution; Sigma Aldrich; St. Louis, MO) film (5 μL) deposited on an electrode, we detected changing concentrations of cholesterol electrochemically. Cholesterol (Alfa Aesar; Ward Hill, MA) is difficult to dissolve in water, so different dissolving agents such as Triton X-100 (Sigma Aldrich) and DMSO (Sigma Aldrich) were investigated for their ability to dissolve it. This is used to determine the best solutions for dissolving cholesterol and giving the most amount of free cholesterol. Furthermore, biofouling can be an issue with sensors, so different semi-permeable polymer membranes including nafion (Alfa Aesar) and poly l-lysine (Sigma) are examined. For both of these studies, the best option is taken as the one that provides the most negative sensitivity.

Results and Discussion.

Cholesterol is difficult to solubilize in water. It forms aggregates in the body as well as in solutions of water. Therefore, a method for de-aggregation is sought. The body uses bile acids and lipoproteins to accomplish this. Many groups have used beta-cyclodextrin/methyl beta-cyclodextrin for dissolving the cholesterol.[131,132] Micellar solutions like surfactants (triton x-100) and organic solvents (ethanol) can also be used for accomplishing de-aggregation. In this study, triton x-100 and different concentrations of DMSO are investigated for methods of dissolution (**Figure A.1**). The higher concentrations of DMSO deactivated the enzyme or possibly opened the enzyme pocket. Because the enzyme denatures, there were non-specific reductions as evidenced by the largely positive sensitivity for 5 and 10% DMSO. Because we want the sensitivity to be oxidative and therefore negative, a combination of 0.5% DMSO and 1% triton x-100 was the best choice and provides the most amount of free cholesterol for testing on the sensor. The concentration of triton x-100 was kept low to maintain biological relevance and produce the most amount of free cholesterol while being able to solubilize it.

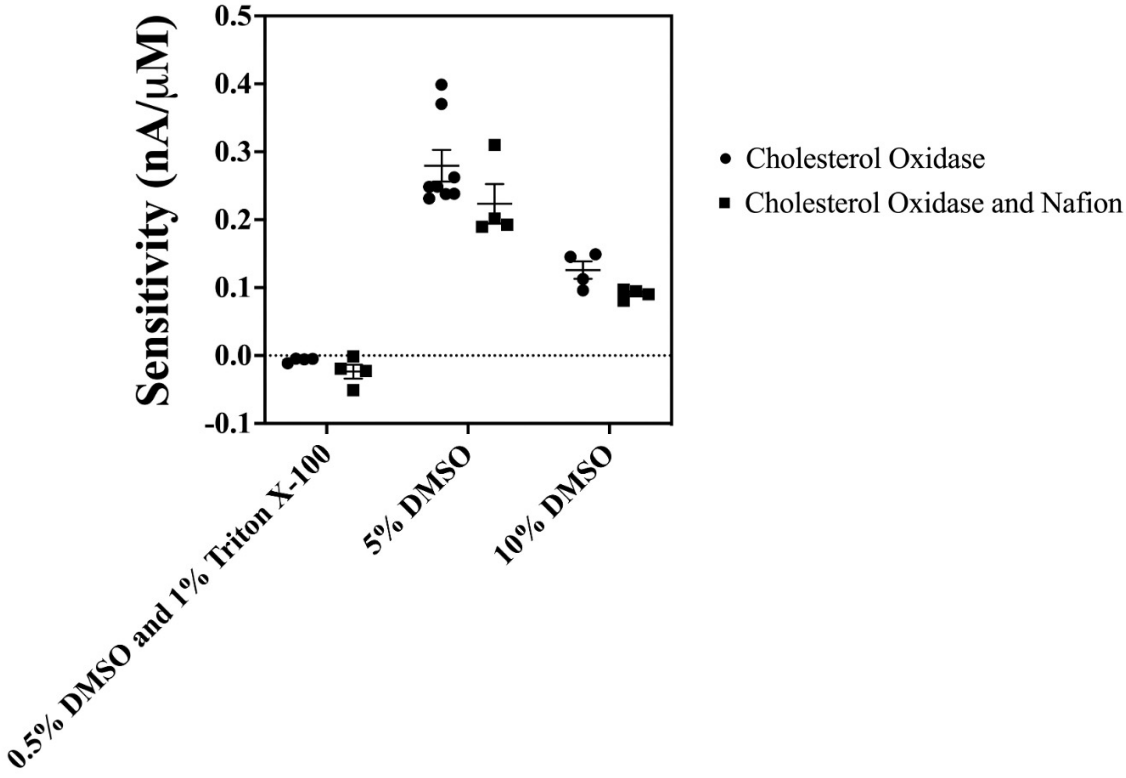

Figure A.1. Comparison of Cholesterol Dissolving Agents. A scatterplot displaying how the dissolving agents and their concentrations affect the sensitivity of the sensor. Experiments were completed in Williams E media, HMM, and 1% FBS (same as LoC samples). Data represented as an average with standard error, n = 4-8.

In addition, biofouling and interference is a large issue for sensors, so much that it can inhibit the sensor from being sensitive to the analyte of interest. Studies were conducted to investigate how to prevent biofouling for this sensor. Semi-permeable polymer membranes can be added on top to increase accuracy and precision of the measurements (**Figure A.2**). Again, the most negative sensitivity is the most desirable for this sensor. Two commonly used polymers and that were investigated here are nafion and poly l-lysine. Poly l-lysine had the largest oxidative current, so it was the best membrane to prevent biofouling. The osmium-polymer developed in chapter three was also utilized to prevent interference from unknown compounds.

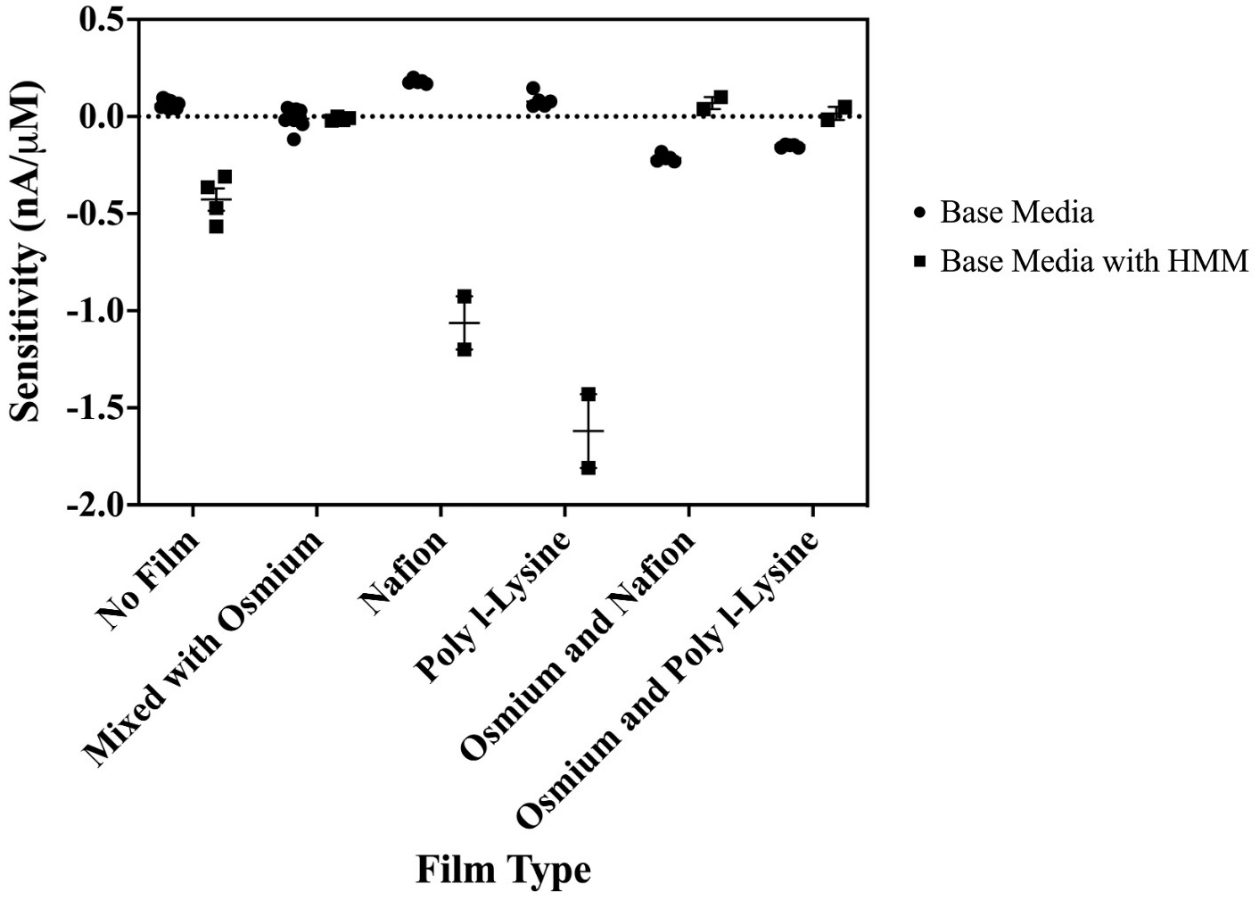

Figure A.2. Comparison of Cholesterol Oxidase Film Modifications. A scatterplot graph that shows how films added on top of the sensor affect the sensitivity as well. Experiments were completed in Williams E media with and without HMM. Poly lysine gives highest sensitivity and prevents biofouling. Data represented as an average with standard error, n = 2-10.

Finally, a cholesterol calibration is completed showing linear response for biologically relevant concentrations (**Figure A.3**). The slope is given by the line, $y = (-0.0135 \pm 0.0010)x - (1.8 \pm 0.2)$. This provides an $R^2 = 0.93$ with n =3, showing the linearity of the sensor measurements. The sensitivity is low, but this is likely due to the conglomerated cholesterol that is still in solution.

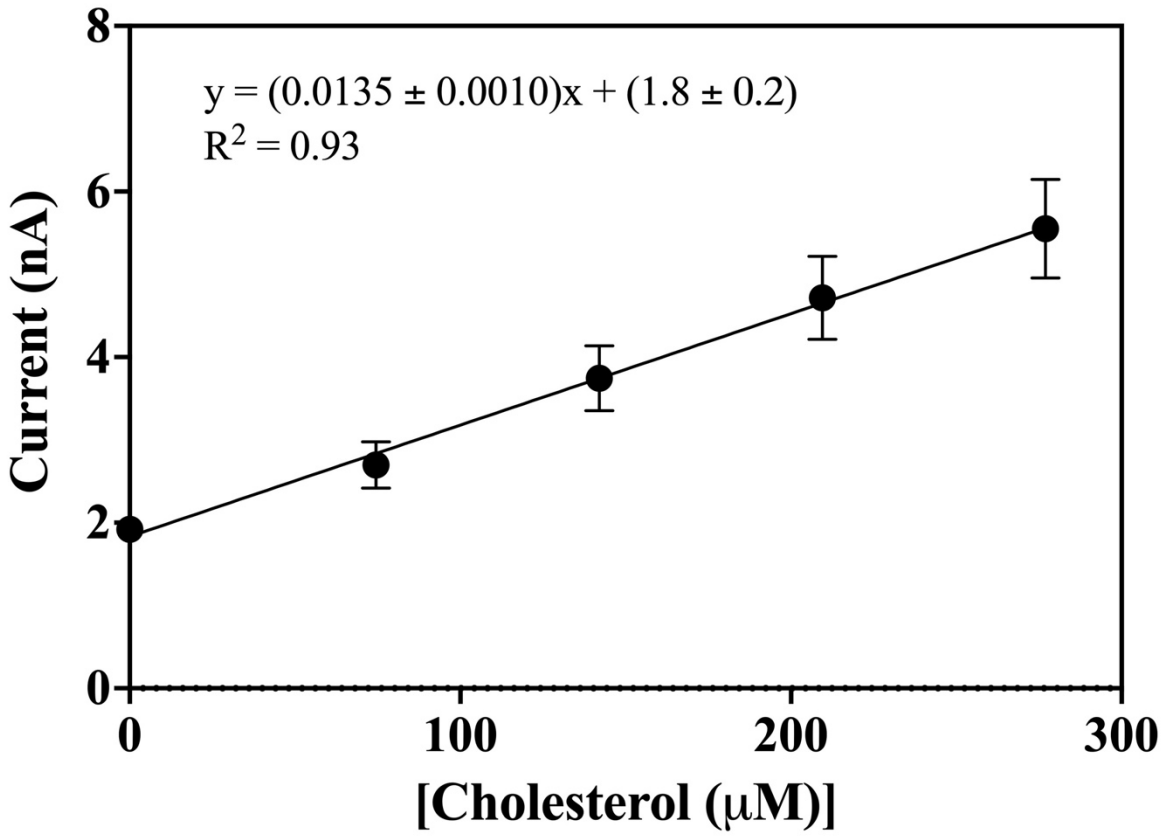

Figure A.3. Cholesterol Calibration Curve. Experiments were completed in a buffered solution (2 mM PBS, 120 mM KCl, 0.5% DMSO, and 1% Triton X-100) in ambient conditions. The slope is represented by the line y = (-0.0135 ± 0.0010) x - (1.8 ± 0.2) with an $R^2 = 0.93$, n = 3.

Conclusions.

Hepatotoxicity is the most common reason for drugs to be taken off the market.[133] Therefore, there is a serious need for increasing pharmacological and toxicological analyses of pharmaceuticals and other xenobiotics. OoC systems provide insight that are difficult with other methods, and improve medicine by assessing the acute and chronic drug effects. By coupling the OoC with the μCA, a fast, robust, low-cost, and sensitive detection method, toxicological studies may be completed in real-time on multiple analytes. Here, we present a cholesterol sensor for use in LoC systems to test the hepatotoxicity of toxins and developing therapeutics. Two dissolving agents, 0.5% DMSO and 1% Triton X-100, were used to dissolve cholesterol while still giving the highest quantity of free cholesterol. A semi-permeable polymer membrane, poly l-lysine, was used to prevent biofouling. Using these discoveries, a cholesterol sensor showed a linear response for biologically relevant concentrations.

Acknowledgments.

This work was also supported in part by the National Institute of Health training grant (ES007028) and EPA (83573601) and using the resources of the Vanderbilt Microfabrication Core operated by the Vanderbilt Institute for Integrative Biosystems Research and Education. The authors would like to thank Dusty Miller and Evan Gizzie for assistance in designing experiments.

Appendix B

ANALYSIS OF LIVER-ON-CHIP SAMPLES USING OSMIUM-BASED ELECTROCHEMICAL BIOSENSORS

A model liver system deemed the liver-on-a-chip (LoC) is key to gaining insight in monitoring toxicity, since the liver acts as a metabolic center. Time dependent analysis is needed to observe metabolic processes and pathways for disease and mechanisms in the organ. The microclinical analyzer (μCA) accomplishes this by simultaneously measuring the concentration of various analytes in the effluent from organs-on-chips (OoCs) via electrochemistry for real-time analysis. The biosignature of the LoC can be analyzed using specific biomarkers for liver stress, ammonium and cholesterol, as well as glucose, lactate, glutamate, dissolved oxygen, and pH biosensors.

Here, we present a study of LoC samples that have been treated with rosiglitazone or a vehicle to understand the effects on glucose and lactate metabolism. Furthermore, these cells were compared between diseased (cancerous tumor that had previously been treated with chemotherapy) and control to determine how the cells glucose and lactate metabolism were affected.

Experimental.

The sensors used to analyze these samples were the same described and developed in chapter three. Four sets of samples were generously provided by the Vernetti group at University of Pittsburgh from patients that had liver tumors.[26] There were two samples: 1) a patient that had a benign tumor and 2) a patient with a cancerous tumor that has been treated with chemotherapeutic drugs. Then, these samples were cultured in a LoC system and treated with a vehicle (DMSO) or rosiglitazone (a known hepatotoxic therapeutic). The media was collected and shipped to us. Media was analyzed using glucose and lactate osmium-based sensors.

Results and Discussion.

To understand the effects of rosiglitazone on the LoC cells, the vehicle and treated cells were compared within the same control or diseased set of cells (**Figure B.1**). Rosiglitazone is a known hepatotoxic therapeutic, so the effects on glucose and lactate metabolism can provide insight into its mechanisms of toxicity.[134] Glucose was not significantly different for the normal control cells ($p = 0.59$) but was significantly decreased in cells treated with rosiglitazone for the diseased cells ($p = 0.02$). Thus, rosiglitazone does have an effect on glucose metabolism if there is another trigger that is affecting the cells as well, compensating for the stress by recruiting more glucose for an inflammatory response.[45] This may also be the result that these diseased liver cells also were treated with chemotherapy before being removed and cultured. The cells treated with rosiglitazone had significantly less lactate compared to the vehicle in the diseased cell ($p = 0.02$) and was trending similarly for the control cells ($p = 0.06$). Lactate metabolism was significantly dysregulated. It is possible that lactate production is slowed from the stress of the toxicity from rosiglitazone. Rosiglitazone dysregulated both glucose and lactate metabolism, indicating possible pathways of toxicity.

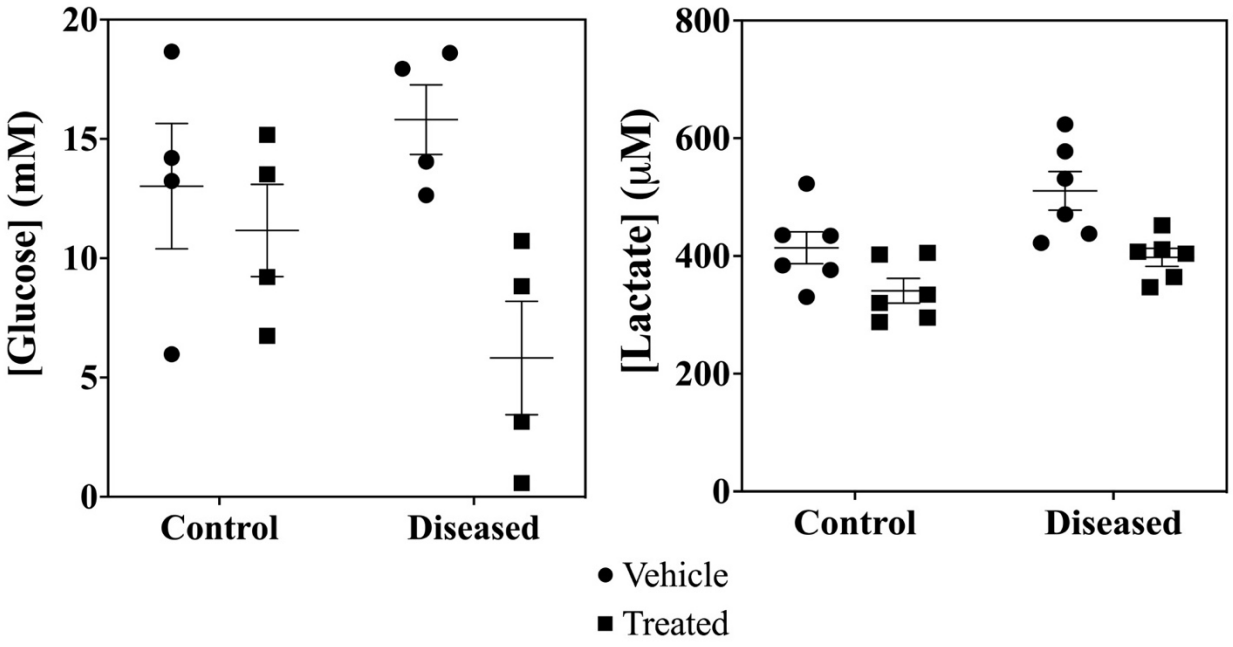

Figure B.1. Glucose and Lactate Metabolism in LoCs after Rosiglitazone Treatment. Scatterplot displaying the glucose (left) and lactate (right) concentrations lactate analyzed using an Os-based sensor vs. sample type including control and diseased samples. Experiments were performed in Williams E media (ambient conditions). Data represented as an average and standard error with n = 4 (glucose) or 6 (lactate) replicates.

In addition, glucose and lactate metabolism was investigated between the control and diseased cells within the same treatments (vehicle or rosiglitazone) (**Figure B.1**). Glucose metabolism was not significantly dysregulated in the diseased cells for the vehicle and rosiglitazone-treated cell ($p = 0.40$ and $p = 0.13$, respectively). However, lactate production was significantly increased in the diseased cells given a vehicle ($p = 0.05$) and trending toward increased for the rosiglitazone-treated diseased cells ($p = 0.06$). Lactate metabolism indicated increased anaerobic respiration. Lactate perhaps depleted the glycogen stores to protect against the stress of the disease or the disease permanently shifted metabolism toward anaerobic respiration.[2,4] Thus, the diseased cells had dysregulated lactate, likely due to the stress of the disease and possibly from the chemotherapeutic treatment.

Conclusions.

The osmium-based amperometric glucose and lactate biosensors were used to investigate glucose and lactate metabolism. Rosiglitazone affects glucose and lactate metabolism by increasing glucose consumption and decreasing lactate production. Those cells that were diseased and had been treated with chemotherapy previously show an exacerbated effect with the rosiglitazone in these same metabolites. The diseased (and treated with chemotherapy) cells showed increased lactate production. Using these sensors, to combine with a OoC system like the LoC will undoubtedly provide new insights and understanding to previously unknown or poorly studies diseases, toxicants, and biological systems.

Acknowledgments.

This work was also supported in part by the National Institute of Health training grant (ES007028) and EPA (83573601) and using the resources of the Vanderbilt Microfabrication Core operated by the Vanderbilt Institute for Integrative Biosystems Research and Education. The authors would like to thank the Vernetti group at the University of Pittsburgh for supplying the samples that were tested.

REFERENCES

(1) Gamache, P. H.; Meyer, D. F.; Granger, M. C.; Acworth, I. N. Metabolomic Applications of Electrochemistry/Mass Spectrometry. *J. Am. Soc. Mass Spectrom.* **2004**, *15* (12), 1717–1726. https://doi.org/10.1016/j.jasms.2004.08.016.

(2) Rui, L. Energy Metabolism in the Liver. *Compr. Physiol.* **2014**, *4* (1), 177–197. https://doi.org/10.1002/cphy.c130024.Energy.

(3) Kimmel, D. W.; Meschievitz, M. E.; Hiatt, L. A.; Cliffel, D. E. Multianalyte Microphysiometry of Macrophage Responses to Phorbol Myristate Acetate, Lipopolysaccharide, and Lipoarabinomannan. *Electroanalysis* **2013**, *25* (7), 1706–1712. https://doi.org/10.1002/elan.201300121.

(4) Davis, A. N.; Travis, A. R.; Miller, D. R.; Cliffel, D. E. Multianalyte Physiological Microanalytical Devices. *Annu. Rev. Anal. Chem* **2017**, *10*, 93–111. https://doi.org/10.1146/annurev-anchem.

(5) Zhou, Y.; Danbolt, N. C. Glutamate as a Neurotransmitter in the Healthy Brain. *Journal of Neural Transmission*. Springer 2014, pp 799–817. https://doi.org/10.1007/s00702-014-1180-8.

(6) Miller, D. R.; McClain, E. S.; Cliffel, D. E. Electrochemical Microphysiometry Detects Cellular Glutamate Uptake. *J. Electrochem. Soc.* **2018**, *165* (12), G3120–G3124. https://doi.org/10.1149/2.0201812jes.

(7) Ko, J. H.; Strafella, A. P. Dopaminergic Neurotransmission in the Human Brain: New Lessons from Perturbation and Imaging. https://doi.org/10.1177/1073858411401413.

(8) Picciotto, M. R.; Higley, M. J.; Mineur, Y. S. Acetylcholine as a Neuromodulator:

Cholinergic Signaling Shapes Nervous System Function and Behavior. *Neuron*. NIH Public Access October 4, 2012, pp 116–129. https://doi.org/10.1016/j.neuron.2012.08.036.

(9) Fukai, T.; Ushio-Fukai, M. Superoxide Dismutases: Role in Redox Signaling, Vascular Function, and Diseases. *Antioxidants and Redox Signaling*. Mary Ann Liebert, Inc. September 15, 2011, pp 1583–1606. https://doi.org/10.1089/ars.2011.3999.

(10) Hiatt, L. A.; McKenzie, J. R.; Deravi, L. F.; Harry, R. S.; Wright, D. W.; Cliffel, D. E. A Printed Superoxide Dismutase Coated Electrode for the Study of Macrophage Oxidative Burst. *Biosens. Bioelectron.* **2012**, *33* (1), 128–133. https://doi.org/10.1016/j.bios.2011.12.038.

(11) Mi, D. J.; Dixit, S.; Warner, T. A.; Kennard, J. A.; Scharf, D. A.; Kessler, E. S.; Moore, L. M.; Consoli, D. C.; Bown, C. W.; Eugene, A. J.; et al. Altered Glutamate Clearance in Ascorbate Deficient Mice Increases Seizure Susceptibility and Contributes to Cognitive Impairment in APP/PSEN1 Mice. *Neurobiol. Aging* **2018**, *71*, 241–254. https://doi.org/10.1016/J.NEUROBIOLAGING.2018.08.002.

(12) Csifféry, G.; Futo, P.; Adányi, N.; Kiss, A. Ascorbate Oxidase-Based Amperometric Biosensor for L-Ascorbic Acid Determination in Beverages. *Food Technol. Biotechnol.* **2016**, *54* (1), 31–35. https://doi.org/10.17113/ftb.54.01.16.4135.

(13) Krueger, W. H.; Tanasijevic, B.; Barber, V.; Flamier, A.; Gu, X.; Manautou, J.; Rasmussen, T. P.; Johnson, R. Cholesterol-Secreting and Statin-Responsive Hepatocytes from Human ES and IPS Cells to Model Hepatic Involvement in Cardiovascular Health. *PLoS One* **2013**, *8* (7). https://doi.org/10.1371/journal.pone.0067296.

(14) Abdelwahab, A. A.; Won, M. S.; Shim, Y. B. Direct Electrochemistry of Cholesterol Oxidase Immobilized on a Conducting Polymer: Application for a Cholesterol Biosensor.

Electroanalysis **2010**, *22* (1), 21–25. https://doi.org/10.1002/elan.200900363.

(15) Adeva, M. M.; Souto, G.; Blanco, N.; Donapetry, C. Ammonium Metabolism in Humans. *Metabolism* **2012**, *61* (11), 1495–1511. https://doi.org/10.1016/J.METABOL.2012.07.007.

(16) Soler, N.; Jain, S.; James, H.; Paton, A. Potassium Status of Patients with Cirrhosis. *Gut* **1976**, *17*, 152–157. https://doi.org/10.1136/gut.17.2.152.

(17) Weaver, C. M. Potassium and Health. *Adv. Nutr.* **2013**, *4* (3), 368S-77S. https://doi.org/10.3945/an.112.003533.

(18) Melow, S.; Miller, D. R.; Gizzie, E. A.; Cliffel, D. E. A Low-Interference, High-Resolution Multianalyte Electrochemical Biosensor. *Anal. Methods* **2020**, 12–15. https://doi.org/10.1039/d0ay00528b.

(19) Hirsch, I. B. History of Glucose Monitoring. *Univ. Washington, Seattle, WA Attempts* **2018**, 2018.

(20) Xu, H.; Wang, Y.; Luo, Z.; Pan, Y. A Miniature All-Solid-State Calcium Electrode Applied to in Situ Seawater Measurement. *Meas. Sci. Technol* **2013**, *24*, 125105–125106. https://doi.org/10.1088/0957-0233/24/12/125105.

(21) McClain, E. S.; Miller, D. R.; Cliffel, D. E. Communication-Microfluidic Electrochemical Acetylcholine Detection in the Presence of Chlorpyrifos. *J. Electrochem. Soc.* **2019**, *166* (16), G178–G181. https://doi.org/10.1149/2.0711916jes.

(22) Tomàs Guinovart; J. Bandodkar, A.; R. Windmiller, J.; J. Andrade, F.; Joseph Wang. A Potentiometric Tattoo Sensor for Monitoring Ammonium in Sweat. *Analyst* **2013**, *138* (22), 7031–7038. https://doi.org/10.1039/C3AN01672B.

(23) Schrimpe-rutledge, A. C.; Codreanu, S. G.; Sherrod, S. D.; Mclean, J. A. Untargeted Metabolomics Strategies -- Challenges and Emerging Directions. *J Am Soc Mass Spectrom.*

2017, *27* (12), 1897–1905. https://doi.org/10.1007/s13361-016-1469-y.Untargeted.

(24) Kimmel, D. W.; Leblanc, G.; Meschievitz, M. E.; Cliffel, D. E. Electrochemical Sensors and Biosensors. *Anal. Chem.* **2012**, *84* (2), 685–707. https://doi.org/10.1021/ac202878q.

(25) Gao, W.; Emaminejad, S.; Nyein, H. Y. Y.; Challa, S.; Chen, K.; Peck, A. Fully Integrated Wearable Sensor Arrays for Multiplexed in Situ Perspiration Analysis. *Nature* **2016**, *529* (7687).

(26) Vernetti, L. A.; Senutovitch, N.; Boltz, R.; DeBiasio, R.; Ying Shun, T.; Gough, A.; Taylor, D. L. A Human Liver Microphysiology Platform for Investigating Physiology, Drug Safety, and Disease Models. *Exp. Biol. Med.* **2016**, *241* (1), 101–114. https://doi.org/10.1177/1535370215592121.

(27) Markwalter, C. F.; Gibson, L. E.; Mudenda, L.; Kimmel, D. W.; Mbambara, S.; Thuma, P. E.; Wright, D. W. Characterization of Plasmodium Lactate Dehydrogenase and Histidine-Rich Protein 2 Clearance Patterns via Rapid on-Bead Detection from a Single Dried Blood Spot. *Am. J. Trop. Med. Hyg.* **2018**, *98* (5), 1389–1396. https://doi.org/10.4269/ajtmh.17-0996.

(28) Picache, J. A.; Rose, B. S.; Balinski, A.; Leaptrot, K. L.; Sherrod, S. D.; May, J. C.; McLean, J. A. Collision Cross Section Compendium to Annotate and Predict Multi-Omic Compound Identities. *Chem. Sci.* **2019**, *10* (4), 983–993. https://doi.org/10.1039/c8sc04396e.

(29) McKenzie, J. R.; Cognata, A.; Davis, A. N.; Wikswo, J. P.; Cliffel, D. E. Real-Time Monitoring of Cellular Bioenergetics with a Multi-Analyte Screen-Printed Electrode. *Anal. Chem.* **2015**, 150630093637003. https://doi.org/10.1021/acs.analchem.5b01533.

(30) Florescu, M.; David, M. Tyrosinase-Based Biosensors for Selective Dopamine Detection. *Sensors (Switzerland)* **2017**, *17* (6). https://doi.org/10.3390/s17061314.

(31) McKenzie, J. R.; Cliffel, D. E.; Wikswo, J. P. Electrochemical Monitoring of Cellular Metabolism. *Encycl. Appl. Electrochem.* **2014**, No. 2008, 522–528.

(32) Marzouk, S. A. M. Improved Eletrodeposited Iridium Oxide PH Sensor Fabricated an Etched Titanium Substrates. *Anal. Chem.* **2003**, *75* (6), 1258–1266.

(33) Silverio, A. A.; Chung, W. Y.; Tsai, V. F. S.; Cheng, C. Multi-Parameter Readout Chip for Interfacing with Amperometric, Potentiometric and Impedometric Sensors for Wearable and Point-of-Care Test Applications. *Microelectronics J.* **2020**, *100*, 104769. https://doi.org/10.1016/j.mejo.2020.104769.

(34) Halldorsson, S.; Lucumi, E.; Gómez-Sjöberg, R.; Fleming, R. M. T. Advantages and Challenges of Microfluidic Cell Culture in Polydimethylsiloxane Devices. *Biosens. Bioelectron.* **2014**, *63*, 218–231. https://doi.org/10.1016/j.bios.2014.07.029.

(35) Hutson, M. S.; Alexander, P. G.; Allwardt, V.; Aronoff, D. M.; Bruner-Tran, K. L.; Cliffel, D. E.; Davidson, J. M.; Gough, A.; Markov, D. A.; Mccawley, L. J.; et al. Organs-on-Chips as Bridges for Predictive Toxicology. *Appl. Vitr. Toxicol.* **2016**, *2* (2), 97–102. https://doi.org/10.1089/aivt.2016.0003.

(36) Barré-Sinoussi, F.; Montagutelli, X. Animal Models Are Essential to Biological Research: Issues and Perspectives. *Future Science OA*. Future Medicine Ltd. November 1, 2015. https://doi.org/10.4155/fso.15.63.

(37) Bruner-Tran, K. L.; Mokshagundam, S.; Herington, J. L.; Ding, T.; Osteen, K. G. Rodent Models of Experimental Endometriosis: Identifying Mechanisms of Disease and Therapeutic Targets. *Curr. Women s Heal. Rev.* **2018**, *14* (2), 173–188. https://doi.org/10.2174/1573404813666170921162041.

(38) Benam, K. H.; Villenave, R.; Lucchesi, C.; Varone, A.; Hubeau, C.; Lee, H. H.; Alves, S.

E.; Salmon, M.; Ferrante, T. C.; Weaver, J. C.; et al. Small Airway-on-a-Chip Enables Analysis of Human Lung Inflammation and Drug Responses in Vitro. *Nat. Methods* **2016**, *13* (2), 151–157. https://doi.org/10.1038/nmeth.3697.

(39) Brown, J. A.; Pensabene, V.; Markov, D. A.; Allwardt, V.; Diana Neely, M.; Shi, M.; Britt, C. M.; Hoilett, O. S.; Yang, Q.; Brewer, B. M.; et al. Recreating Blood-Brain Barrier Physiology and Structure on Chip: A Novel Neurovascular Microfluidic Bioreactor. *Biomicrofluidics* **2015**, *9* (5), 1–15. https://doi.org/10.1063/1.4934713.

(40) Perrier, R.; Pirog, A.; Jaffredo, M.; Gaitan, J.; Catargi, B.; Renaud, S.; Raoux, M.; Lang, J. Bioelectronic Organ-Based Sensor for Microfluidic Real-Time Analysis of the Demand in Insulin. *Biosens. Bioelectron.* **2018**, *117*, 253–259. https://doi.org/10.1016/J.BIOS.2018.06.015.

(41) Zhang, Y. S.; Aleman, J.; Shin, S. R.; Kilic, T.; Kim, D.; Mousavi Shaegh, S. A.; Massa, S.; Riahi, R.; Chae, S.; Hu, N.; et al. Multisensor-Integrated Organs-on-Chips Platform for Automated and Continual in Situ Monitoring of Organoid Behaviors. *Proc. Natl. Acad. Sci. U. S. A.* **2017**, *114* (12), E2293–E2302. https://doi.org/10.1073/pnas.1612906114.

(42) Loria, P.; Lonardo, A.; Anania, F. Liver and Diabetes. A Vicious Circle. *Hepatol. Res.* **2013**, *43* (1), 51–64. https://doi.org/10.1111/j.1872-034X.2012.01031.x.

(43) Bruner-Tran, K. L.; Gnecco, J.; Ding, T.; Glore, D. R.; Pensabene, V.; Osteen, K. G. Exposure to the Environmental Endocrine Disruptor TCDD and Human Reproductive Dysfunction: Translating Lessons from Murine Models. https://doi.org/10.1016/j.reprotox.2016.07.007.

(44) Khan, K. N.; Fujishita, A.; Hiraki, K.; Kitajima, M.; Nakashima, M.; Fushiki, S.; Kitawaki, J. Bacterial Contamination Hypothesis: A New Concept in Endometriosis. *Reproductive*

Medicine and Biology. John Wiley and Sons Ltd April 1, 2018, pp 125–133. https://doi.org/10.1002/rmb2.12083.

(45) Fensterheim, B. A.; Young, J. D.; Luan, L.; Kleinbard, R. R.; Stothers, C. L.; Patil, N. K.; McAtee-Pereira, A. G.; Guo, Y.; Trenary, I.; Hernandez, A.; et al. The TLR4 Agonist Monophosphoryl Lipid A Drives Broad Resistance to Infection via Dynamic Reprogramming of Macrophage Metabolism. *J. Immunol.* **2018**, *200* (11), 3777–3789. https://doi.org/10.4049/jimmunol.1800085.

(46) Miller, D. R.; Schaffer, D. K.; Neely, M. D.; McClain, E. S.; Travis, A. R.; Block, F. E.; Mckenzie, J.; Werner, E. M.; Armstrong, L.; Markov, D. A.; et al. A Bistable, Multiport Valve Enables Microformulators Creating Microclinical Analyzers That Reveal Aberrant Glutamate Metabolism in Astrocytes Derived from a Tuberous Sclerosis Patient. *Sensors Actuators B Chem.* **2021**, *341*, 129972. https://doi.org/10.1016/j.snb.2021.129972.

(47) Heller, A.; Feldman, B. Electrochemical Glucose Sensors and Their Applications in Diabetes Management. *Chem. Rev.* **2008**, *108*, 2482–2505. https://doi.org/10.1021/cr068069y.

(48) Smutok, O.; Karkovska, M.; Smutok, H.; Gonchar, M. Flavocytochrome B_2-Based Enzymatic Method of L-Lactate Assay in Food Products. *ScientificWorldJournal.* **2013**, *2013*, 461284. https://doi.org/10.1155/2013/461284.

(49) Perry, S. C.; Gateman, S. M.; Sifakis, J.; Pollegioni, L.; Mauzeroll, J. Enhancement of the Enzymatic Biosensor Response through Targeted Electrode Surface Roughness. *J. Electrochem. Soc.* **2018**, *165* (12), G3074–G3079. https://doi.org/10.1149/2.0121812jes.

(50) McLamore, E. S.; Shi, J.; Jaroch, D.; Claussen, J. C.; Uchida, A.; Jiang, Y.; Zhang, W.; Donkin, S. S.; Banks, M. K.; Buhman, K. K.; et al. A Self Referencing Platinum

Nanoparticle Decorated Enzyme-Based Microbiosensor for Real Time Measurement of Physiological Glucose Transport. *Biosens. Bioelectron.* **2011**, *26* (5), 2237–2245. https://doi.org/10.1016/j.bios.2010.09.041.

(51) Wang, J. Electrochemical Glucose Biosensors. *Chemical Reviews*. February 2008, pp 814–825. https://doi.org/10.1021/cr068123a.

(52) Basu, A.; Veettil, S.; Dyer, R.; Peyser, T.; Basu, R. Direct Evidence of Acetaminophen Interference with Subcutaneous Glucose Sensing in Humans: A Pilot Study. *Diabetes Technol. Ther.* **2016**, *18 Suppl 2* (Suppl 2), S243-7. https://doi.org/10.1089/dia.2015.0410.

(53) Smith, S. K.; Lee, C. A.; Dausch, M. E.; Horman, B. M.; Patisaul, H. B.; McCarty, G. S.; Sombers, L. A. Simultaneous Voltammetric Measurements of Glucose and Dopamine Demonstrate the Coupling of Glucose Availability with Increased Metabolic Demand in the Rat Striatum. *ACS Chem. Neurosci.* **2017**, *8* (2), 272–280. https://doi.org/10.1021/acschemneuro.6b00363.

(54) Wang, J. Electrochemical Glucose Biosensors. *Chem. Rev.* **2008**, *108*, 814–825. https://doi.org/10.1016/B978-012373738-0.50005-2.

(55) Xiao, L.; Chen, J.; Cha, C. Elimination of the Interference of Ascorbic Acid in the Amperometric Detection of Biomolecules in Body Fluid Samples and the Simple Detection of Uric Acid in Human Serum and Urine by Using the Powder Microelectrode Technique. *J. Electroanal. Chem.* **2000**, *495*, 27–35.

(56) Deng, H.; Teo, A. K. L.; Gao, Z. An Interference-Free Glucose Biosensor Based on a Novel Low Potential Redox Polymer Mediator. *Sensors Actuators B Chem.* **2014**, *191*, 522–528. https://doi.org/10.1016/J.SNB.2013.10.059.

(57) Bharathi, S.; Nogami, M. A Glucose Biosensor Based on Electrodeposited Biocomposites

of Gold Nanoparticles and Glucose Oxidase Enzyme. *Analyst* **2001**, *126* (11), 1919–1922.

(58) Dodevska, T.; Horozova, E.; Dimcheva, N. Electrocatalytic Reduction of Hydrogen Peroxide on Modified Graphite Electrodes: Application to the Development of Glucose Biosensors. *Anal. Bioanal. Chem.* **2006**, *386* (5), 1413–1418. https://doi.org/10.1007/s00216-006-0682-0.

(59) Sakslund, H.; Wang, J.; Lu, F.; Hammerich, O. Development and Evaluation of Glucose Microsensors Based on Electrochemical Codeposition of Ruthenium and Glucose Oxidase onto Carbon Fiber Microelectrodes. *J. Electroanal. Chem.* **1995**, *397* (1–2), 149–155. https://doi.org/10.1016/0022-0728(95)04152-0.

(60) Yu, G.; Wu, W.; Pan, X.; Zhao, Q.; Wei, X.; Lu, Q. High Sensitive and Selective Sensing of Hydrogen Peroxide Released from Pheochromocytoma Cells Based on Pt-Au Bimetallic Nanoparticles Electrodeposited on Reduced Graphene Sheets. *Sensors* **2015**, *15* (2), 2709–2722. https://doi.org/10.3390/s150202709.

(61) Degani, Y.; Heller, A. Electrical Communication between Redox Centers of Glucose Oxidase and Electrodes via Electrostatically and Covalently Bound Redox Polymers. *J. Am. Chem. Soc.* **1989**, *111*, 2357–2358.

(62) Ohara, T. J.; Rajagopalan, R.; Heller, A. Glucose Electrodes Based on Cross-Linked [Os(Bpy)2Cl]+/2+ Complexed Poly(1-Vinylimidazole) Films. *Anal. Chem.* **1993**, *65* (23), 3512–3517. https://doi.org/10.1021/ac00071a031.

(63) Kurbanoglu, S.; Zafar, M. N.; Tasca, F.; Aslam, I.; Spadiut, O.; Leech, D.; Haltrich, D.; Gorton, L. Amperometric Flow Injection Analysis of Glucose and Galactose Based on Engineered Pyranose 2-Oxidases and Osmium Polymers for Biosensor Applications. *Electroanalysis* **2018**, *30* (7), 1496–1504. https://doi.org/10.1002/elan.201800096.

(64) Bollella, P.; Medici, L.; Tessema, M.; Poloznikov, A. A.; Hushpulian, D. M.; Tishkov, V. I.; Andreu, R.; Leech, D.; Megersa, N.; Marcaccio, M.; et al. Highly Sensitive, Stable and Selective Hydrogen Peroxide Amperometric Biosensors Based on Peroxidases from Different Sources Wired by Os-Polymer: A Comparative Study. *Solid State Ionics* **2018**, *314*, 178–186. https://doi.org/10.1016/J.SSI.2017.10.015.

(65) Mao, L.; Yamamoto, K. Amperometric Biosensor for Glutathione Based on Osmium-Polyvinylpyridine Gel Polymer and Glutathione Sulfhydryl Oxidase. *Electroanalysis* **2000**, *12* (8), 577–582. https://doi.org/10.1002/(SICI)1521-4109(200005)12:8<577::AID-ELAN577>3.0.CO;2-9.

(66) Kato, T.; Liu, J. K.; Yamamoto, K.; Osborne, P. G.; Niwa, O. Detection of Basal Acetylcholine Release in the Microdialysis of Rat Frontal Cortex by High-Performance Liquid Chromatography Using a Horseradish Peroxidase-Osmium Redox Polymer Electrode with Pre-Enzyme Reactor. *J. Chromatogr. B Biomed. Sci. Appl.* **1996**, *682* (1), 162–166. https://doi.org/10.1016/0378-4347(96)00079-5.

(67) Sherwin, R. S. Role of the Liver in Glucose Homeostasis. *Diabetes Care* **1980**, *3* (2), 261–265.

(68) Sefried, S.; Häring, H.-U.; Weigert, C.; Eckstein, S. S. Suitability of Hepatocyte Cell Lines HepG2, AML12 and THLE-2 for Investigation of Insulin Signalling and Hepatokine Gene Expression. *Open Biol.* **2018**, *8* (10), 180147. https://doi.org/10.1098/rsob.180147.

(69) Nagarajan, S. R.; Paul-Heng, M.; Krycer, J. R.; Fazakerley, D. J.; Sharland, A. F.; Andrew, X.; Hoy, J. Lipid and Glucose Metabolism in Hepatocyte Cell Lines and Primary Mouse Hepatocytes: A Comprehensive Resource for in Vitro Studies of Hepatic Metabolism. *Am J Physiol Endocrinol Metab* **2019**, *316*, 578–589.

https://doi.org/10.1152/ajpendo.00365.2018.-The.

(70) Badura, A.; Guschin, D.; Esper, B.; Kothe, T.; Neugebauer, S.; Schuhmann, W. Photo-Induced Electron Transfer Between Photosystem 2 Via. *Electroanalysis* **2008**, *20* (10), 1043–1047. https://doi.org/10.1002/elan.200804191.

(71) Zafar, M. N.; Wang, X.; Sygmund, C.; Ludwig, R.; Gorton, L. Electron-Transfer Studies with a New Flavin Adenine Dinucleotide Dependent Glucose Dehydrogenase and Osmium Polymers of Different Redox Potentials. *Anal. Chem.* **2012**, *84* (334–341), 334.

(72) Kober, E. M.; Caspar, J. V; Sullivan, B. P.; Meyer, T. J. Synthetic Routes to New Polypyridyl Complexes of Osmium(II). *Inorg. Chem.* **1988**, *27*, 4587–4598.

(73) Polk, B. J.; Stelzenmuller, A.; Mijares, G.; MacCrehan, W.; Gaitan, M. Ag/AgCl Microelectrodes with Improved Stability for Microfluidics. *Sensors Actuators, B Chem.* **2006**, *114* (1), 239–247. https://doi.org/10.1016/j.snb.2005.03.121.

(74) Wang, J. Selectivity Coefficients for Amperometric Sensors. *Talanta* **1994**, *41* (6), 857–863.

(75) Cha, K. H.; Meyerhoff, M. E. Compatibility of Nitric Oxide Release with Implantable Enzymatic Glucose Sensors Based on Osmium (III/II) Mediated Electrochemistry. **2018**, *28*, 32. https://doi.org/10.1021/acssensors.7b00430.

(76) Park, T.-M.; Iwuoha, E. I.; Smyth, M. R.; Freaney, R.; McShane, A. J. Sol-Gel Based Amperometric Biosensor Incorporating an Osmium Redox Polymer as Mediator for Detection of l-Lactate. *Talanta* **1997**, *44* (6), 973–978. https://doi.org/10.1016/S0039-9140(96)02164-9.

(77) Ohara, T. J.; Rajagopalan, R.; Heller, A. “Wired” Enzyme Electrodes for Amperometric Determination of Glucose or Lactate in the Presence of Interfering Substances. *Anal. Chem.*

1994, *66* (15), 2451–2457. https://doi.org/10.1021/ac00087a008.

(78) Eklund, S. E.; Taylor, D.; Kozlov, E.; Prokop, A.; Cliffel, D. E. A Microphysiometer for Simultaneous Measurement of Changes in Extracellular Glucose, Lactate, Oxygen, and Acidification Rate. *Anal. Chem.* **2004**, *76* (3), 519–527. https://doi.org/10.1021/ac034641z.

(79) Antiochia, R.; Gorton, L. Development of a Carbon Nanotube Paste Electrode Osmium Polymer-Mediated Biosensor for Determination of Glucose in Alcoholic Beverages. *Biosens. Bioelectron.* **2007**, *22* (11), 2611–2617. https://doi.org/10.1016/J.BIOS.2006.10.023.

(80) Hollaender, J. Rapid Assessment of Food/Package Interactions by Electrochemical Impedance Spectroscopy (EIS). *Food Addit. Contam.* **1997**, *14* (6–7), 617–626. https://doi.org/10.1080/02652039709374574.

(81) Winter, M.; Brodd, R. J. What Are Batteries, Fuel Cells, and Supercapacitors? *Chem. Rev.* **2004**, *104*, 4245–4269. https://doi.org/10.1021/cr020730k.

(82) Pourbaix, M. Applications of Electrochemistry in Corrosion Science and in Practice. *Corros. Sci.* **1974**, *14* (1), 25–82. https://doi.org/10.1016/S0010-938X(74)80006-5.

(83) Hu, X.; Dong, S. Metal Nanomaterials and Carbon Nanotubes—Synthesis, Functionalization and Potential Applications towards Electrochemistry. *J. Mater. Chem.* **2008**, *18* (12), 1279. https://doi.org/10.1039/b713255g.

(84) Acetaminophen Drug Level - Health Encyclopedia - University of Rochester Medical Center https://www.urmc.rochester.edu/encyclopedia/content.aspx?contenttypeid=167&contentid=acetaminophen_drug_level (accessed Apr 30, 2020).

(85) Bravo, I.; Revenga-Parra, M.; Pariente, F.; Lorenzo, E. Reagent-Less and Robust Biosensor

for Direct Determination of Lactate in Food Samples. *Sensors (Basel).* **2017**, *17* (144). https://doi.org/10.3390/s17010144.

(86) Kalgutkar, A. S.; Soglia, J. R. Minimising the Potential for Metabolic Activation in Drug Discovery. *Expert Opin. Drug Metab. Toxicol.* **2005**, *1* (1), 91–142. https://doi.org/10.1517/17425255.1.1.91.

(87) Eisenstein, M. Honey, I Shrunk the Lungs. *Nature* **2015**, *519*, S16–S18.

(88) Marx, V. Organs from the Lab. *Nature* **2015**, *522*, 373–377.

(89) Ware, B. R.; Khetani, S. R. Engineered Liver Platforms for Different Phases of Drug Development. https://doi.org/10.1016/j.tibtech.2016.08.001.

(90) Hutson, M. S.; Alexander, P. G.; Allwardt, V.; Aronoff, D. M.; Bruner-Tran, K. L.; Cliffel, D. E.; Davidson, J. M.; Gough, A.; Markov, D. A.; McCawley, L. J.; et al. Organs-on-Chips as Bridges for Predictive Toxicology. *Appl. Vitr. Toxicol.* **2016**, *2* (2), 97–102. https://doi.org/10.1089/aivt.2016.0003.

(91) Nyein, H. Y. Y.; Gao, W.; Shahpar, Z.; Emaminejad, S.; Challa, S.; Chen, K.; Fahad, H. M.; Tai, L. C.; Ota, H.; Davis, R. W.; et al. A Wearable Electrochemical Platform for Noninvasive Simultaneous Monitoring of Ca2+ and PH. *ACS Nano* **2016**, *10* (7), 7216–7224. https://doi.org/10.1021/acsnano.6b04005.

(92) Marquitan, M.; Bobrowski, T.; Ernst, A.; Wilde, P.; Clausmeyer, J.; Ruff, A.; Schuhmann, W. Miniaturized Amperometric Glucose Sensors Based on Polymer/ Enzyme Modified Carbon Electrodes in the Sub-Micrometer Scale. *J. Electrochem. Soc.* **2018**, *165* (12), G3008–G3014. https://doi.org/10.1149/2.0021812jes.

(93) Correia, D. P. A.; Magalhães, J. M. C. S.; Machado, A. A. S. C. Array of Potentiometric Sensors for Simultaneous Analysis of Urea and Potassium. *Talanta* **2005**, *67*, 773–782.

https://doi.org/10.1016/j.talanta.2005.04.003.

(94) Bollella, P.; Gorton, L. Enzyme Based Amperometric Biosensors. *Curr. Opin. Electrochem.* **2018**, *10*, 157–173. https://doi.org/10.1016/J.COELEC.2018.06.003.

(95) McClain, E. S. Development and Application and Enzymatic Biosensors in the Investigation of Organophosphate Toxicity and Neurotransmission, Vanderbilt University, 2021.

(96) Lima, E. A.; Snider, R. M.; Reiserer, R. S.; McKenzie, J. R.; Kimmel, D. W.; Eklund, S. E.; Wikswo, J. P.; Cliffel, D. E. Multichamber Multipotentiostat System for Cellular Microphysiometry. *Sensors Actuators, B Chem.* **2014**, *204*, 536–543. https://doi.org/10.1016/j.snb.2014.07.126.

(97) Gholivand, M. B.; Khodadadian, M. Amperometric Cholesterol Biosensor Based on the Direct Electrochemistry of Cholesterol Oxidase and Catalase on a Graphene/Ionic Liquid-Modified Glassy Carbon Electrode. *Biosens. Bioelectron.* **2014**, *53*, 472–478. https://doi.org/10.1016/J.BIOS.2013.09.074.

(98) Antiochia, R.; Gorton, L.; Mannina, L. Rapid Determination of Sucrose in Fruit Juices: A New Sensitive Carbon Nanotube Paste Osmium-Polymer Mediated Biosensor. *J. Food Res.* **2014**, *3* (4), 101. https://doi.org/10.5539/jfr.v3n4p101.

(99) Alpeeva, I. S.; Vilkanauskyte, A.; Ngounou, B.; Csöregi, E.; Sakharov, I. Y.; Gonchar, M.; Schuhmann, W. Bi-Enzyme Alcohol Biosensors Based on Genetically Engineered Alcohol Oxidase and Different Peroxidases. *Microchim. Acta* **2005**, *152* (1–2), 21–27. https://doi.org/10.1007/s00604-005-0407-7.

(100) McKenzie, J. R.; Palubinsky, A. M.; Brown, J. E.; McLaughlin, B.; Cliffel, D. E. Metabolic Multianalyte Microphysiometry Reveals Extracellular Acidosis Is an Essential Mediator of

Neuronal Preconditioning. *ACS Chem. Neurosci.* **2012**, *3* (7), 510–518. https://doi.org/10.1021/cn300003r.

(101) Rocchitta, G.; Spanu, A.; Babudieri, S.; Latte, G.; Madeddu, G.; Galleri, G.; Nuvoli, S.; Bagella, P.; Demartis, M. I.; Fiore, V.; et al. Enzyme Biosensors for Biomedical Applications: Strategies for Safeguarding Analytical Performances in Biological Fluids. *Sensors (Switzerland)*. MDPI AG June 1, 2016. https://doi.org/10.3390/s16060780.

(102) Rathee, K.; Dhull, V.; Dhull, R.; Singh, S. Biosensors Based on Electrochemical Lactate Detection: A Comprehensive Review. *Biochem. Biophys. Reports* **2016**, *5*, 35–54. https://doi.org/10.1016/J.BBREP.2015.11.010.

(103) Chen, C.; Xie, Q.; Yang, D.; Xiao, H.; Fu, Y.; Tan, Y.; Yao, S. Recent Advances in Electrochemical Glucose Biosensors: A Review. *RSC Adv.* **2013**, *3*, 4473–4491. https://doi.org/10.1039/c2ra22351a.

(104) Eckman, J.; Dixit, S.; Nackenoff, A.; Schrag, M.; Harrison, F. E. Oxidative Stress Levels in the Brain Are Determined by Post-Mortem Interval and Ante-Mortem Vitamin C State but Not Alzheimer's Disease Status. *Nutrients* **2018**, *10* (7). https://doi.org/10.3390/nu10070883.

(105) Kimmel, D. W.; Meschievitz, M. E.; Hiatt, L. A.; Cliffel, D. E. Multianalyte Microphysiometry of Macrophage Responses to Phorbol Myristate Acetate, Lipopolysaccharide, and Lipoarabinomannan. *Electroanalysis* **2013**, *25* (7), 1706–1712. https://doi.org/10.1002/elan.201300121.

(106) Hiatt, L. A.; Mckenzie, J. R.; Deravi, L. F.; Harry, R. S.; Wright, D. W.; Cliffel, D. E. A Printed Superoxide Dismutase Coated Electrode for the Study of Macrophage Oxidative Burst. *Biosens. Bioelectron.* **2011**, *33*, 128–133. https://doi.org/10.1016/j.bios.2011.12.038.

(107) Kimmel, D. W.; Dole, W. P.; Cliffel, D. E. Application of Multianalyte Microphysiometry to Characterize Macrophage Metabolic Responses to Oxidized LDL and Effects of an ApoA-1 Mimetic. *Biochem. Biophys. Res. Commun.* **2013**, *431* (2), 181–185. https://doi.org/10.1016/j.bbrc.2012.12.140.

(108) Zhang, H.; Qi, J.; Wang, Y.; Sun, J.; Li, Z.; Sui, L.; Fan, J.; Liu, C.; Shang, Y.; Kong, L.; et al. Progesterone Regulates Glucose Metabolism Through Glucose Transporter 1 to Promote Endometrial Receptivity. *Front. Physiol.* **2020**, *11*, 543148. https://doi.org/10.3389/fphys.2020.543148.

(109) Ratter, J. M.; Rooijackers, H. M. M.; Hooiveld, G. J.; Hijmans, A. G. M.; de Galan, B. E.; Tack, C. J.; Stienstra, R. In Vitro and in Vivo Effects of Lactate on Metabolism and Cytokine Production of Human Primary PBMCs and Monocytes. *Front. Immunol.* **2018**, *9*, 2564. https://doi.org/10.3389/fimmu.2018.02564.

(110) Diskin, C.; Pålsson-McDermott, E. M. Metabolic Modulation in Macrophage Effector Function. *Frontiers in Immunology*. Frontiers Media S.A. February 19, 2018, p 270. https://doi.org/10.3389/fimmu.2018.00270.

(111) Harry, R. S.; Hiatt, L. A.; Kimmel, D. W.; Carney, C. K.; Halfpenny, K. C.; Cliffel, D. E.; Wright, D. W. Metabolic Impact of 4-Hydroxynonenal on Macrophage-like RAW 264.7 Function and Activation. *Chem. Res. Toxicol.* **2012**, *25* (8), 1643–1651. https://doi.org/10.1021/tx3001048.

(112) Du, X.; Wang, R.; Zhai, J.; Li, X.; Xie, X. Ionophore-Based Ion-Selective Nanosensors from Brush Block Copolymer Nanodots. *ACS Appl. Nano Mater.* **2020**, *3* (1), 782–788. https://doi.org/10.1021/acsanm.9b02286.

(113) Henriksen, G. H.; Bloom, A. J.; Spanswick, R. M. Measurement of Net Fluxes of

Ammonium and Nitrate at the Surface of Barley Roots Using Ion-Selective Microelectrodes. *Plant Physiol.* **1990**, *93* (1), 271–280. https://doi.org/10.1104/pp.93.1.271.

(114) Fresser, F.; Moser, H.; Mair, N. *INTRA-AND EXTRACELLULAR USE AND EVALUATION OF AMMONIUM-SELECTIVE MICROELECTRODES*; 1991; Vol. 147.

(115) Ghauri, M. S.; Thomas, J. D. R. Evaluation of an Ammonium Ionophore for Use in Poly(Vinyl Chloride) Membrane Ion-Selective Electrodes: Solvent Mediator Effects. *Analyst* **1994**, *119* (11), 2323–2326. https://doi.org/10.1039/AN9941902323.

(116) Ma, S. C.; Chaniotakis, N. A.; Meyerhoff, M. E. Response Properties of Ion-Selective Polymeric Membrane Electrodes Prepared with Aminated and Carboxylated Poly(Vinyl Chloride). *Anal. Chem.* **1988**, *60* (20), 2293–2299. https://doi.org/10.1021/ac00171a027.

(117) Ghauri, M. S.; Thomas, J. D. R. Poly(Vinyl Chloride) Type Ammonium Ion-Selective Electrodes Based on Nonactin: Solvent Mediator Effects. *Anal. Proc.* **1994**, *31* (181).

(118) Cuartero, M.; Colozza, N.; Fernández-Pérez, B. M.; Crespo, G. A. Why Ammonium Detection Is Particularly Challenging but Insightful with Ionophore-Based Potentiometric Sensors-an Overview of the Progress in the Last 20 Years. *Analyst* **2020**, *145* (9), 3188–3210. https://doi.org/10.1039/d0an00327a.

(119) Lingenfelter, P.; Bartoszewicz, B.; Migdalski, J.; Sokalski, T.; Bućko, M. M.; Filipek, R.; Lewenstam, A. Reference Electrodes with Polymer-Based Membranes—Comprehensive Performance Characteristics. *Membranes (Basel).* **2019**, *9* (12). https://doi.org/10.3390/membranes9120161.

(120) Miyake, M.; Chen, L. D.; Pozzi, G.; Bühlmann, P. Ion-Selective Electrodes with Unusual Response Functions: Simultaneous Formation of Ionophore-Primary Ion Complexes with

Different Stoichiometries. *Anal. Chem.* **2012**, *84* (2), 1104–1111. https://doi.org/10.1021/ac202761x.

(121) Karakuş, E.; Pekyardimci, Ş.; Kiliç, E. A New Potentiometric Ammonium Electrode for Biosensor Construction. *Artif. Cells, Blood Substitutes, Biotechnol.* **2006**, *34* (5), 523–534. https://doi.org/10.1080/10731190600862910.

(122) Weiner, I. D. Roles of Renal Ammonia Metabolism Other than in Acid–Base Homeostasis. *Pediatric Nephrology*. Springer Verlag June 1, 2017, pp 933–942. https://doi.org/10.1007/s00467-016-3401-x.

(123) WHITE, L. P.; PHEAR, E. A.; SUMMERSKILL, W. H.; SHERLOCK, S.; Cole, M. Ammonium Tolerance in Liver Disease: Observations Based on Catheterization of the Hepatic Veins. *J. Clin. Invest.* **1955**, *34* (2), 158–168. https://doi.org/10.1172/JCI103070.

(124) Ferrannini, E.; Galvan, A. Q.; Santoro, D.; Natali, A. Potassium as a Link between Insulin and the Renin-Angiotensin-Aldosterone System. In *Journal of Hypertension*; J Hypertens Suppl, 1992; Vol. 10. https://doi.org/10.1097/00004872-199204001-00002.

(125) Singh, K.; Lou, B.-S.; Her, J.-L.; Pang, S.-T.; Pan, T.-M. Super Nernstian PH Response and Enzyme-Free Detection of Glucose Using Sol-Gel Derived RuOx on PET Flexible-Based Extended-Gate Field-Effect Transistor. *Sensors Actuators B Chem.* **2019**, *298*, 126837. https://doi.org/10.1016/J.SNB.2019.126837.

(126) Zakir Hossain, S. M.; Luckham, R. E.; Smith, A. M.; Lebert, J. M.; Davies, L. M.; Pelton, R. H.; Filipe, C. D. M.; Brennan, J. D. Development of a Bioactive Paper Sensor for Detection of Neurotoxins Using Piezoelectric Inkjet Printing of Sol-Gel-Derived Bioinks. *Anal. Chem.* **2009**, *81* (13), 5474–5483. https://doi.org/10.1021/ac900660p.

(127) Pandit, A.; Sachdeva, T.; Bafna, P. Drug-Induced Hepatotoxicity: A Review. *J. Appl.*

Pharm. Sci. **2011**, *02* (2012), 233–243. https://doi.org/10.7324/JAPS.2012.2541.

(128) Blesso, C. N.; Fernandez, M. L. Dietary Cholesterol, Serum Lipids, and Heart Disease: Are Eggs Working for or Against You? *Nutrients* **2018**, *10* (4). https://doi.org/10.3390/nu10040426.

(129) Zhao, B.; Natarajan, R.; Ghosh, S. Human Liver Cholesteryl Ester Hydrolase: Cloning, Molecular Characterization, and Role in Cellular Cholesterol Homeostasis.

(130) Meyer, D. F.; Gamache, P. H.; Acworth, I. N. The Application of Electrochemistry to Metabolic Profiling. In *Metabolome Analyses: Strategies for Systems Biology*; Vaidyanathan, S., Harrigan, G. G., Goodacre, R., Eds.; Springer US, 2005; pp 119–135.

(131) Hargrove, T. Y.; Wawrzak, Z.; Lamb, D. C.; Guengerich, F. P.; Lepesheva, G. I. Structure-Functional Characterization of Cytochrome P450 Sterol 14α-Demethylase (CYP51B) from Aspergillus Fumigatus and Molecular Basis for the Development of Antifungal Drugs. *J. Biol. Chem.* **2015**, *290* (39), 23916–23934. https://doi.org/10.1074/jbc.M115.677310.

(132) Portilho, D. M.; Soares, C. P.; Morrot, A.; Thiago, L. S.; Butler-Browne, G.; Savino, W.; Costa, M. L.; Mermelstein, C. Cholesterol Depletion by Methyl-β-Cyclodextrin Enhances Cell Proliferation and Increases the Number of Desmin-Positive Cells in Myoblast Cultures. *Eur. J. Pharmacol.* **2012**, *694* (1–3), 1–12. https://doi.org/10.1016/J.EJPHAR.2012.07.035.

(133) Onakpoya, I. J.; Heneghan, C. J.; Aronson, J. K. Post-Marketing Withdrawal of 462 Medicinal Products Because of Adverse Drug Reactions: A Systematic Review of the World Literature. *BMC Med.* **2016**, *14* (10). https://doi.org/10.1186/s12916-016-0553-2.

(134) Scheen, A. J. Hepatotoxicity with Thiazolidinediones: Is It a Class Effect? *Drug Saf.* **2001**, *24* (12), 873–888.

Sara L. Melow

118 Pine Grove Road, Mt. Juliet, TN 37122 ♦ (503) 871-6932
salyme8@yahoo.com ♦ linkedin.com/in/saramelow

EDUCATION

Ph.D. in Chemistry (GPA: 3.787) **May 2021**
Vanderbilt University, Nashville, TN

Bachelor of Science in Chemistry and Mathematics (GPA: 3.909) **2016**
Elmira College, Elmira, NY

RELEVANT EXPERIENCE

Science Communication Intern **2021-Present**
Advisor: Karisa Calvitti; Vanderbilt Institute of Infection, Immunology, and Inflammation, Vanderbilt University Medical Center, Nashville, TN

- Generated written content and images on current research and discoveries for social media campaigns
- Assisted in making marketing creative materials for community outreach programs
- Developed a podcast on COVID and public health for community outreach

Graduate Research Assistant/Ph.D. Candidate **2016-Present**
Advisor: Dr. David Cliffel; Department of Chemistry, Vanderbilt University, Nashville, TN

- Developed eight electrochemical sensors for testing with model organ systems in applications of toxicological studies and presented at weekly lab meetings and at several conferences
- Collaborated with Vanderbilt-Pittsburgh Resource for Organotypic Models for Predictive Toxicology to adapt electrochemical sensors for testing on model liver system

Research Assistant **2013-2016**
Advisor: Dr. Jared Baker; Department of Chemistry, Elmira College, Elmira, NY

- Collaborated with a local whiskey distillery to develop a portable Arduino sensor to determine methanol (0%) and ethanol content (40-80%) in the field for regulation purposes
- Characterized whiskey flavor profiles using techniques such as fluorimetry and GC-MS by evaluating various compounds (i.e. total acidity, calcium, and scopoletin)

Research Assistant **May 2015-July 2015**
Advisor: Dr. Lisa Holland; Department of Chemistry, West Virginia University, Morgantown, WV

- Developed and investigated a self-directed project, and presented findings in two presentations
- Assembled and standardized procedures for an Inductively Coupled Plasma – Optical Emission Spectrometry (ICP-OES) instrument for colleagues and independent project use

Research Mentor **2018-Present**
Department of Chemistry, Vanderbilt University, Nashville, TN

- Organized projects for seven undergraduate/PhD students: monitored their progress, provided feedback, and reviewed their presentations for internal use and external institutions
- Directed experimental design and provided technical training for students in instruments (potentiostat) and techniques (cyclic voltammetry and cell culture)

Teaching Assistant **2016-2017**
Department of Chemistry, Vanderbilt University, Nashville, TN

- Supervised and facilitated general and organic chemistry labs
- Guided and coordinated experiments for 18-24 students in each class twice a week

AWARDS

T32 Trainee in Environmental Toxicology Program, Vanderbilt University
2017- 2020
Algernon DeWaters Gorman Prize, Elmira College
2015
Chemical Rubber Company Basic Chemistry Prize, Elmira College
2013

LEADERSHIP POSITIONS

Secretary/PR Chair, Younger Chemists Committee of ACS Nashville chapter **2020-Present**
Secretary, Graduate Student Council at Vanderbilt University **2020-2021**
Founder/President, Gamma Sigma Epsilon – Elmira College chapter **2016-Present**
Member/President, American Chemical Society – Elmira College chapter **2013-Present**

PROFESSIONAL AFFILIATIONS

Member, Electrochemical Society **2019-2020**
Member, Sigma Zi **2017-2019**
Member, Phi Beta Kappa **2016-Present**
Member, Omicron Delta Kappa at Elmira College **2014-Present**
Member, Phi Eta Sigma at Elmira College **2013-Present**

PRESENTATIONS

Oral

Melow, S. L., Miller, D. R., Gizzie, E. A., and Cliffel, D. E. High-Resolution Multianalyte Biosensor Array for Analysis of Model Organ Systems, Electrochemical Society Meeting, 2019, Atlanta, GA

Melow, S. L. and Cliffel, D. E. Electrochemical Biosensors for Predictive Toxicology, Vanderbilt University Toxicology Seminar, 2019, Nashville, TN

Melow, S. L., Miller, D. R., Gizzie, E. A., and Cliffel, D. E. High-Resolution Multianalyte Biosensor Array for Analysis of Model Liver Systems, SERMACS, 2018, Augusta, GA

Melow, S. L. and Cliffel, D. E. Electrochemical Biosensors for Predictive Toxicology in Model Liver Systems, Vanderbilt University Chemistry Department Seminar, 2018, Nashville, TN

Melow, S. L. and Cliffel, D. E. Electrochemical Biosensors for Predictive Toxicology, Vanderbilt University Toxicology Seminar, 2018, Nashville, TN

Poster

Melow, S. L., Miller, D. R., Gizzie, E. A., and Cliffel, D. E. High-Resolution Multianalyte Biosensor Array for Analysis of Model Organ Systems, Cellular and Molecular Mechanisms of Toxicity – Gordon Research Seminar/Conference, 2019, Andover, NH

Melow, S. L., Ellington, M. C., and Holland, L. A. Assessment of Titanium Dioxide Nanoparticles in Aquatic Tanks, Pittsburgh Conference on Analytical Chemistry and Applied Spectroscopy, 2016, Atlanta, GA

Melow, S. L., Ellington, M. C., and Holland, L. A. Assessment of Titanium Dioxide Nanoparticles in Aquatic Tanks, Summer Undergraduate Research Symposium, 2015, Morgantown, WV

PUBLICATIONS

Melow, S. L., Miller, D. R., Gizzie, E. A., and Cliffel, D. E. A Low-Interference, High-Resolution Multianalyte Electrochemical Biosensor. *Anal. Methods* **2020**, 12–15. https://doi.org/10.1039/d0ay00528b.

Melow, S. L., Tuladhar, P., Stevens, V., Osteen, K., and Cliffel, D. E. Development and Application of a Dual Amperometric and Potentiometric Multianalyte Electrochemical Biosensor. *In preparation for submission*. (Estimated submission date: June 2021).

Melow, S. L., Stevens, V., Osteen, K., and Cliffel, D. E. Multianalyte Amperometric Electrochemical Biosensor Platform for Analysis of Model Organ Systems. *In preparation for submission*. (Estimated submission date: June 2021).